# Analyzing Cellular Properties with Dielectrophoresis

by

Shannon Louise Hilton

A Dissertation Presented in Partial Fulfillment
of the Requirements for the Degree
Doctor of Philosophy

Approved April 2019 by the
Graduate Supervisory Committee:

Mark A. Hayes, Chair
Chad Borges
Pierre Herckes

ARIZONA STATE UNIVERSITY

May 2019

ABSTRACT

Dielectrophoresis (DEP) is a technique that influences the motion of polarizable particles in an electric field gradient. DEP can be combined with other effects that influence the motion of a particle in a microchannel, such as electrophoresis and electroosmosis. Together, these three can be used to probe properties of an analyte, including charge, conductivity, and zeta potential. DEP shows promise as a high-resolution differentiation and separation method, with the ability to distinguish between subtly-different populations. This, combined with the fast (on the order of minutes) analysis times offered by the technique, lend it many of the features necessary to be used in rapid diagnostics and point-of-care devices.

Here, a mathematical model of dielectrophoretic data is presented to connect analyte properties with data features, including the intercept and slope, enabling DEP to be used in applications which require this information. The promise of DEP to distinguish between analytes with small differences is illustrated with antibiotic resistant bacteria. The DEP system is shown to differentiate between methicillin-resistant and -susceptible *Staphylococcus aureus*. This differentiation was achieved both label-free and with bacteria that had been fluorescently-labeled. *Klebsiella pneumoniae* carbapenemase-positive and -negative *Klebsiella pneumoniae* were also distinguished, demonstrating the differentiation for a different mechanism of antibiotic resistance. Differences in dielectrophoretic behavior as displayed by *S. aureus* and *K. pneumoniae* were also shown by *Staphylococcus epidermidis*. These differences were exploited for a separation in space of gentamicin-resistant and -susceptible *S. epidermidis*. Besides

establishing the ability of DEP to distinguish between populations with small biophysical differences, these studies illustrate the possibility for the use of DEP in applications such as rapid diagnostics.

To my family – you made this possible, and worth it

ACKNOWLEDGEMENTS

Much thanks is due to my advisor, Dr. Mark Hayes. I am truly grateful for your guidance, direction, and support over my graduate career, without which this dissertation would not be what it is. I also thank my committee members, Dr. Chad Borges and Dr. Pierre Herckes, for support and encouragement.

To the Hayes group members with whom I have crossed paths, thank you. You are wonderful people to work with and have all have helped make me a better scientist. Dr. Paul Jones, thank you for your willingness to teach and help me get my feet under me when starting graduate school. Dr. Claire Crowther, thank you for the Friday afternoon discussions, the proofreading, and the friendship. Thanks to Dr. Jie Ding for your insights into DEP. Fanyi Zhu and Yameng Liu, thank you for your kindness and your willingness to help. Ryan Yanashima, Paige Davis, Alex Ramirez, Jared Smithers, and Brennan Copp, thank you for helping me refine my understanding of my work.

There are many outside of the Hayes group who have worked with me and helped this dissertation come to be. Jolene Bowers, Michael Valentine, and Dave Engelthaler of TGen North, thank you for being such wonderful collaborators and answering my many questions. Alex McLaren, thank you for your insights into all things clinical. Dr. Wade Van Horn, thank you for assistance in such a variety of things over my time as a graduate student.

My friends and family in Arizona, thank you. You all have given me support and encouragement and made the time I spent researching and writing this dissertation even

sweeter. Thanks especially to Shane and Megan Hilton, Robin and Bruce Goldthorpe, and Joe and Claudia Hilton.

To my family, this is all possible thanks to you. I lack the words to appropriately thank you all. I couldn't possibly list everything for which I am grateful. To my parents: thank you for supporting me, encouraging me, and believing in me. Your continued encouragement of my love of science helped me to get to now. None of this would be possible without you. Finally, to Jacob. Thank you for exploring with me, helping me find just the right word, laughing with me, understanding weird hours and late nights, baking with me, and so much more. Thank you for always believing in me and having my back.

TABLE OF CONTENTS

Page

LIST OF FIGURES ..... xi

CHAPTER

1 INTRODUCTION ..... 1

1.1 Bioparticle Analysis ..... 1

1.2 Separations ..... 2

1.3 Microfluidics ..... 4

1.4 Clinical Analysis ..... 5

1.5 Dissertation Overview ..... 7

1.6 References ..... 8

2 OVERVIEW AND THEORY OF DIELECTROPHORESIS ..... 13

2.1 Dielectrophoresis Theory ..... 13

2.1.1 Electroosmosis ..... 13

2.1.2 Electrophoresis ..... 15

2.1.3 Electrokinetic Mobility ..... 17

2.1.4 Dielectrophoresis ..... 18

2.1.5 Capture in Dielectrophoresis ..... 21

2.2 Microfluidic Device Fabrication ..... 22

2.3 Applications of Dielectrophoresis ..... 25

2.4 References ..... 29

CHAPTER Page

3 A MATHEMATICAL MODEL OF DIELECTROPHORETIC DATA TO CONNECT MEASUREMENTS WITH CELL PROPERTIES ..... 33

3.1 Introduction ..... 33

3.2 Theory ..... 36

3.2.1 Channel Effects ..... 36

3.2.1.1 Electroosmosis and Electrophoresis ..... 37

3.2.1.2 Dielectrophoresis ..... 38

3.2.2 Particle Properties ..... 40

3.2.2.1 Conductivity and Permittivity ..... 40

3.2.2.2 Surface Charge Density ..... 41

3.2.2.3 Charge Distribution and Multipoles ..... 42

3.3 Materials and Methods ..... 44

3.4 Results and Discussion ..... 44

3.4.1 Development of a Mathematical Model of Dielectrophoretic Data ..... 44

3.4.1.1 Varying Potential ..... 47

3.4.1.2 Conditions of Capture ..... 48

3.4.1.3 Capture Onset Potential ..... 49

3.4.1.4 Varying Time ..... 50

3.4.2 Features of Data and Interpretation with the Model ..... 50

3.4.3 Applications with Known Particle Properties ..... 51

3.4.3.1 Conductivity and Permittivity ..... 52

CHAPTER Page

3.4.3.2 Zeta Potential ..... 56

3.4.3.3 Surface Charge Density ..... 58

3.4.3.4 Charge Distribution/Multipoles and Dipoles ..... 62

3.5 Conclusion ..... 62

3.6 References ..... 63

4 BIOPHYSICAL DIFFERENTIATION OF SUSCEPTIBILITY AND CHEMICAL DIFFERENCES IN *STAPHYLOCOCCUS AUREUS* ..... 69

4.1 Introduction ..... 69

4.2 Theory ..... 72

4.3 Materials and Methods ..... 75

4.3.1 Microdevice Fabrication ..... 75

4.3.2 Bacterial Preparation and Labeling ..... 76

4.3.3 DEP Experiments ..... 78

4.3.4 Data Modeling ..... 79

4.3.5 Safety Considerations ..... 81

4.4 Results ..... 81

4.5 Discussion ..... 83

4.6 Conclusion ..... 89

4.7 References ..... 90

5 DIELECTROPHORESIS OF KPC-POSITIVE AND -NEGATIVE *KLEBSIELLA PNEUMONIAE* AND POST-HOC ASSESSMENT OF DIFFERENCES ..... 94

CHAPTER Page

5.1 Introduction ..... 94

5.2 Theory ..... 96

5.3 Materials and Methods ..... 97

5.3.1 Fabrication of the Microdevice ..... 97

5.3.2 Cell Culture ..... 99

5.3.3 Dielectrophoresis Experiments ..... 100

5.3.4 Data Modeling ..... 100

5.3.5 Polymerase Chain Reaction (PCR) Methods ..... 101

5.3.6 Safety Considerations ..... 102

5.4 Results and Discussion ..... 103

5.5 Conclusion ..... 107

5.6 References ..... 107

6 DIELECTROPHORETIC SEPARATION OF GENTAMICIN-RESISTANT AND -SUSCEPTIBLE *STAPHYLOCOCCUS EPIDERMIDIS* ..... 112

6.1 Introduction ..... 112

6.1.1 Antibiotic Resistance ..... 112

6.1.2 Dielectrophoresis ..... 113

6.1.3 DEP Separations ..... 114

6.2 Theory ..... 116

6.3 Materials and Methods ..... 118

6.3.1 Device Fabrication and Assembly ..... 118

CHAPTER Page

6.3.2 Bacterial Culture ..... 120

6.3.3 Labeling ..... 121

6.3.4 Experimental ..... 122

6.3.5 Safety Considerations ..... 123

6.4 Results and Discussion ..... 123

6.5 Conclusions ..... 129

6.6 References ..... 129

7 SUMMARY AND CONCLUSIONS ..... 134

7.1 Summary ..... 134

7.2 Future Outlook ..... 135

7.3 Antimicrobial Susceptibility Testing ..... 136

7.4 Dielectrophoresis As A Point-Of-Care Device ..... 137

7.5 Other Applications of Dielectrophoresis ..... 139

7.6 References ..... 140

REFERENCES ..... 142

APPENDIX

A VALIDATION OF THE MATHEMATICAL MODEL OF DIELECTROPHORETIC DATA ..... 167

B PUBLISHED PORTIONS ..... 171

LIST OF FIGURES


| Figure | | Page |
|---|---|---|
| 1.1 | Resolution and the Relationship to Chromatographic Peaks | 3 |
| 1.2 | Number of Microfluidics Papers 2010-2018 | 5 |
| 2.1 | Electroosmosis Theory | 14 |
| 2.2 | Electrophoresis Analyte Direction | 17 |
| 2.3 | Dielectrophoresis Theory | 20 |
| 2.4 | Capture in Dielectrophoresis | 21 |
| 2.5 | Photolithography Methods for Microfluidic Devices | 24 |
| 2.6 | Assembly of a Dielectrophoretic Channel | 25 |
| 3.1 | Illustration of Channel, Typical Analyte Collection, and Data Structures | 46 |
| 3.2 | Calculated DEP Data for Varying Conductivities | 53 |
| 3.3 | Calculated DEP Data Using Shell Model with Varying Conductivities | 55 |
| 3.4 | Calculated DEP Data with Varying Zeta Potentials | 57 |
| 3.5 | Calculated DEP Data with Varying Surface Charge Density and Softness | 60 |
| 4.1 | Typical Data Structure Illustration with Images of Capture | 81 |
| 4.2 | Plots of Dielectrophoretic Capture Data of *Staphylococcus aureus* | 82 |
| 4.3 | Surface Charge Density Map of PBP2a | 86 |
| 4.4 | Structure of NHS-Rhodamine and Modeled Surface Charge Difference | 88 |
| 5.1 | Illustration of Capture and Dielectrophoretic Data Structures | 103 |
| 5.2 | DEP Data of KPC-Positive and KPC-Negative *Klebsiella pneumoniae* | 104 |
| 5.3 | DEP Data from Old and New Plates of *Klebsiella pneumoniae* | 105 |

Figure Page

5.4 PCR of New Plate of *Klebsiella pneumoniae* .....106

6.1 Illustration of Analyte Collection over Time and Separation in Space .....118

6.2 Schematic of Microchannel Designs .....120

6.3 Plots of *Staphylococcus epidermidis* Dielectrophoretic Data .....124

6.4 Separation of Resistant and Susceptible *Staphylococcus epidermidis* .....126

6.5 Separation of *Staphylococcus epidermidis* with Switched Dyes .....127

6.6 Structure of NHS-Rhodamine and NHS-Fluorescein .....128

# CHAPTER 1

# INTRODUCTION

The world is teeming with microscopic life. These microbes, from viruses and fungi to bacteria and archaea, surround and impact the world in numerous ways. Some are helpful, some neutral, while others cause harm. They affect the appearance of the world, the types of food available, and human health. Microbes, including bacteria and archaea, contribute to the myriad of colors in the pools of Yellowstone [1, 2]. The making of cheese and yogurt is enabled by bacteria [3, 4]. Bacteria and algae fix nitrogen in the soil, supporting the growth of food and plants [5]. Everyone has a microbiome, with bacteria living commensally in and on the body [6]. Harmful microbes include bacteria and viruses that cause infection. In order to understand this complex microscopic world, people have discovered ways to detect and analyze microbes.

## 1.1 Bioparticle Analysis

Traditionally, microscopes have been used to study particles too small to be seen by the human eye unassisted. Conventional light microscopy has been used to study cells and allow viewing and identification of organelles [7]. Various microscopy techniques can give information not only about size and shape, but about organelles in a cell, depth of an analyte, and even responses to stimuli. When combined with fluorescence and immunocytochemistry techniques, microscopy becomes even more advanced in its ability to detect and localize proteins and nucleic acids. Dyes sensitive to atoms or small molecules, such as calcium, allow signaling to be studied with microscopy. However, conventional light microscopes have a lower limit of particle sizes it can be used to study,

about 0.25 μm [7]. The advent of electron microscopy has increased the range of analyte sizes that can be investigated with microscopy [7]. Electron microscopy methods can give higher-resolution imaging and has been used to determine the structure of proteins [8].

Other properties of biological analytes can be studied using other techniques. Electrophysiology provides information about ion channels and the electrical properties of cell membranes [9, 10]. Polymerase chain reaction and DNA sequencing techniques inform about the genomic makeup of a cell [11]. Blotting methods and gel separation techniques can identify and quantify the protein contents of a sample [12, 13]. Mass spectrometry can be used to learn about the identity of components and sequence of proteins [14]. Nuclear magnetic resonance (NMR) spectroscopy and crystallography give atomic-level structural information [15, 16]. NMR can also provide information regarding dynamic motions of proteins that give rise to their function [17]. Studying microbes with various methods to obtain a variety of information gives a more complete picture of these microscopic life forms.

### 1.2 Separations

In many chemical, biochemical, and biological analyses, separation is the first step. While most real-world samples are complicated mixtures, a pure, or somewhat pure, sample is required to manipulate and study the analyte. The goal of all separation techniques is to result in distinct populations of each desired species. The quality of the separation is characterized by its resolution.

Resolution ($R$) is determined from the distance between the center of two populations ($\Delta X$) and the spread of each population ($\sigma$), according to the equation [18]

$$R = \frac{\Delta X}{4\sigma} \tag{1}$$

Two populations are considered to be resolved with a resolution of $R \geq 1$, while $R \geq 1.5$ is usually desired to consider two populations to be separated [19, 20]. Assuming peaks have a Gaussian distribution, $R = 1$ corresponds to an overlap of 2.3% of each population, while $R = 1.5$ corresponds to a 0.13% overlap [21-23]. To improve resolution, either the centers of the two populations must be further apart (increasing $\Delta X$) or the spread of the populations must be decreased (decreasing $\sigma$) (Figure 1.1).

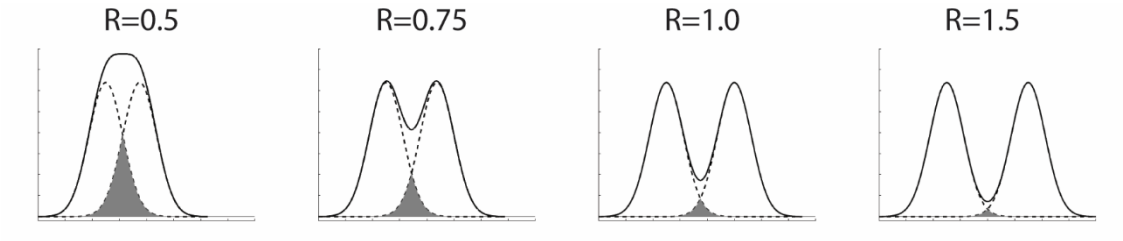



Figure 1.1 Gaussian chromatographic peaks (dashed lines) and their combination (solid line) for R = 0.5, 0.75, 1.0 and 1.5 (left to right). The overlap between the peaks is shaded grey.

While numerous separation techniques exist, only those directly relevant to this work will be mentioned here. Chromatography is a widely-used separation technique with numerous variations, including high-performance liquid chromatography, gas chromatography, and column chromatography, among others. Each method separates based on various properties of the analytes, including size, affinity for a specific ligand, or other properties [19, 20, 24]. Centrifugation methods separate based on density or analyte mass [25]. Electrophoresis methods include capillary electrophoresis and gel

electrophoresis. The separation of analytes is based on the size and the charge (small particles) or zeta potential (large particles) [19, 26-28]. The theory of electrophoresis will be discussed more in Chapter 2. Distillation relies on the difference in volatility of two populations [29]. Extraction separates two populations between two different phases [30].

All separation methods are useful for specific applications, but have limitations which make them less useful under certain conditions. Each one separates based on different features of the analyte, or can be used to separate a certain number of analytes. Some allow for recovery of analytes for further analysis, while others are used for identification purposes and the analyte cannot be recovered. Appropriate separation methods are chosen in each case based on the application.

### 1.3 Microfluidics

The term "microfluidics" describes the use of small volumes of liquid. This encompasses many applications, from medical diagnostics to genetic sequencing [10, 31-36]. While some microfluidic methods are miniaturizations of existing techniques [37-44], solely microfluidic methods exist as well [45-49]. The number of papers published each year on microfluidics is increasing, showing that this field is growing (Figure 1.2).

Advantages of microfluidics over traditional counterparts often include small sample and reagent volumes and portability. In addition to these advantages, many microfluidic analyses have fast analysis times and are relatively inexpensive compared to larger-scale techniques. These features of microfluidic devices match well with the World Health Organization's ASSURED criteria for point-of-care diagnostic devices

[50]. These criteria stipulate that such a device should be affordable, sensitive, specific, user-friendly, rapid and robust, equipment-free, and deliverable to end users. Many microfluidic devices have been developed with the goal of being used in low-resource settings [31, 42, 51-56].

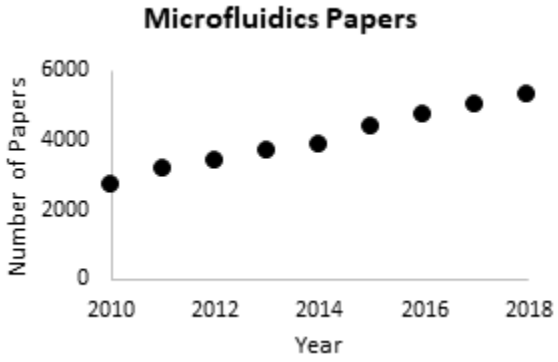



Figure 1.2 Number of microfluidics papers published each year from 2010 to 2018. The number of papers was determined with a Web of Science search for "microfluidic*" in the year published.

### 1.4 Clinical Analysis

Clinical laboratories, those which analyze samples from patients, perform diagnostic tests to aid in the diagnosis, monitoring, or screening of disease [57]. Tests performed by clinical laboratories include antimicrobial susceptibility testing, detection and identification of bacteria, yeast, and viruses, diagnosis of blood-borne parasites, and detection of specific antibodies [58]. Most methods used in clinical laboratories involve complex equipment and controlled conditions to limit false positives or negatives. Of these, antibiotic resistance and susceptibility testing is central to this dissertation.

The era of antimicrobials is often considered to have begun in 1928 with Alexander Fleming's discovery of penicillin [59-61]. This followed Paul Ehrlich's successful search for a treatment of *Treponema pallidium* in 1909 and the first use of an

antibiotic in a hospital setting in 1899, against *Pseudomonas aeruginosa*, developed by Emmerich and Low [59]. In the years following Fleming's discovery and the subsequent purification of penicillin, numerous antibiotics and antibiotic classes were discovered and developed [59]. These therapies could treat all sorts of illnesses that had long been considered fatal. Unfortunately, antimicrobial resistance accompanied these discoveries [59, 60].

Resistance to penicillin was reported as early as the 1940s, in the form of an enzyme now known as penicillinase, a $\beta$-lactamase [60]. As new antibiotics were developed and put into clinical use, resistance appeared soon after their introduction. In some cases, resistance was reported less than a year after antibiotic introduction, or even before the antibiotic was put into use as a therapeutic [59, 60, 62]. In many cases, it was less than 5 years from the time of introduction of the antibiotic to reports of resistance [63]. Antibiotic resistance is associated with at least 700,000 deaths per year worldwide, although this number is assumed to be an underestimate [64]. The Centers for Disease Control and Prevention state that each year in the United States, around 2 million people will be infected with antibiotic resistant organisms, and 23,000 of those will die as a direct result of their infections [65].

Resistance mechanisms fall into four categories: modification of the antibiotic to render it ineffective, modification of the target so that the antibiotic cannot bind or otherwise disrupt cell processes, the addition of an alternative pathway to perform the task the antibiotic disrupts, or the presence of efflux pumps to lower the concentration of an antibiotic in a cell [66]. In each case, the cell acquires or expresses new genetic

material, resulting in a biophysical difference between the resistant and susceptible cells. These biophysical differences between resistant and susceptible bacteria may be minor. The susceptibility of a strain can be determined though standard microbiological techniques. Standard methods used in clinical laboratories to determine the minimum inhibitory concentrations of organisms causing infections include disk diffusion and broth or agar dilution methods [67, 68]. These methods take days [69]. When a treatment decision must be made quickly, this lag in analysis poses a problem. Effective treatment in a reasonable amount of time is crucial to positive patient outcomes, and delays in proper treatment by as little as one hour has been associated with increased mortality rates [70]. The World Health Organization, the Centers for Disease Control and Prevention, and others have all called for development of rapid diagnostics to identify resistant infections and enable proper treatment [64, 71, 72].

### 1.5 Dissertation Overview

This dissertation describes the development and application of gradient insulator-based dielectrophoresis in the study of various analytes, specifically groups of antibiotic resistant and susceptible strains of the same species. Chapter 2 discusses dielectrophoresis theory, an overview of dielectrophoretic applications to this point, and a description of microfluidic device fabrication methods, providing background and placing this work in context.

A mathematical model of dielectrophoretic data is presented in Chapter 3. This model connects biophysical properties of bacteria to the features of dielectrophoretic data, enabling the cellular properties to be more closely connected with features within

the data. Chapter 4 describes the differentiation of methicillin-resistant and -susceptible *Staphylococcus aureus* using dielectrophoresis. Labeled and unlabeled populations of each of these strains were studied, giving further insight into the effects of chemical differences on dielectrophoretic data. KPC-positive and -negative *Klebsiella pneumoniae* are studied in Chapter 5. This chapter also describes the detection of previously unknown differences in bacterial populations. Chapter 6 presents the separation of gentamicin-resistant and -susceptible *Staphylococcus epidermidis*, and discusses the effects a label may have on this separation. Finally, chapter 7 presents conclusions which may be drawn from this work, along with a future outlook.

**1.6 References**


1. B. M. Davis, *Science*, 1897, *6*, 145-157.
2. P. W. Nugent, J. A. Shaw and M. Vollmer, *Applied Optics*, 2015, *54*, B128-B139.
3. G. Smit, B. A. Smit and W. J. M. Engels, *FEMS Microbiology Reviews*, 2005, *29*, 591-610.
4. A. Zourari, J. P. Accolas and M. J. Desmazeaud, *Lait*, 1992, *72*, 1-34.
5. R. C. Burns and R. W. F. Hardy, *Nitrogen fixation in bacteria and higher plants*, Springer-Verlag, Berlin, 1975.
6. L. V. Hooper and J. I. Gordon, *Science*, 2001, *292*, 1115-1118.
7. D. E. Chandler and R. W. Roberson, *Bioimaging: Current Concepts in Light and Electron Microscopy*, Jones and Bartlett Publishers, Sudbury, MA, 2009.
8. Y. Cheng, *Science*, 2018, *361*, 876-880.
9. D. L. Armstrong, C. Erxleben and J. A. White, in *Calcium in Living Cells*, ed. M. Whitaker, Academic Press, Burlington, MA, 2010, vol. 99.
10. B. Sakmann and E. Neher, *Annual Review of Physiology*, 1984, *46*, 455-472.

11. J. W. Dale and M. von Schantz, *From Genes to Genomes: Concepts and Applications of DNA Technology*, John Wiley & Sons, West Sussex, England, 2002.

12. J. A. Cooper, B. R. Mintz, S. L. Palumbo and W.-J. Li, in *Characterization of Biomaterials*, eds. M. Jaffe, W. Hammond, P. Tolias and T. Arinzeh, Woodhead Publishing, Cambridge, 2013, DOI: 10.1533/9780857093684.101, pp. 101-137.

13. R. Spillman, W. Kopaciewicz and A. J. Weiss, in *Encyclopedia of Separation Science*, ed. I. D. Wilson, Academic Press, 2007.

14. J. T. Watson and O. D. Sparkman, *Introduction to Mass Spectrometry: Instrumentation, Applications and Strategies for Data Interpretation*, John Wiley & Sons, Hoboken, NJ, 2007.

15. S. Nerli, A. C. McShan and N. G. Sgourakis, *Progress in Nuclear Magnetic Resonance Spectroscopy*, 2018, *106-107*, 1-25.

16. T. W. Ni, M. A. Tofanelli and C. J. Ackerson, in *Protected Metal Clusters - From Fundamentals to Applications*, eds. T. Tsukuda and H. Hakkinen, 2015, DOI: 10.1016/b978-0-08-100086-1.00005-1, pp. 103-125.

17. M. Kovermann, P. Rogne and M. Wolf-Watz, *Quarterly Reviews of Biophysics*, 2016, *49*.

18. J. C. Giddings, *Dynamics of Chromatography*, M. Dekker, New York, 1965.

19. D. C. Harris, *Quantitative Chemical Analysis*, W. H. Freeman, New York, 7th edn., 2007.

20. J. M. Miller, *Chromatography : Concepts and Contrasts*, Wiley, Hoboken, N.J., 2nd ed.. edn., 2005.

21. T. F. Bidleman, *Journal of Chemical Education*, 1979, *56*, 293.

22. Chemical Rubber Company, *CRC handbook of chemistry and physics*, CRC Press : Taylor & Francis, Boca Raton, Fla., Electronic ed.. edn., 1978.

23. R. Tijssen, in *Handbook of HPLC*, eds. E. Katz, R. Eksteen, P. Schoenmakers and N. Miller, Marcel Dekker, New York, 2011.

24. C. F. Poole, in *Encyclopedia of Separation Science*, ed. I. D. Wilson, Academic Press, 2000.

25. D. N. Taulbee and M. M. Maroto-Valer, in *Encyclopedia of Separation Science*, ed. I. D. Wilson, Academic Press, 2000.

26. N.-T. Nguyen and S. T. Wereley, *Fundamentals and Applications of Microfluidics*, Artech House, Boston, 2nd edn., 2006.

27. D. Perrett, in *Encyclopedia of Separation Science*, ed. I. D. Wilson, Academic Press, 2000.

28. P. Tabeling, *Introduction to Microfluidics*, Oxford University Press, New York, 2005.

29. R. Smith and M. Jobson, in *Encyclopedia of Separation Science*, ed. I. D. Wilson, Academic Press, 2000.

30. D. E. Raynie, in *Encyclopedia of Separation Science*, ed. I. D. Wilson, Academic Press, 2000.

31. C. D. Chin, V. Linder and S. K. Sia, *Lab on a Chip*, 2012, *12*, 2118-2134.

32. C. J. Easley, J. M. Karlinsey, J. M. Bienvenue, L. A. Legendre, M. G. Roper, S. H. Feldman, M. A. Hughes, E. L. Hewlett, T. J. Merkl, J. P. Ferrance and J. P. Landers, *PNAS*, 2006, *103*, 19272-19277.

33. F. Lan, B. Demaree, N. Ahmed and A. R. Abate, *Nature Biotechnology*, 2017, *35*, 640-646.

34. L. R. Volpatti and A. K. Yetisen, *Trends in Biotechnology*, 2014, *32*, 347-350.

35. L. Y. Yeo, H.-C. Chang, P. P. Y. Chan and J. R. Friend, *Small*, 2011, *7*, 12-48.

36. A. K. Yetisen, M. S. Akram and C. R. Lowe, *Lab on a Chip*, 2013, *13*, 2210-2251.

37. S. B. Cheng, C. D. Skinner, J. Taylor, S. Attiya, W. E. Lee, G. Picelli and D. J. Harrison, *Analytical Chemistry*, 2001, *73*, 1472-1479.

38. E. Eteshola and B. Michal, *Biomedical Microdevices*, 2004, *6*, 7-9.

39. A. Fernández-la-Villa, V. Bertrand-Serrador, D. F. Pozo-Ayuso and M. Castaño-Álvarez, *Analytical Methods*, 2013, *5*, 1494-1501.

40. D. Hoegger, P. Morier, C. Vollet, D. Heini, F. Reymond and J. S. Rossier, *Analytical and Bioanalytical Chemistry*, 2007, *387*, 267-275.

41. J. S. Mellors, V. Gorbounov, R. S. Ramsey and J. M. Ramsey, *Analytical Chemistry*, 2008, *80*, 6881-6887.

42. S. Park, Y. Zhang, S. Lin, T.-H. Wang and S. Yang, *Biotechnology Advances*, 2011, *29*, 830-839.

43. E. A. Redman, J. S. Mellors, J. A. Starkey and J. M. Ramsey, *Analytical Chemistry*, 2016, *88*, 2220-2226.

44. T. Wang, M. Zhang, D. D. Dreher and Y. Zeng, *Lab on a Chip*, 2013, *13*, 4190-4197.

45. E. B. Cummings and A. K. Singh, *Analytical Chemistry*, 2003, *75*, 4724-4731.

46. D. R. Gossett, W. M. Weaver, A. J. Mach, S. C. Hur, H. T. K. Tse, W. Lee, H. Amini and D. Di Carlo, *Analytical and Bioanalytical Chemistry*, 2010, *397*, 3249-3267.

47. P. V. Jones, S. J. R. Staton and M. A. Hayes, *Analytical and Bioanalytical Chemistry*, 2011, *401*, 2103-2111.

48. S. J. R. Staton, K. P. Chen, T. J. Taylor, J. R. Pacheco and M. A. Hayes, *Electrophoresis*, 2010, *31*, 3634-3641.

49. Y. Zheng, J. Nguyen, Y. Wei and Y. Sun, *Lab on a Chip*, 2013, *13*, 2464-2483.

50. H. Kettler, K. White and S. Hawkes, *Mapping the landscape of diagnostics for sexually transmitted infections*, World Health Organization, 2004.

51. A. E. Herr, A. V. Hatch, D. J. Throckmorton, H. M. Tran, J. S. Brennan, W. V. Giannobile and A. K. Singh, *PNAS*, 2007, *104*, 5268-5273.

52. X. Mao and T. J. Huang, *Lab on a Chip*, 2012, *12*, 1412-1416.

53. N. M. Myers, E. N. Kernisan and M. Lieberman, *Analytical Chemistry*, 2015, *87*, 3764-3770.

54. V. Srinivasan, V. K. Pamula and R. B. Fair, *Lab on a Chip*, 2004, *4*, 310-315.

55. W. Su, X. Gao, L. Jiang and J. Qin, *Journal of Chromatography A*, 2015, *1377*, 13-26.

56. A. A. Weaver, H. Reiser, T. Barstis, M. Benvenuti, D. Ghosh, M. Hunckler, B. Joy, L. Koenig, K. Raddell and M. Lieberman, *Analytical Chemistry*, 2013, *85*, 6453-6460.

57. C. Kaplan, in *Clinical Methods: The History, Physical, and Laboratory Examinations*, eds. H. K. Walker, W. D. Hall and J. W. Hurst, Butterworths, Boston, 3rd edn., 1990.

58. Clinical and Laboratory Standards Institute, Microbiology: Standards, https://clsi.org/standards/products/microbiology/documents/, (accessed February 22, 2019).

59. R. I. Aminov, *Frontiers in Microbiology*, 2010, *1*, 134.

60. J. Davies and D. Davies, *Microbiology and Molecular Biology Reviews*, 2010, *74*, 417-433.

61. A. Fleming, *British Journal of Experimental Pathology*, 1929, *10*, 226-236.

62. E. P. Abraham and E. Chain, *Reviews of Infectious Diseases*, 1988, *10*, 677-678.

63. K. Bush, *Clinical Microbiology and Infection*, 2004, *10 Suppl 4*, 10-17.

64. J. O'Neill, *Tackling Drug-Resistant Infections Globally: Final Report and Recommendations*, 2016.

65. Centers for Disease Control and Prevention, *Antibiotic Resistance Threats in the United States, 2013*, 2013.

66. F. C. Tenover, *American Journal of Infection Control*, 2006, *34*, S3-S10.

67. J. H. Jorgensen and J. D. Turnidge, in *Manual of Clinical Microbiology*, eds. J. H. Jorgensen and M. A. Pfaller, ASM Press, Washington, DC, 11th edn., 2015.

68. F. P. Maurer, M. Christner, M. Hentschke and H. Rohde, *Infectious Disease Reports*, 2017, *9*, 18-27.

69. J. D. Turnidge, in *Manual of Clinical Microbiology*, eds. J. H. Jorgensen and M. A. Pfaller, ASM Press, Washington, DC, 11th edn., 2015.

70. A. Kumar, D. Roberts, K. E. Wood, B. Light, J. E. Parrillo, S. Sharma, R. Suppes, D. Feinstein, S. Zanotti, L. Taiberg, D. Gurka, A. Kumar and M. Cheang, *Critical Care Medicine*, 2006, *34*, 1589-1596.

71. Centers for Disease Control and Prevention, Antibiotic/Antimicrobial Resistance: Combat Antimicrobial Resistance Globally, https://www.cdc.gov/drugresistance/intl-actvities.html, (accessed 25 February, 2019).

72. World Health Organization, Antimicrobial resistance, https://www.who.int/en/news-room/fact-sheets/detail/antimicrobial-resistance, (accessed February 13, 2019).

# CHAPTER 2

# OVERVIEW AND THEORY OF DIELECTROPHORESIS

## 2.1 Dielectrophoresis Theory

A particle in a microchannel experiences a number of forces, including electroosmosis, electrophoresis, dielectrophoresis, and hydrodynamics. These forces govern the motion of the particle and are affected by the size and geometry of the microchannel as well as the magnitude and shape of an applied electric field. Electroosmosis, electrophoresis, and dielectrophoresis all arise from various properties of the particle, the microchannel, the solution, and the interactions between them. To understand the behavior of a particle in a microchannel, it is necessary to first understand the forces behind its motion.

### 2.1.1 Electroosmosis

Electroosmosis describes the motion of a fluid in a microchannel. This motion arises due to the electrical double layer which is formed by the immobilized charge on the walls of the microchannel interacting with the electrolyte solution. This double layer is composed of two distinct regions, the Stern layer nearest the wall and the diffuse layer towards the bulk fluid (Figure 2.1). The Stern layer is thin and composed of charges opposite that of the wall that are stationary. The diffuse layer is thicker than the Stern layer and is able to move when a lateral electric field is applied. The plane between the Stern and diffuse layers is called the shear surface. The zeta potential of the wall is the potential at this surface [1].

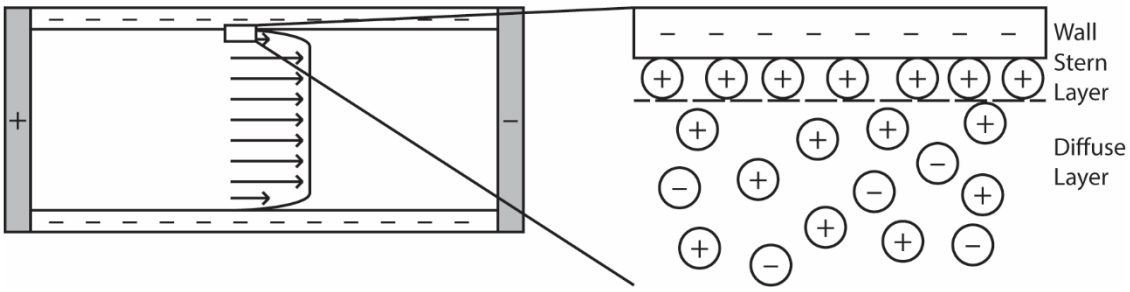



Figure 2.1 Electroosmosis is the flow of a fluid in a microchannel in response to an applied electric field. The flow profile from electroosmosis is shown (left). The Stern layer, nearest the wall, is composed of ions oppositely-charged than the wall. The diffuse layer is further away from the wall (right). This depiction is not to scale, as a typical electric double layer thickness is approximately 10 nm and characteristic channel dimensions are in the tens of microns.

When an electric field is applied, the diffuse layer moves in response to the Coulomb forces, and the bulk fluid moves with this layer through viscous effects. From the Stokes approximation, this movement is given by the equation

$$0 = -\nabla p + \eta \Delta \boldsymbol{v} + \rho_e \boldsymbol{E} \tag{1}$$

or

$$0 = -\nabla p + \eta \nabla^2 \boldsymbol{v} + \rho_e \boldsymbol{E} \tag{2}$$

where $p$ is the pressure, $\boldsymbol{v}$ is the velocity of the fluid, $\eta$ is the viscosity of the fluid, $\rho_e$ is the electrical density of the ionic charges, and $\boldsymbol{E}$ is the electric field [1, 2]. This can also be written in terms of the electric potential, according to Poisson, as

$$0 = -\nabla p + \eta \nabla^2 \boldsymbol{v} - \varepsilon \nabla^2 \boldsymbol{\psi} \tag{3}$$

where $\varepsilon$ is the permittivity and $\boldsymbol{\psi}$ is the potential [1]. Considering the flow to be between two planes along direction $x$, with the $y$-coordinate normal to the wall, this becomes

$$0 = -\frac{\delta p}{\delta x} + \eta \frac{\delta^2 u}{\delta y^2} - \varepsilon E_x \frac{\delta^2 \psi}{\delta y^2} \tag{4}$$

where $u$ is the speed. With the pressure gradient at zero ($\delta p = 0$), rearranging this equation gives

$$\eta \frac{\delta^2 u}{\delta y^2} = E_x \frac{\delta^2 \psi}{\delta y^2} \tag{5}$$

After integrating, this becomes

$$\boldsymbol{v} = \frac{\varepsilon E_x}{\eta} (\psi - \zeta_m) \tag{6}$$

with $\zeta$ as the zeta potential of the wall [2]. Since $\psi$ is zero in the Debye-Huckel layer, the velocity is

$$\boldsymbol{v} = -\frac{\varepsilon E_x \zeta_m}{\eta} \tag{7}$$

which is known as the Helmholtz-Smoluchowski velocity [1, 2]. From this, we define the electroosmotic mobility to be

$$\mu_{EOF} = -\frac{\varepsilon \zeta_m}{\eta} \tag{8}$$

such that

$$\boldsymbol{v} = \mu_{EOF} \boldsymbol{E}_x \tag{9}$$

describes the electroosmotic velocity.

### 2.1.2 Electrophoresis

A charged particle will move in an electric field toward its opposite charge (Figure 2.2). This motion is called electrophoresis. Large and small particles move differently in an electric field and how they are considered mathematically is dependent on the Debye-Huckel length. This length is given by

$$\lambda_B = \sqrt{\frac{D\varepsilon}{\sigma}} \tag{10}$$

where $\lambda_B$ is the double layer size, $D$ is the molecular diffusion coefficient, and $\sigma$ is the conductivity. This size determines whether a particle is considered large or small, and which equations govern its motion. Generally, for the case of a particle in an electrolyte solution, this is about ten nanometers [2]. A particle is considered "small" when it is small compared to the Debye-Huckel length, and "large" when the Debye-Huckel length is much smaller than the particle, generally for particles greater than 100 nm in diameter [1]. In the case of small particles with a low Reynolds number, the velocity of the particle can be found by balancing the drag force with the electrical force. This gives

$$6\pi\eta \boldsymbol{v}_{EP} r = q\boldsymbol{E} \tag{11}$$

where $r$ is the radius of the particle, $\boldsymbol{v}_{EP}$ is the velocity of the particle relative to the fluid, and $q$ is the charge. Rearranging gives

$$\boldsymbol{v}_{EP} = \frac{q}{6\pi\eta r}\boldsymbol{E} \tag{12}$$

Small particles include ions, small molecules, short DNA strands, and small ionized proteins.

Many biological analytes, such as bacteria and other cells, are considered to be large particles relative to their Debye-Huckel length. In the case of a large particle, the double layer acts similarly as to in electroosmosis, and the same logic as in developing the electroosmotic velocity can be followed. The velocity of the particle again is the Helmholtz-Smoluchowski velocity,

$$\boldsymbol{v} = \frac{\varepsilon \zeta_p}{\eta} \boldsymbol{E} = \mu_{EP} \boldsymbol{E} \tag{13}$$

where $\zeta_p$ is the zeta potential of the particle rather than the wall [1, 2]. The electrophoretic mobility, $\mu_{EP}$, can then be defined as

$$\mu_{EP} = \frac{\varepsilon \zeta_p}{\eta} \tag{14}$$

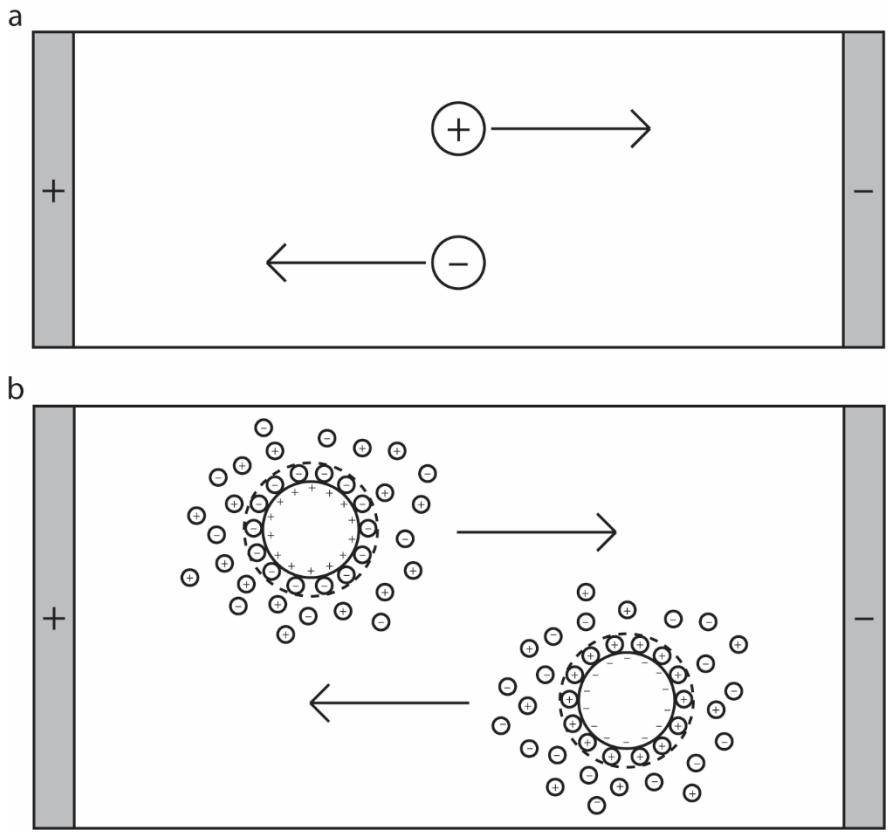



Figure 2.2 Electrophoresis of small (a) and large (b) particles. Particles are considered small when they are small compared to the Debye-Huckel length (equation 10), which generally encompasses particles less than 100 nm in diameter. Otherwise, particles are considered large. This illustration is not to scale, as microchannels typically have features (length, width) of tens to hundreds of microns.

### 2.1.3 Electrokinetic Mobility

Electroosmosis and electrophoresis are proportional to the magnitude of the applied electric field. As such, they are considered here together, and termed the

electrokinetic force [3, 4]. The electrokinetic velocity is the sum of the electroosmotic and the electrophoretic velocities, according to the equation

$$\boldsymbol{v}_{EK} = \boldsymbol{v}_{EOF} + \boldsymbol{v}_{EP} = (\mu_{EOF} + \mu_{EP})\boldsymbol{E} \tag{15}$$

The electroosmotic and electrophoretic mobilities can be combined to become the electrokinetic mobility, $\mu_{EK}$. This mobility is given as

$$\mu_{EK} = (\mu_{EOF} + \mu_{EP}) = \frac{-\varepsilon(\zeta_m - \zeta_p)}{\eta} \tag{16}$$

where $\zeta_m$ is the zeta potential of the medium (typically also the wall zeta potential). The electrokinetic velocity can then be written as

$$\boldsymbol{v}_{EK} = \mu_{EK}\boldsymbol{E} \tag{17}$$

Thus, the electrokinetic velocity is related to the properties of both the particle and the solution.

### 2.1.4 Dielectrophoresis

The movement of a polarizable particle when in an electric field gradient is called dielectrophoresis (DEP). This motion doesn't require a charged particle, but rather arises from the distribution of dipoles in a particle [5]. These dipoles are normally randomly distributed but will align when an electric field is applied. In the case where this field is not uniform, this will allow for a force that is oriented either towards regions of high field (positive dielectrophoresis, pDEP) or away from regions of high field (negative dielectrophoresis, nDEP) (Figure 2.3). This force is given by the equation

$$\boldsymbol{F} = 2\pi r^3 \varepsilon f_{CM} \nabla |E|^2 \tag{18}$$

where $f_{CM}$ is the Clausius-Mossotti factor [6]. For a spherical particle, this factor is given by

$$f_{CM} = \frac{\varepsilon^*{}_p - \varepsilon^*{}_m}{\varepsilon^*{}_p + 2\varepsilon^*{}_m} \tag{19}$$

where $\varepsilon^*{}_p$ and $\varepsilon^*{}_m$ are the complex permittivities of the particle and medium, respectively. The complex permittivity is defined as

$$\varepsilon^* = \varepsilon - \frac{j\sigma}{\omega} \tag{20}$$

where $\sigma$ is the conductivity, $\omega$ is the angular frequency of the applied potential, and $j = \sqrt{-1}$. As the frequency varies, so will the relative impact of the conductivity and the permittivity on the complex permittivity. For DC fields, the Clausius-Mossotti factor simplifies to [3]

$$f_{CM} = \frac{\sigma_p - \sigma_m}{\sigma_p + 2\sigma_m} \tag{21}$$

This factor is affected by similar properties of the system for other shaped particles. Nakano et al. gave the Clausius-Mossotti factor for an ellipsoidal particle in DC fields as

$$f_{CM,ellipse} = \frac{\sigma_p - \sigma_m}{Z\sigma_p + (1 - Z)\sigma_m} \tag{22}$$

where $Z$ is the depolarization factor [7]. When the Clausius-Mossotti factor is positive, the particle will experience positive dielectrophoresis (pDEP). When $f_{CM}$ is negative, the particle will experience negative dielectrophoresis (nDEP). In DC fields, pDEP will occur when the conductivity of the particle is greater than that of the medium, and nDEP will occur in the opposite case.

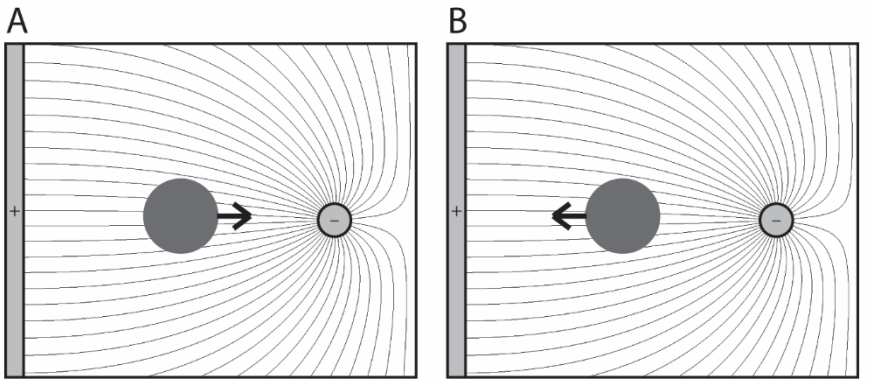



Figure 2.3 Positive dielectrophoresis (A) occurs when the particle conductivity is greater than that of the medium. In this case, the force is oriented such that particles are attracted to regions of high field gradient. Negative dielectrophoresis (B) occurs in the opposite case, and particles are repelled from regions of high field gradient.

The dielectrophoretic velocity can be found by balancing the DEP force with the drag force [2],

$$\boldsymbol{F}_{drag} = 6\pi r\eta \boldsymbol{v}_{\boldsymbol{DEP}} \tag{23}$$

such that

$$2\pi r^3 \varepsilon f_{CM} \nabla |E|^2 = 6\pi r\eta \boldsymbol{v}_{\boldsymbol{DEP}} \tag{24}$$

Rearranging gives the dielectrophoretic velocity to be

$$\boldsymbol{v}_{\boldsymbol{DEP}} = \frac{\varepsilon r^2 f_{CM}}{3\eta} \nabla |\boldsymbol{E}|^2 \tag{25}$$

The dielectrophoretic mobility, $\mu_{DEP}$, is then defined as

$$\mu_{DEP} = \frac{\varepsilon r^2 f_{CM}}{3\eta} \tag{26}$$

and the dielectrophoretic velocity is

$$\boldsymbol{v}_{DEP} = \mu_{DEP} \nabla |\boldsymbol{E}|^2 \tag{27}$$

### 2.1.5 Capture in Dielectrophoresis

When the flux of particles past a point in a microchannel is zero due to the particles stopping at that location, it is termed capture or trapping. Capture allows for the concentration and separation of various particles away from differing particles. Capture occurs when

$$(\boldsymbol{v}_{EK} + \boldsymbol{v}_{DEP}) \cdot \boldsymbol{E} > 0 \tag{28}$$

Substituting equations 17 and 27 for the electrokinetic and dielectrophoretic velocities, respectively, gives

$$(\mu_{EK}\boldsymbol{E} + \mu_{DEP}\nabla|\boldsymbol{E}|^2) \cdot \boldsymbol{E} > 0 \tag{29}$$

Rearranging this equation gives the condition that must be satisfied in order for capture to occur,

$$\frac{\mu_{EK}}{\mu_{DEP}} \leq \frac{\nabla|E|^2}{E} \tag{30}$$

This shows that differences in either the electrokinetic or dielectrophoretic mobility will cause differences in the capture conditions of the particles (Figure 2.4) [3, 8].

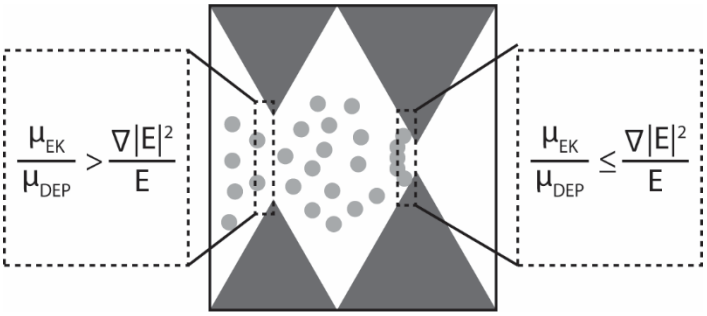



Figure 2.4 Capture in dielectrophoresis. The conditions for capture are depicted (right). When these conditions are not met, capture will not occur (left). The ratio of $\frac{\nabla|E|^2}{E}$ can be increased either by increasing the applied potential or by increasing the gradient, as occurs with a smaller constriction.

## 2.2 Microfluidic Device Fabrication

The methods for fabrication of microfluidic devices are varied, depending on the quantity to be produced, required geometric features and resolution, and desired qualities in the completed device. Commonly, photolithography methods are used for the fabrication of a microfluidic device. These techniques require the use of a cleanroom to keep dust and other contaminants away from the area during fabrication. Other fabrication methods do exist and have successfully been employed to create microfluidic devices. Three-dimensional printing is one such method, and numerous examples can be found [9-13]. Another involves the use of laser cutters to form the channel [14]. Hot embossing has also been used to fabricate microchannels [15]. Inexpensive, rapid fabrication methods that have been developed include using desktop craft cutters or laser cutters to cut readily-available materials, such as overhead transparencies [16, 17]. These methods all have various advantages as well as drawbacks, which may include ease of fabrication, cost, reproducibility, resolution, and access to specialized equipment.

Some devices, such as those made entirely of glass, are made almost completely in the cleanroom with photolithography techniques. The methods used to form the microchannel include various etching and deposition of material techniques [1]. These are often time-consuming and expensive, which can be prohibitive for some applications.

Labs that work on proof-of-concept or that aim to test numerous devices, however, often make casts of a silicon wafer master using poly(dimethyl) siloxane (PDMS) or poly(methyl methacrylate) (PMMA). Such polymers are chosen for their low cost, ease of use for small numbers of a single channel design, and availability [1, 18].

This method of making a master wafer still requires the use of photolithography and a cleanroom, but one master wafer can be used in the fabrication of hundreds of individual devices from the polymer for testing in the laboratory.

One of the more complicated steps of this process is the fabrication of the silicon wafer master. In general, the master is made by coating a silicon wafer with photoresist. A mask is used to allow UV exposure only in the channel area when negative photoresist is used, or everywhere but the channel pattern when positive photoresist is used. This mask is either brought into contact with the coated wafer (contact printing), brought close to the wafer (proximity printing), or kept farther away from the wafer (projection printing). Each of these methods give a different resolution of the channel pattern irradiated, although the resolution for each is based on the wavelength of the light used. The depth of focus, or the depth irradiated at the optimal resolution, varies for each method as well [1]. The wafer is then developed, which washes the photoresist off the wafer in all areas except in the pattern of the channel. This can either be used as the master as-is, or an etching step can be used. This allows for a deeper channel to be made. Either way, the end result is a wafer with a raised area in the pattern of the channel (Figure 2.5).

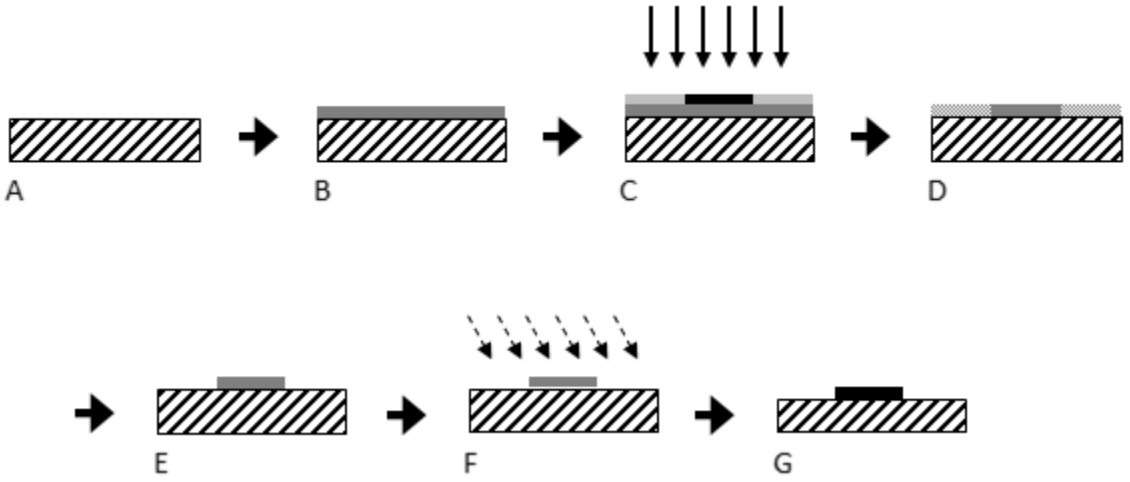



Figure 2.5 This outlines the basic steps of creating an etched wafer via soft lithography techniques. A silicon wafer (A) is coated with photoresist (B), then exposed to UV light through a chrome mask (C). The situation depicted shows positive photoresist being used, which means that the area to be removed is irradiated while the channel pattern is blocked from the light by the chrome. The exposed photoresist is then removed (E). The wafer is etched (F), resulting in a wafer with a raised area in the pattern of the channel (G).

This master wafer is then used to create casts, often in PDMS. In this process, PDMS is poured over the wafer and allowed to cure. The resulting PDMS cast can be bonded to a glass slide to create a completed device with three walls of PDMS and one wall of glass (Figure 2.6) [18]. The bonding process most often relies on exposure to oxygen plasma. PDMS is composed of repeating silicon and oxygen atoms, with two methyl groups bonded to each silicon. The plasma treatment removes the methyl groups and forms silanol groups in their place [19, 20]. This treatment allows for a bond between the glass and PDMS, as well as decreasing the hydrophobicity of the PDMS surface [19, 21].

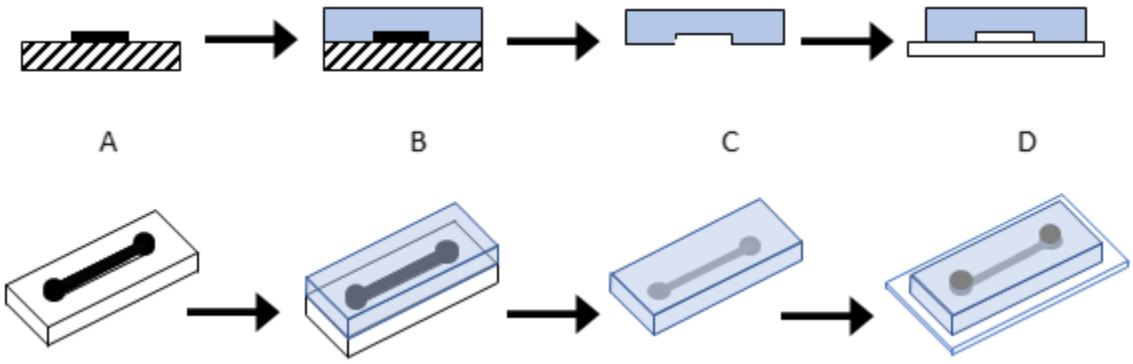



Figure 2.6 The process of making a PDMS cast from a silicon master wafer, shown from a side view (top) and a corner view (bottom). The master wafer has a raised area in the shape of the microchannel (A). PDMS is then poured over the wafer and cured (B). The resulting PDMS cast is peeled from the wafer, leaving an indented area in the channel pattern in the PDMS (C). Access holes are punched into the PDMS, and the PDMS is then bonded to a glass slide (D), resulting in a completed channel with three walls of PDMS and one wall of glass.

Of course, this process could be modified to add numerous features into a microchannel including pumps, valves, and three-dimensional components. While posts can be made as part of the channel geometry with the process described above, nanoposts are smaller than can be made with traditional photolithography techniques and have been created using focused ion beam milling [22]. Valves have been used to direct the flow of the particles and buffers. This allows for the introduction of specific sample and buffer combinations, or the locating of a separated or concentrated sample to a separate reservoir for follow-up analysis [23-26]. External pumps or control of valves can give an added flow [23, 26-28]. Three-dimensional components can add other separation and analysis factors to the device [29-31].

**2.3 Applications of Dielectrophoresis**

The electric fields and field gradients required for DEP were originally created using patterned electrodes [5, 6, 32, 33]. This electrode-based dielectrophoresis (eDEP)

uses AC fields. Many applications using eDEP rely on differences in the behavior of analytes with varying frequencies of the AC field [34-39]. This eliminates the presence of electrokinetics, and the motion of particles is instead based on whether a particle displays positive or negative DEP in a given system, as well as any other forces that may be included, such as hydrodynamic flow. While eDEP has advantages including the application of relatively low potentials to generate high electric field strengths, it also can have problems with electrode fouling and Joule heating.

In 2002, Chou et al. introduced electrodeless DEP [40]. This was followed in 2003 by Cummings and Singh reporting a method of DEP using patterned insulators, rather than electrodes, to create the field gradients [41]. This became known as insulator-based dielectrophoresis (iDEP). Electrodes are placed at the ends of a microchannel, rather than at the site of analysis, and insulating material is patterned to create constrictions which result in electric field gradients. Either AC or DC fields can be used with iDEP, as can an AC field with a DC offset. When DC fields or a DC offset are used, electroosmosis and electrophoresis can be used for transport of particles in the microchannel, and capture is governed by the requirements described above.

Dielectrophoresis has been used for the analysis of numerous analytes, using both eDEP and iDEP. Particles ranging in size from nanometer-scale proteins, viruses, and DNA to micron-sized bacteria, stem cells, and blood cells have been studied [36-38, 40, 42-55]. While only a small number of notable applications will be summarized here, many further applications have appeared in the literature.

The dielectrophoresis of proteins was demonstrated as early as 1994 by Washizu et al. [55]. While larger molecules, including longer strands of DNA, had been investigated before this time [56], this work demonstrated the DEP of molecules in the kDa range. This work also showed the collection of particles from a solution as it is passed through a microchannel, resulting in a separation of the trapped particles from the rest of the solution.

The use of viruses is another case of sub-micron sized particles being studied with DEP. Morgan and Green showed the manipulation of a rod-shaped virus using eDEP [50]. They were able to assign a conductivity and permittivity to the particle from their data. More recently, Ding et al. captured a spherical virus with iDEP, using a microchannel with constrictions designed to provide the high electric field gradients necessary for smaller particles [45].

Separations of particles of varying sizes have been shown. Ding et al. have shown the capture of red blood cells from a mixture of the blood cells and protein biomarkers using iDEP [57]. They first demonstrated the idea using polystyrene spheres as a model system for red blood cells, and then were able to repeat the experiment with the cells. At low applied potentials, neither the red blood cells nor the protein biomarkers are captured. As higher potentials were applied, however, the red blood cells were seen to capture and be concentrated in a patterned region of the microchannel, while the proteins continued to pass through the channel.

Larger particles have also been studied extensively with DEP. The separation of tumor cells from blood cells was shown by Gascoyne et al. [58]. This was accomplished

by using DEP to perform field flow fractionation, which separated particles along the height of a microchannel as they were flowed down the length. The tumor cells were attracted to electrodes on the bottom of the channel, and blood cells were repelled. The fluid flow profile influenced the velocity of the particles, with the particles in the middle of the channel moving more quickly than those near the edges of the channel. This separated the particles in time as well as in space; the blood cells eluted from the channel before the tumor cells. Becker et al. had previously used similar properties to separate cancer cells from blood using eDEP; a frequency was chosen to allow the tumor cells to capture while the blood cells did not, and could be washed from the channel [44].

Other low-abundance cells have also been separated and concentrated out of a mixture. LaLonde et al. have shown a separation and concentration of larger polystyrene particles from a mixture containing a relatively high concentration of smaller polystyrene particles, up to 1 part in 1 million [59]. Yeast cells were also captured from a solution with a much larger concentration of polystyrene particles.

Many applications involving bacteria have appeared in the literature. Lapizco-Encinas et al. used iDEP to separate live and dead *E. coli* cells [49]. When applying lower potentials across the microchannel, only the live cells captured while the dead bacteria continued to pass through the channel. Upon application of a higher potential, separate bands of the live and dead bacteria appeared due to the differences in the conditions required for capture. These differences were attributed to the difference in conductivity between live and dead bacterial cells. Later, different serotypes of live *E. coli* were differentiated through DEP [47]. The strains distinguished included both

pathogenic and non-pathogenic *E. coli*, and each required different conditions (field strengths and electric field gradients) for capture to occur.

These varied studies of DEP show its wide applicability to diverse analytes and to the study of several properties, including size, shape, surface charge, deformability, and conductivity. Small biophysical differences in the analytes are detectable by DEP, which could find use in studying minute variations in populations, or even in identifying changes in a population without prior knowledge of the alteration.

## 2.4 References


1. N.-T. Nguyen and S. T. Wereley, *Fundamentals and Applications of Microfluidics*, Artech House, Boston, 2nd edn., 2006.
2. P. Tabeling, *Introduction to Microfluidics*, Oxford University Press, New York, 2005.
3. A. Lalonde, A. Gencoglu, M. F. Romero-Creel, K. S. Koppula and B. H. Lapizco-Encinas, *Journal of Chromatography A*, 2014, *1344*, 99-108.
4. H. Moncada-Hernandez, J. L. Baylon-Cardiel, V. H. Perez-Gonzalez and B. H. Lapizco-Encinas, *Electrophoresis*, 2011, *32*, 2502-2511.
5. H. A. Pohl, *Journal of Applied Physics*, 1951, *22*, 869-871.
6. H. A. Pohl, *Dielectrophoresis The behavior of neutral matter in nonuniform electric fields*, Cambridge University Press, New York, 1978.
7. A. Nakano, F. Camacho-Alanis and A. Ros, *Analyst*, 2015, *140*, 860-868.
8. C. V. Crowther and M. A. Hayes, *Analyst*, 2017, *142*, 1608-1618.
9. M. J. Beauchamp, H. Gong, A. T. Woolley and G. P. Nordin, *Micromachines*, 2018, *9*.
10. A. Enders, I. G. Siller, K. Urmann, M. R. Hoffmann and J. Bahnemann, *Small*, 2019, *15*, 1804326.
11. H. Gong, A. T. Woolley and G. P. Nordin, *Lab on a Chip*, 2016, *16*, 2450-2458.
12. A. Lambert, S. Valiulis and Q. Cheng, *ACS Sensors*, 2018, *3*, 2475-2491.

13. M. F. Santangelo, S. Libertino, A. P. F. Turner, D. Filippini and W. C. Mak, *Biosensors and Bioelectronics*, 2018, *99*, 464-470.

14. Y. Huang, S. Liu, W. Yang and C. Yu, *Applied Surface Science*, 2010, *256*, 1675-1678.

15. B. G. Hawkins, A. E. Smith, Y. A. Syed and B. J. Kirby, *Analytical Chemistry*, 2007, *79*, 7291-7300.

16. B. L. Thompson, Y. Ouyang, G. R. Duarte, E. Carrilho, S. T. Krauss and J. P. Landers, *Nature Protocols*, 2015, *10*, 875-886.

17. P. K. Yuen and V. N. Goral, *Lab on a Chip*, 2010, *10*, 384-387.

18. H. Becker and C. Gartner, *Electrophoresis*, 2000, *21*, 12-26.

19. S. Bhattacharya, A. Datta, J. M. Berg and S. Gangopadhyay, *Journal of Microelectromechanical Systems*, 2005, *14*, 590-597.

20. H.-J. Hettlich, F. Otterbach, C. Mittermayer, R. Kaufmann and D. Klee, *Biomaterials*, 1991, *12*, 521-524.

21. H. Hillborg and U. W. Gedde, *Polymer*, 1998, *39*, 1991-1998.

22. F. Camacho-Alanis, L. Gan and A. Ros, *Sensors and Actuators B: Chemical*, 2012, *173*, 668-675.

23. J. Melin and S. R. Quake, *Annual Review of Biophysics and Biomolecular Structure*, 2007, *36*, 213-231.

24. A. Mohammadzadeh, A. E. Fox-Robichaud and P. R. Selvaganapathy, *Journal of Micromechanics and Microengineering*, 2019, *29*, 015013.

25. H. S. Rho, Y. Yang, A. T. Hanke, M. Ottens, L. W. M. M. Terstappen and H. Gardeniers, *Lab on a Chip*, 2016, *16*, 305-311.

26. M. A. Unger, H.-P. Chou, T. Thorsen, A. Scherer and S. R. Quake, *Science*, 2000, *228*, 113-116.

27. C. J. Lee, H. J. Sheen, H. C. Chu, C. J. Hsu and T. H. Wu, *Journal of Micromechanics and Microengineering*, 2007, *17*, 439-446.

28. Y. Temiz, J. Skorucak and E. Delamarche, *Journal of Micro/Nanolithography, MEMS, and MOEMS*, 2014, *13*, 033018.

29. C.-S. Chen, D. N. Breslauer, J. I. Luna, A. Grimes, W.-c. Chin, L. P. Lee and M. Khine, *Lab on a Chip*, 2008, *8*, 622-624.

30. B.-H. Jo, L. M. Van Lerberghe, K. M. Motsegood and D. J. Beebe, *Journal of Microelectromechanical Systems*, 2000, *9*, 76-81.

31. A. R. Schor and C. R. Buie, *Journal of Micromechanics and Microengineering*, 2016, *26*, 105010.

32. T. B. Jones, *Electromechanics of Particles*, Cambridge University Press, New York, 1995.

33. R. Pethig, *Dielectrophoresis : theory, methodology and biological applications*, Hoboken, NJ : John Wiley & Sons, Ltd, 1st edn., 2017.

34. M. Castellarnau, A. Errachid, C. Madrid, A. Juarez and J. Samitier, *Biophysical Journal*, 2006, *91*, 3937-3945.

35. J. S. Crane and H. A. Pohl, *Journal of The Electrochemical Society*, 1968, *115*, 584-586.

36. F. H. Labeed, J. Lu, H. J. Mulhall, S. A. Marchenko, K. F. Hoettges, L. C. Estrada, A. P. Lee, M. P. Hughes and L. A. Flanagan, *PLoS One*, 2011, *6*, e25458.

37. G. H. Markx, Y. Huang, X.-F. Zhou and R. Pethig, *Microbiology*, 1994, *140*, 585-591.

38. S. K. Srivastava, P. R. Daggolu, S. C. Burgess and A. R. Minerick, *Electrophoresis*, 2008, *29*, 5033-5046.

39. X.-B. Wang, Y. Huang, J. P. H. Burt, G. H. Markx and R. Pethig, *Journal of Physics D: Applied Physics*, 1993, *26*, 1276-1285.

40. C.-F. Chou, J. O. Tegenfeldt, O. Bakajin, S. S. Chan, E. C. Cox, N. Darnton, T. Duke and R. H. Austin, *Biophysical Journal*, 2002, *83*, 2170-2179.

41. E. B. Cummings and A. K. Singh, *Analytical Chemistry*, 2003, *75*, 4724-4731.

42. T. N. G. Adams, A. Y. L. Jiang, P. D. Vyas and L. A. Flanagan, *Methods*, 2018, *133*, 91-103.

43. C. Asbury, L., A. H. Dierks and G. van den Engh, *Electrophoresis*, 2002, *23*, 2658-2666.

44. F. F. Becker, X.-B. Wang, Y. Huang, R. Pethig, J. Vykoukal and P. R. C. Gascoyne, *Proceedings of the National Academy of Sciences of the United States of America*, 1995, *92*, 860-864.

45. J. Ding, R. M. Lawrence, P. V. Jones, B. G. Hogue and M. A. Hayes, *Analyst*, 2016, *141*, 1997-2008.

46. M. P. Hughes, H. Morgan, F. J. Rixon, J. P. H. Burt and R. Pethig, *Biochimica et Biophysica Acta*, 1998, *1425*, 119-126.

47. P. V. Jones, A. F. DeMichele, L. Kemp and M. A. Hayes, *Analytical and Bioanalytical Chemistry*, 2014, *406*, 183-192.

48. B. H. Lapizco-Encinas, S. Ozuna-Chacon and M. Rito-Palomares, *Journal of Chromatography A*, 2008, *1206*, 45-51.

49. B. H. Lapizco-Encinas, B. A. Simmons, E. B. Cummings and Y. Fintschenko, *Analytical Chemistry*, 2004, *76*, 1571-1579.

50. H. Morgan and N. G. Green, *Journal of Electrostatics*, 1997, *42*, 279-293.

51. S. Otto, U. Kaletta, F. F. Bier, C. Wenger and R. Holzel, *Lab on a Chip*, 2014, *14*, 998-1004.

52. J. Regtmeier, T. T. Duong, R. Eichhorn, D. Anselmetti and A. Ros, *Analytical Chemistry*, 2007, *79*, 3925-3932.

53. H. Song, J. M. Rosano, Y. Wang, C. J. Garson, B. Prabhakarpandian, K. Pant, G. J. Klarmann, A. Perantoni, L. M. Alvarez and E. Lai, *Lab on a Chip*, 2015, *15*, 1320-1328.

54. S. J. R. Staton, P. V. Jones, G. Ku, S. D. Gilman, I. Kheterpal and M. A. Hayes, *Analyst*, 2012, *137*, 3227-3229.

55. M. Washizu, S. Suzuki, O. Kurosawa, T. Nishizaka and T. Shinohara, *IEEE Transactions on Industry Applications*, 1994, *30*, 835-843.

56. M. Washizu and O. Kurosawa, *IEEE Transactions on Industry Applications*, 1990, *26*, 1165-1172.

57. J. Ding, C. Woolley and M. A. Hayes, *Analytical and Bioanalytical Chemistry*, 2017, *409*, 6405-6414.

58. P. R. C. Gascoyne, J. Noshari, T. J. Anderson and F. F. Becker, *Electrophoresis*, 2009, *30*, 1388-1398.

59. A. LaLonde, M. F. Romero-Creel, M. A. Saucedo-Espinosa and B. H. Lapizco-Encinas, *Biomicrofluidics*, 2015, *9*, 064113.

# CHAPTER 3

# A MATHEMATICAL MODEL OF DIELECTROPHORETIC DATA TO CONNECT MEASUREMENTS WITH CELL PROPERTIES

Reprinted by permission from Springer Nature: Springer *Analytical and Bioanalytical Chemistry* A mathematical model of dielectrophoretic data to connect measurements with cell properties, S.H. Hilton, M. A. Hayes © 2019

## 3.1 Introduction

The ability to distinguish subtle biophysical differences in analytes is a major element in realizing the potential of dielectrophoresis (DEP). For cells, these differences are a result of mutations, gene expression levels, post-translational modifications, environmental effects, glycosylation variations, and lipid composition. They are difficult to assess, although tremendous efforts have been put forth to measure them. In bacterial cells, these physical variations can reflect anything from harmless, normal population variance to indications of transferred genes and possible acquisition of antibiotic resistance or an increase in virulence. Specific structures of the cells which are responsible for the physical changes have not yet been assigned to any quantitative changes in the dielectrophoretic data. Literature values for cellular properties are examined here for their effects on dielectrophoretic results, informing the qualitative features of dielectrophoretic data structures and defining reasonable values which can be expected.

Dielectrophoresis describes the motion of polarizable particles in the presence of electric field gradients. It was described and named by Herbert Pohl in 1951, although it

was exploited before that time [1]. The phenomenon interfaces well with microfluidics, the advantages of which include small sample and reagent volume, portability, and often-fast analysis times, while bringing its own advantages, such as the ability to probe small differences in electrophysical properties of the cell through accurate and precise determination of electrokinetic and dielectrophoretic mobilities. In recent years, the study of DEP has increased [2], encompassing many analytes ranging from DNA and proteins, to bacteria and yeast cells, to tumor and blood cells [3-16].

The theory of DEP has been well-developed by many researchers [1, 17-21] . Electrode-based DEP (eDEP) was originally used and continues to be implemented today. In eDEP, electrodes embedded into a device create the electric fields and gradients necessary for DEP to occur and particles to capture. The behavior of particles under applied AC fields and with varying frequencies has been extensively described [1, 18, 22, 23].

More recently, insulator-based DEP (iDEP) has emerged as an alternative to eDEP [24]. In iDEP, insulating features rather than patterned electrodes create the gradients in the electric field. Electrodes are placed farther away from these insulating features, often in an inlet and an outlet located at the two ends of a microfluidic channel.

The technique of iDEP allows for the use of DC fields, permitting electroosmosis and electrophoresis to be employed to move particles down a microchannel. While the forces in these systems are well known and many descriptive works for various analytes have appeared, less attention has been given to connecting the features of the dielectrophoretic data to the properties of the analytes.

Dielectrophoretic capture models have shown success in demonstrating experimental results closely matching predicted values [13]. Cells have been separated based on whether they exhibited positive or negative DEP at a given frequency, including mixtures of *E. coli* and *M. lysodeikticus*, and *S. cerevisiae* and *M. lysodeikticus* [9]. Cancer cells have also been separated from blood cells by trapping all cells under positive dielectrophoresis; the applied field was then adjusted to release blood cells, allowing the tumor cells to stay trapped [25]. With both eDEP and iDEP, AC fields have been used to assess the properties of cells and the frequency has often played a large role in this assessment. This technique has evaluated properties including the whole-cell membrane capacitance of neural stem cells [26], mitochondrial modifications [27], and the polysaccharides on the surface of cells for the characterization of blood types [28]. Using iDEP, live and dead *E. coli* cells have been separated [8]. Dielectrophoretic field-flow fractionation was used to separate circulating tumor cells from blood cells to an efficiency approaching 90% [5]. DEP has also been used to separate a mixture of two bacterial strains of the same species [29].

The fact that the physical properties of cells define their dielectrophoretic behavior is the underlying theme of these experiments. Differences in size, conductivity, surface charge, and other properties have been shown to result in different dielectrophoretic behaviors of particles [30-35]. Even slight differences in cells, such as the presence of a new enzyme in one bacterial strain versus another, can be discerned with a well-designed DEP system.

To help determine what types of physical changes lead to a given outcome in dielectrophoretic measurements, this chapter will introduce and develop a new mathematical model of dielectrophoretic data. This model will aid in the connection between the biophysical properties of an analyte, specifically bacteria, and the data obtained from DEP experiments. Common properties of cells and their effect on DEP behavior based on the model will also be discussed. The typical high and low values for important cellular properties which have appeared in the literature are used to plot and quantify expected behaviors of cells in dielectrophoresis. Some cell properties, such as whole cell conductivity, have major influence, where others, like surface softness, have minor effects. Some features strongly influence electrophoresis, while others affect dielectrophoresis, each with characteristic effects on the data structure and its quantification.

## 3.2 Theory

### 3.2.1 Channel Effects

The motion of particles in a buffer-filled microchannel with an applied potential is described by a number of effects, each of which may influence the behavior of analytes and therefore the structure of data sets acquired from such systems. These effects include electroosmosis, electrophoresis, and dielectrophoresis. These each arise from various properties of the particle, the microchannel, the solution, the applied field, and the interactions between them. Higher order effects, such as relaxation, retardation, thermophoresis, and field-induced electroosmosis, among others, may also be present. However, these occur for a relatively narrow set of conditions that are unlikely to be

present in currently-used operations of dielectrophoretic microdevice designs and will not be included in this discussion. In some specific applications, these may need to be introduced to fully account for experimentally observed effects.

#### 3.2.1.1 Electroosmosis and Electrophoresis

Electroosmosis, the motion of the bulk fluid in a microchannel upon application of a longitudinal electric field, is described with the zeta potential ($\zeta_m$) of the channel walls. Electroosmotic mobility ($\mu_{EOF}$) is defined by the Helmholtz-Smoluchowski equation as

$$\mu_{EOF} = -\frac{\varepsilon\zeta_m}{\eta} \tag{1}$$

where $\varepsilon_m$ is the permittivity and $\eta$ is the viscosity of the medium [36-38]. The fluid velocity ($\boldsymbol{v}_{EOF}$) is

$$\boldsymbol{v}_{EOF} = \mu_{EOF}\boldsymbol{E} \tag{2}$$

where $E$ is the electric field.

Electrophoresis refers to the motion of charged particles in a solution in the presence of an electric field. The size of the double layer surrounding these particles affects how these particles are considered. A particle is defined as small when the Debye-Huckel length is much larger than the particle and considered large in the opposite case. For cells under physiological conditions, the Debye-Huckel length is much smaller than the particle, which is generally the case for particles greater than 100 nm in diameter [37]. Here, only the large particle case will be considered. For a discussion of the case of small particles, see Tabeling 2005 and Nguyen and Wereley 2006 [37, 38]. In the

large particle case, the velocity of the particle again is the Helmholtz-Smoluchowski velocity [36-38]. The electrophoretic mobility can then be defined as:

$$\mu_{EP} = \frac{\varepsilon \zeta_p}{\eta} \tag{3}$$

where $\zeta_p$ is the zeta potential of the particle (rather than the wall), with the electrophoretic velocity ($\boldsymbol{v}_{EP}$) as

$$\boldsymbol{v}_{EP} = \mu_{EP}\boldsymbol{E} \tag{4}$$

Electroosmosis and electrophoresis are considered together as the electrokinetic force. These mobilities can be combined to become the electrokinetic mobility, $\mu_{EK}$, given as the sum of the electroosmotic and electrophoretic mobilities. The electrokinetic velocity ($\boldsymbol{v}_{EK}$) is

$$\boldsymbol{v}_{EK} = \mu_{EK}\boldsymbol{E} \tag{5}$$

#### 3.2.1.2 Dielectrophoresis

Dielectrophoresis (DEP) refers to the motion of a polarizable particle in the presence of a non-uniform electric field [1]. With no electric field present, a dielectric particle will have dipoles distributed in random directions. When a particle is exposed to an electric field, the dipoles align with the field. A force is induced that is oriented either towards (positive dielectrophoresis) or away from (negative dielectrophoresis) regions of high field gradient. This force ($\boldsymbol{F}$) is described by

$$\boldsymbol{F} = 2\pi r^3 \varepsilon_m f_{CM} \nabla |\boldsymbol{E}|^2 \tag{6}$$

where $r$ is the radius of the particle, $\varepsilon_m$ is the permittivity of the medium, and $f_{CM}$ is the Clausius-Mossotti factor. For a spherical particle, $f_{CM}$ is

$$f_{CM} = \frac{\varepsilon^*{}_p - \varepsilon^*{}_m}{\varepsilon^*{}_p + 2\varepsilon^*{}_m} \tag{7}$$

where $\varepsilon^*{}_p$ and $\varepsilon^*{}_m$ are the complex permittivity of the particle and medium, respectively. For DC fields, $f_{CM}$ simplifies to

$$f_{CM} = \frac{\sigma_p - \sigma_m}{\sigma_p + 2\sigma_m} \tag{8}$$

where $\sigma_p$ and $\sigma_m$ are the conductivity of the particle and medium, respectively. The dielectrophoretic force can also be described for particles of other shapes [18, 39, 40].

The dielectrophoretic mobility, $\mu_{DEP}$, is defined as

$$\mu_{DEP} = \frac{\varepsilon_m r^2 f_{CM}}{3\eta} \tag{9}$$

and the dielectrophoretic velocity, $v_{DEP}$, is

$$\boldsymbol{v}_{DEP} = \mu_{DEP} \nabla |\boldsymbol{E}|^2 \tag{10}$$

From this, it is seen that the effect of the radius on the dielectrophoretic mobility is trivially understood, and thus will not be considered in more depth here.

Capture in DEP occurs when the flux of particles at a given point in the channel is zero. Written in terms of mobilities, this is

$$(\mu_{EK} \boldsymbol{E} + \mu_{DEP} \nabla |\boldsymbol{E}|^2) \cdot \boldsymbol{E} > 0 \tag{11}$$

Rearranging this equation defines the condition that must be satisfied for capture to occur:

$$\frac{\mu_{EK}}{\mu_{DEP}} \leq \frac{\nabla |E|^2}{E} \tag{12}$$

The applied potential required for capture to begin to occur is called the capture onset potential.

### 3.2.2 Particle Properties

Properties of particles will affect their electrokinetic and dielectrophoretic mobilities, which in turn affect their behavior in a microchannel. These properties and their influence on these two mobilities are summarized here.

#### 3.2.2.1 Conductivity and Permittivity

The conductivity or permittivity of a sphere made up of multiple shells is described by the multishell model [18, 34, 41]. In this model, a cell is assumed to be a collection of concentric spheres representing the cytoplasm (conductivity $\sigma_1$, permittivity $\varepsilon_1$, and radius $R_1$), the membrane (conductivity $\sigma_2$, permittivity $\varepsilon_2$, and radius $R_2$), and the cell wall (conductivity $\sigma_3$, permittivity $\varepsilon_3$, and radius $R_3$). The conductivity of the two inner shells is given by

$$\sigma_{2shell} = \sigma_2 \left[ \frac{\left(\frac{R_2}{R_1}\right)^3 + 2\left(\frac{\sigma_1 - \sigma_2}{\sigma_1 + 2\sigma_2}\right)}{\left(\frac{R_2}{R_1}\right)^3 - \left(\frac{\sigma_1 - \sigma_2}{\sigma_1 + 2\sigma_2}\right)} \right] \tag{13}$$

and the overall conductivity of the three shells is

$$\sigma_{3shell} = \sigma_3 \left[ \frac{\left(\frac{R_3}{R_2}\right)^3 + 2\left(\frac{\sigma_{2shell} - \sigma_3}{\sigma_{2shell} + 2\sigma_3}\right)}{\left(\frac{R_3}{R_2}\right)^3 - \left(\frac{\sigma_{2shell} - \sigma_3}{\sigma_{2shell} + 2\sigma_3}\right)} \right] \tag{14}$$

Thus, factors which affect the conductivity of the cell wall, the membrane, or the cytoplasm will change the overall conductivity of the cell.

The same model can be applied to the permittivity of each layer of a cell. The permittivity of the inner two shells is

$$\varepsilon_{2shell} = \varepsilon_2 \left[ \frac{\left(\frac{R_2}{R_1}\right)^3 + 2\left(\frac{\varepsilon_1 - \varepsilon_2}{\varepsilon_1 + 2\varepsilon_2}\right)}{\left(\frac{R_2}{R_1}\right)^3 - \left(\frac{\varepsilon_1 - \varepsilon_2}{\varepsilon_1 + 2\varepsilon_2}\right)} \right] \tag{15}$$

and the overall permittivity of a three-shell system is

$$\varepsilon_{3shell} = \varepsilon_3 \left[ \frac{\left(\frac{R_3}{R_2}\right)^3 + 2\left(\frac{\varepsilon_{2shell} - \varepsilon_3}{\varepsilon_{2shell} + 2\varepsilon_3}\right)}{\left(\frac{R_3}{R_2}\right)^3 - \left(\frac{\varepsilon_{2shell} - \varepsilon_3}{\varepsilon_{2shell} + 2\varepsilon_3}\right)} \right] \tag{16}$$

This pattern can be followed to determine the conductivity or permittivity for a system of four or more shells. The shell model is more complex for an ellipsoid [42, 43].

#### 3.2.2.2 Surface Charge Density

Ohshima and Kondo, along with others, have described the electrophoretic mobility of a particle as it relates to the charges on the surface of the particle [44-46]. These equations well-describe soft particles such as bacteria and have been used to determine the surface softness ($\lambda^{-1}$) and surface charge density ($N_c$) of bacterial cells ($N$ in the original work). With a specific set of assumptions described in the original work, they found the expression for the electrophoretic mobility to be

$$\mu_{EP} = \frac{\varepsilon_m \varepsilon_o}{\eta} \frac{\frac{\psi(0)}{\kappa_m} + \frac{\psi_{DON}}{\lambda}}{\frac{1}{\kappa_m} + \frac{1}{\lambda}} + \frac{zeN_c}{\eta\lambda^2} \tag{17}$$

where $z$ is the valence of the charged groups on the particle, $e$ is the electric unit charge, and $\kappa_m$ (the Debye-Huckel parameter of the surface charge layer), $\psi(0)$ (the potential at the boundary between the surface-charge layer and the solution), $\psi_{DON}$ (the Donnan potential), and $\lambda$ are as described in the original work [45]. Each of the parameters $\kappa_m$, $\psi(0)$, and $\psi_{DON}$ are influenced by the surface charge density and parameters $z$ and/or $N_c$.

The softness parameter is larger for cells with more polymer on the surface, and small as cells become "hard". For the limit where the softness parameter becomes zero (hard particles), this equation reduces to the familiar Smoluchowski equation, which is commonly used to describe electrophoretic mobility. This analysis has been used to study analytes including bacteria, microgel particles, and latex particles bound to immunoglobulin G [47-50].

#### 3.2.2.3 Charge Distribution and Multipoles

Pysher and Hayes, Anderson, and Fair and Anderson discuss how multipoles affect the electrophoretic mobility [51-53]. Multipoles affect the zeta potential of a particle. Generally, particles are considered to be a point charge with spherically symmetric charge distribution, but this assumption does not hold true for biological particles.

Multipole expansions of the zeta potential have been described. The model developed by Anderson gives the electrophoretic mobility, using the first three multipole moments of the expansion of the zeta potential, as

$$\mu_{EP} = \frac{\varepsilon}{4\pi\eta}\left[\beta_0 I - \frac{1}{2}\beta_2\right] \tag{18}$$

where $\beta_0$ is the monopole moment, $\beta_2$ is the quadrupole moment, and $I$ is the identity tensor. This shows that the quadrupole moment is affected by the distribution as well as by the magnitude of the surface charge in a particle.

Pethig summarizes the dielectrophoretic force as it is affected by multipoles [19]. The DEP force acts on the *n*th-order multipole in a spherical particle according to the equation

$$\langle \boldsymbol{F}_{DEP_n} \rangle = \mathrm{Re}\left[\frac{p_n[\,\cdot\,]^n(\nabla)^n \boldsymbol{E}}{n!}\right] \tag{19}$$

where $p_n$ is the effective *n*th-order multipolar moment given by the equation

$$p_n = \frac{4\pi\varepsilon_m r^{2n+1}}{(2n-1)!!} CM_{(n)}(\nabla)^{n-1}E \tag{20}$$

and $CM_{(n)}$ is the general multipole form of the Clausius-Mossotti factor, given by the equation

$$CM_{(n)} = \frac{\varepsilon^*{}_P - \varepsilon^*{}_m}{n\varepsilon^*{}_p + (n+1)\varepsilon^*{}_m} \tag{21}$$

with $[\,\cdot\,]^n$ representing *n* dot products performed on the dyadic tensors, $(\nabla)^n$ representing *n* vector $\nabla$ operations, $r$ as the radius of a spherical dielectric particle, and $E$ as the sinusoidal steady-state field vector to which the particle is subjected.

For nonspherical particles, $p_n$ becomes

$$p_n = 4\pi\varepsilon_m r_{int}^{n+1} \frac{2n+1}{2} \int_0^\pi \phi_{r_{int}} P_n(cos\theta) sin\theta d\theta \tag{22}$$

where $P_n(cos\theta)$ are the Legendre polynomials, using spherical coordinates, and $\phi_{r_{int}}$ is the electric potential due to the particle over a spherical surface of radius $r_{int}$.

Recent efforts focused on developing more accurate models of electrophoresis and dielectrophoresis include the polarized solute-solvent interface [54-59]. This approach indicates a greater degree of descriptive differentiation for complex particles such as proteins and cells. Given the potential high-resolution separations theoretically predicted and the experimental results beginning to support this high-resolution capability, more nuanced theoretical descriptions will likely be of greater applicability.

## 3.3 Materials and Methods

Modeling of the effects of various cell properties on dielectrophoretic data was performed with Matlab (version 9.5 R2018b, MathWorks, Natick, MA). The equations governing each property presented above were used in combination with the piecewise function of the mathematical model developed (see below) to determine the expected features of dielectrophoretic data of varying cellular properties.

Finite element commercial software (COMSOL version 5.1 with AC/DC module, COMSOL, Inc., Burlington, MA) was used to interrogate the distribution of the electric field and find values of $E_{ave}(V)$, $E_{max}$, and $\nabla|E|^2{}_{max}$, as they relate to the specific channels used in these studies. The microchannel has a decreasing size of constrictions, formed by triangles, from the outlet to the inlet and has been previously described in-depth [6, 12, 16, 29, 35]. The second microchannel used to demonstrate the applicability of the model to other systems uses multi-length scale insulators, and has also been previously described [60]. Here, this channel was 3.2 cm long with a constriction of 37 $\mu$m. The values used were determined from centerline measurements.

## 3.4 Results and Discussion

### 3.4.1 Development of a Mathematical Model of Dielectrophoretic Data

A mathematical model is developed for dielectrophoretic data, when either the electric field or time is varied. When one of these is altered, the capture behavior of two or more particle populations can be compared [6, 7, 12, 29, 30, 32, 61-68]. This model of the data relies on electrophoresis and electroosmosis for particle transport and assumes a DC field is present, but could be modified to account for an AC field with a DC offset.

Differences in either the electrokinetic or dielectrophoretic mobility of particles will produce unique capture conditions (equation 12). While the model, as developed, uses fluorescence intensity as the metric of detection, other concentration-sensitive methods could be used with only a slight adaptation of the model. Possible other detection methods include impedance and light or dark field illumination [69], but could also include other methods to measure the number of bacterial cells present. Particle properties will also be considered and expected variations in the data due to changes in these properties noted. The model developed here will advance the ability to compare particles based on their behavior in the microchannel.

Assuming a homogeneous population of particles with average velocity $v$ in a microchannel, the particles will travel distance $d = vt$ in time $t$. The particles that will reach the gate within time $t$ are then, before any potential is applied, found within a volume with length $d$ ending at the capture zone, height $h$ the height of the channel, and width $w$, the average width of the channel (Figure 3.1a). The number of particles ($N$) that reach the capture point in time *t* is

$$N = nvtwh \tag{23}$$

where $n$ is the average particle density.

The average electric field ($E_{ave}$) is the average magnitude of the field across the entire channel and reservoir length, whereas the local magnitude of the electric field ($E$) varies dramatically within a microchannel due to the insulating features. The local maxima of the electric field magnitude ($E_{max}$) occurs near each gate and is associated with the location of capture. The applied potential ($V$) is the voltage applied across the

entire microchannel and provides a convenient way to relate $E_{ave}$ and $E_{max}$ to this same externally controlled value. The values $E_{ave}(V)$ and $E_{max}(V)$ are the average electric field and the local maximum magnitude of the electric field, respectively, as a function of the applied potential.

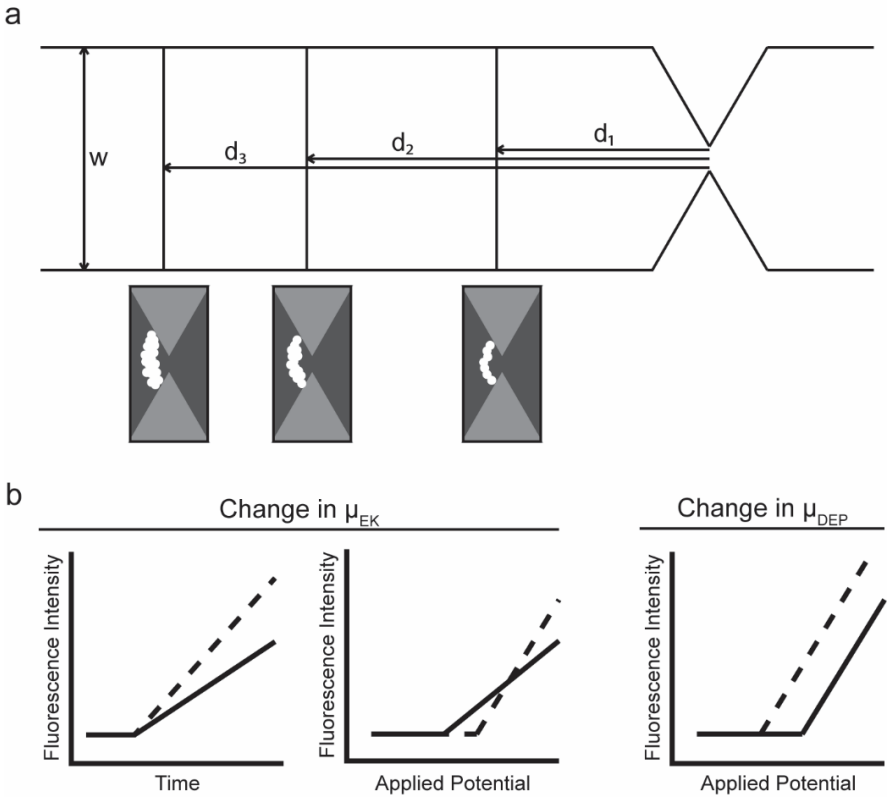



Figure 3.1 Schematic diagram of the channel (a, top), typical particle collection pattern (a, bottom), and data structures resulting from changes in electrokinetic and dielectrophoretic properties (b). Notable variables used in the mathematical model include channel width, *w*, and the distance, *d*, from which particles can reach the gate and capture (a, top). This distance increases with increasing voltage (*V*) or increasing time (*t*). The channel height, $h$, is perpendicular to the paper. This channel is on the microscale, with dimensions of about 1 mm for *w* and about 20 μm for $h$. The number of particles captured and a brighter fluorescence intensity result from larger *d* (a, bottom). An increase in $\mu_{EK}$ (dashed line) will result in a larger slope in time-dependent data, along with a larger slope and higher onset capture potential in voltage-dependent data (b, left). An increase in $\mu_{DEP}$ (dashed line) will result in a smaller capture onset potential in voltage-dependent data, but will not affect the slope (b, right); time-dependent data will not be affected by changes in $\mu_{DEP}$. The opposite cases (solid lines) induce the opposite effect.

The number of particles can be determined relative to the electric field using equations 5 and 23:

$$N = n\mu_{EK} twh E_{ave} \tag{24}$$

Fluorescence intensity ($FI$) is established by multiplying $N$ by nominal integrated fluorescence signal for an average particle, $\gamma$:

$$FI = \gamma N = \gamma n\mu_{EK} twh E_{ave} \tag{25}$$

The value of $\gamma$ for the fluorescence signal from an average particle may be substituted for the signal detected in a different method, if the overall signal is concentration-dependent. A correction factor, $s$, accounts for potential stacking of the analyte, scattering of the light, saturation of the detection method, or other issues in detecting all analytes. When using fluorescence as the detection method, this also accounts for the particles not visible due to the depth of the channel, either due to stacking or to the depth-of-focus. The expression for the observed fluorescence intensity then becomes

$$FI_{obs} = \gamma n\mu_{EK} twhs E_{ave} \tag{26}$$

Data is captured and assessed via two methods, holding $t$ constant and varying $E_{ave}$, or by holding $E_{ave}$ constant and varying $t$ (Figure 3.1b).

#### 3.4.1.1 Varying Potential

The magnitude of the local electric field varies as a function of applied potential ($V$). An expression for how this varies within a specific system can be determined using COMSOL. For the specific channel under study, this relationship was found to be

$$E_{ave}(V) = 0.24 \cdot V \tag{27}$$

This expression, $E_{ave}(V)$, can then be substituted into equation 26 to determine the fluorescence intensity as a function of applied potential, resulting in

$$FI(V) = \gamma n \mu_{EK} twhs E_{ave}(V) \tag{28}$$

For the specific channel under study, equation 27 can be combined with equation 28 to find

$$FI(V) = \gamma n \mu_{EK} twhs \cdot (0.24V) \tag{29}$$

To extend this work to other microchannel geometries, other expressions for $E_{ave}(V)$ could be found and used in place of the values shown here.

**3.4.1.2 Conditions of Capture**

At low values of applied voltage, no capture takes place. The above expression only holds true when capture is occurring. A function is necessary that describes the full data, including the region of no capture, the capture onset potential, and capture with a linear rise in $FI$. The behavior is best described by a piecewise function. At values less than the capture point, $y = 0$, while at values higher than the capture point, $FI$ will increase linearly as described above. The intercept of this function is related to the applied potential at which capture begins to occur ($V = c$). Setting $FI(c) = 0$ and using algebra to determine the intercept of the linear rise part of the piecewise function results in the expression

$$FI(V) = \begin{cases} 0 & if\ V < c \\ 0.24\gamma n \mu_{EK} twhs(V - c) & if\ V \geq c \end{cases} \tag{30}$$

### 3.4.1.3 Capture Onset Potential

COMSOL was used to find finite element software-derived values for the function $\frac{\nabla|E|^2{}_{max}}{E_{max}}(V)$ in the specific device under study

$$\left[\frac{\nabla|E|^2{}_{max}}{E_{max}}(V)\right] = [1.4 \cdot 10^7 \cdot V] \tag{31}$$

When the value of $V$ is set to the onset capture potential ($c$), the entire equation can be set equal to $\frac{\mu_{EK}}{\mu_{DEP}}$. Doing this and then solving for $c$ yields

$$\left[\frac{\nabla|E|^2{}_{max}}{E_{max}}(c)\right] = [1.4 \cdot 10^7] \cdot c = \frac{\mu_{EK}}{\mu_{DEP}} \tag{32}$$

$$c = \frac{1}{1.4 \cdot 10^7}\left(\frac{\mu_{EK}}{\mu_{DEP}}\right) \tag{33}$$

Again, an expression can be found for other microchannel systems, and the appropriate values substituted in this equation.

This expression can be substituted into the piecewise function of equation 30:

$$FI(V) = \begin{cases} 0 & if\ V < \frac{1}{1.4 \cdot 10^7}\left(\frac{\mu_{EK}}{\mu_{DEP}}\right) \\ 0.24\gamma n \mu_{EK} twhs\left[V - \frac{1}{1.4 \cdot 10^7}\left(\frac{\mu_{EK}}{\mu_{DEP}}\right)\right] & if\ V \geq \frac{1}{1.4 \cdot 10^7}\left(\frac{\mu_{EK}}{\mu_{DEP}}\right) \end{cases} \tag{34}$$

This reflects that the fluorescence intensity of captured particles, as well as the capture onset potential, is related to known parameters. This final function can be fitted to data collected from a specific particle population to find properties of that population. Differences in both $\mu_{EK}$ and $\mu_{DEP}$ will affect the shape of the data when the potential is varied (Figure 3.1b). As before, an expression for other microchannel systems can be found by using the appropriate expressions for $\frac{\nabla|E|^2{}_{max}}{E_{max}}(V)$ and $E_{ave}(V)$.

One such system, previously described in-depth [60], uses a multi-length scale insulator rather than the triangles of the system used in the case above. For this system, it was calculated that

$$E_{ave}(V) = 0.29 \cdot V \tag{35}$$

and

$$\frac{\nabla|E|^2{}_{max}}{E_{max}}(V) = [1.9 \cdot 10^6] \cdot V \tag{36}$$

Thus, the final equation can be written as

$$FI(V) = \begin{cases} 0 & if\ V < \frac{1}{1.9 \cdot 10^6}\left(\frac{\mu_{EK}}{\mu_{DEP}}\right) \\ 0.29\gamma n \mu_{EK} twhs\left[V - \frac{1}{1.9 \cdot 10^6}\left(\frac{\mu_{EK}}{\mu_{DEP}}\right)\right] & if\ V \geq \frac{1}{1.9 \cdot 10^6}\left(\frac{\mu_{EK}}{\mu_{DEP}}\right) \end{cases} \tag{37}$$

which demonstrates how this model could be applied to other dielectrophoretic systems.

#### 3.4.1.4 Varying Time

Rearranging equation 29, holding the applied potential $V$ and therefore $E_{ave}$ constant, and allowing *t* to vary gives

$$FI = 0.24V\gamma n \mu_{EK} whst \tag{38}$$

where expressions for $E_{ave}(V)$ from other devices can be substituted.

### 3.4.2 Features of Data and Interpretation with the Model

The equations derived for $FI$ reflect that differences in the electrokinetic mobility appear as a change in both the slope in voltage- and time-based data, as well as in the voltage at which capture begins to occur. Differences in the dielectrophoretic mobility, however, will only appear as a difference in the onset voltage and the slope of the data remains unchanged (Figure 3.1). Other devices and systems can also be interpreted with

this approach by using the data from other microchannel geometries [30, 32, 34, 61, 68, 70-74] and these general features of the data would remain unchanged, although quantitative details will vary depending on the configuration. Specific dimensions and operating parameters for a common device design were used in the calculations presented here. Some other systems may require additional factors, such as the addition of pressure driven flow [75].

Typical data demonstrates a linear increase in $FI$ with increasing $V$, consistent with equations 29 and 34, starting at the value of $c$ where capture begins [6, 29]. There is a limited range of linearity, beyond which the signal falls below the values predicted by the model. The non-linearity has two possible origins: saturation of the capture zones with particles (causing release or visual occlusion) or preceding capture zones collecting particles, reducing the available pool.

### 3.4.3 Applications with Known Particle Properties

Various particle properties are known to affect $\mu_{EK}$, $\mu_{DEP}$, or both, but with unique mechanisms for each. Variations in these properties can cause differences in capture onset potential and/or slope, and the magnitude of this difference will depend on the property. Here, differences in bacterial cell conductivity and permittivity, surface charge density, and zeta potential, and their effect on the data according to the model developed will be considered. The results discussed below and shown in Figures 3.2-3.5 are a direct application of the model to real data, from values for these properties found in the literature. The influence of multipoles will also be discussed. Shape, deformability,

and the mobility of surface charges will be briefly considered within the influence in multipoles.

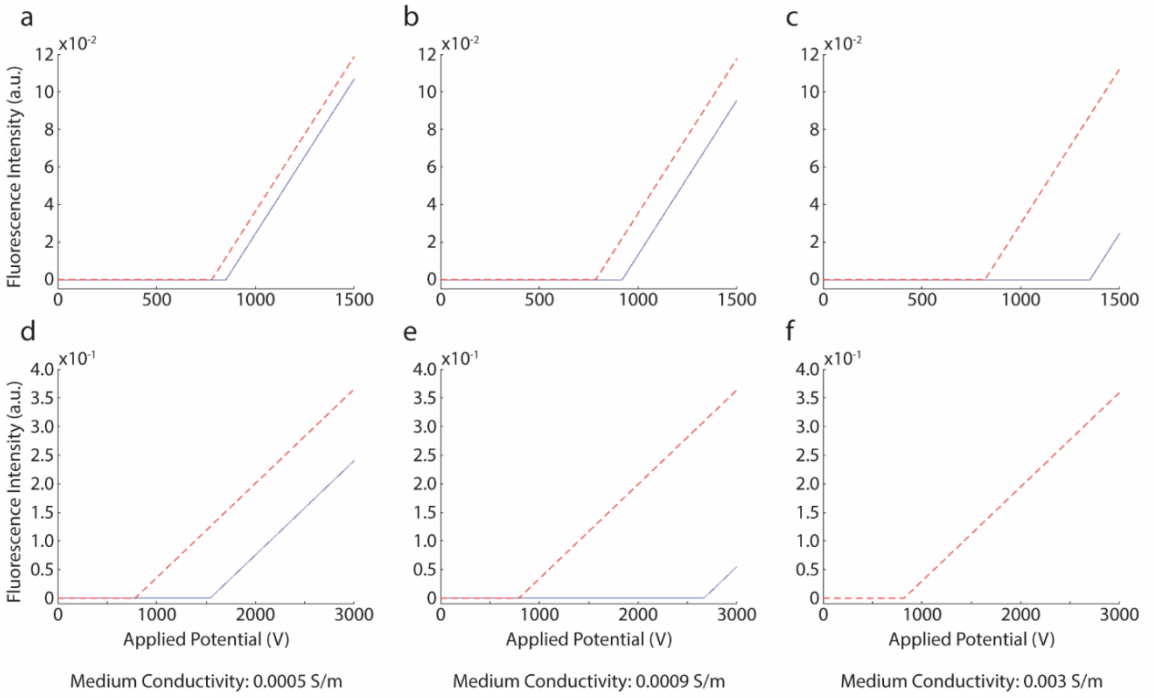
#### 3.4.3.1 Conductivity and Permittivity

The conductivity and permittivity of the cell directly impact the dielectrophoretic mobility (equations 7-9) and helps to define the capture onset potential. Changes in $\mu_{DEP}$ do not influence the slope of the $FI$ (equation 34 and Figure 3.1b).

Differences in conductivity were examined using high and low literature values for various microorganisms. The overall conductivity of a cell can range from about 0.002 to 0.1 S/m for gram-negative bacteria, a range of about two orders of magnitude. In gram-positive species, this range is about 0.015 to 0.15 S/m, about one order of magnitude [76]. These values are used to model expected dielectrophoretic behavior and provide graphical evidence of reasonable changes in dielectrophoretic behavior arising from this variable (Figures 3.2a, d, and g). Values for other properties not mentioned specifically are averages of values found in the literature. The same holds true for the considerations of zeta potential and surface charge density below.

The magnitude of the difference in capture onset potential, however, is dependent on the conductivity of the medium. When the cell and the medium conductivity are similar, there is a larger difference in capture onset potential (Figure 3.2). This is more clearly shown for gram-positive species; the difference in capture onset potential is much greater when the medium conductivity is closer to the values of the particle conductivity (Figure 3.2a-c). Varying the medium permittivity or the viscosity of the medium will shift the potential at which capture occurs but does not affect the difference in capture

onset potentials between two species. Varying medium conductivity could be exploited to determine if the differences seen in capture onset potential are likely related to the conductivity of the particles, or if other possibilities should be considered.




g

| | Conductivity | | Onset Potential | |
|---|---|---|---|---|
| | Blue Solid | Red Dashed | Blue Solid | Red Dashed |
| a | 0.015 S/m | 0.15 S/m | 851 V | 779 V |
| b | | | 919 V | 785 V |
| c | | | 1350 V | 819 V |
| d | 0.002 S/m | 0.1 S/m | 1540 V | 783 V |
| e | | | 2660 V | 792 V |
| f | | | 6170 V | 843 V |

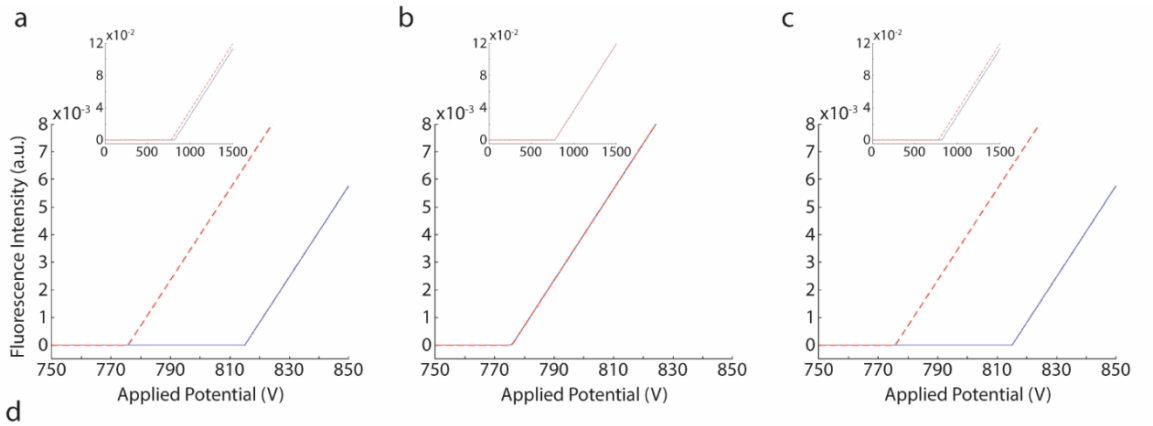
Figure 3.2 Calculated dielectrophoretic data for model cells with high and low values of overall cell conductivity (Gram-positive: a, b, c; Gram-negative: d, e, f) with respect to a range of medium conductivities (left to right: low, 0.0005 S/m; mid-range, 0.0009 S/m; high, 0.003 S/m). The high (dashed red line) and low (solid blue line) overall cell conductivity literature values are used to calculate dielectrophoretic properties, while all other properties were assigned an average from across the literature. In f, the low cell conductivity value is smaller than the medium conductivity, leading to positive dielectrophoresis. The capture onset potential for this situation is outside the plotted *x*-axis (at $6.0 \cdot 10^3$ V), and thus the line is not plotted. A table summarizes the changed variables and resulting capture onset potentials for each situation (g).

As reflected in the shell model, the conductivity or permittivity of any layer of a cell can affect the overall conductivity or permittivity, and thus each layer can affect the dielectrophoretic mobility (equations 13-14) [18, 72]. These relationships, for both a sphere and an ellipsoid, show that a change in thickness in any layer will affect the overall conductivity of the particle. An increase in conductivity of the cell will lead to an increase in the capture onset potential. The same is true for an increase in the permittivity. The impact of a single layer will be affected by the radius of that layer. For three layers that are the same thickness, a change in the outermost layer would cause the largest change in the overall conductivity or permittivity; however, this is not the case in bacterial cells where the three layers are the cell wall, the membrane, and the cytoplasm, each with its characteristic thickness (Figure 3.3).

The cell wall and the cytoplasm conductivities can vary by about an order of magnitude, with reasonable values of the conductivity for each being between 0.5 and 0.05 S/m (Figure 3.3a and 3.3c). The membrane conductivity also varies by approximately an order of magnitude, with a reasonable value being $10^{-7}$ S/m [17, 76, 77]. As this variation generates a difference in the capture onset potential in the $6^{th}$ decimal place, two orders of magnitude were considered, changing conductivity from $10^{-7}$ to $10^{-9}$ S/m (Figure 3.3b and d).

This modeling shows that a change in conductivity solely in one layer of the cell will cause a much smaller effect on the capture onset potential compared with whole cell conductivity (Figures 3.2 and 3.3). The same logic can be applied to permittivity to examine the effect of a variation in each layer. The effect on total conductivity of a cell

differs to varying degrees depending upon which layer is changed. A difference in conductivity in either the cell wall and the cytoplasm could solely be responsible for a small difference in overall conductivity and thus the capture onset potential. A variation in the membrane conductivity, however, could only be responsible for a very small difference in the capture onset potential. Thus, it is unlikely that a difference in capture onset potential between two cell populations could be assigned exclusively to a difference in the membrane conductivity.




d

| | Conductivity | | Onset Potential | |
|---|---|---|---|---|
| | Blue Solid | Red Dashed | Blue Solid | Red Dashed |
| a (cell wall conductivity varied) | 0.05 S/m | 0.5 S/m | 815 V | 776 V |
| b (membrane conductivity varied) | $1 \cdot 10^{-9}$ S/m | $1 \cdot 10^{-7}$ S/m | 776 V | 776 V |
| c (cytoplasm conductivity varied) | 0.05 S/m | 0.5 S/m | 815 V | 776 V |

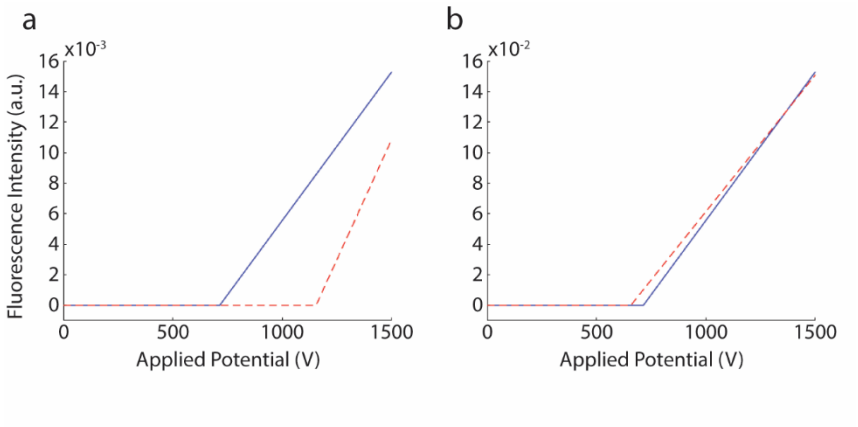
Figure 3.3 Calculated biophysical data from modeled cells in a dielectrophoretic system influenced by changes in the conductivity of the cell wall (a, blue solid 0.05 S/m, red dashed 0.5 S/m), membrane (b, blue solid $1 \cdot 10^{-9}$ S/m, red dashed $1 \cdot 10^{-7}$ S/m), and cytoplasm (c, blue solid 0.05 S/m, red dashed 0.5 S/m). A representative high (red dashed) and low (blue solid) value for conductivity of each layer was chosen. The shell model (equation 14) is used to determine the effect of the conductivity. Larger *x*- and *y*-axis values consistent with other data presented is shown (insets), allowing for visual comparison of the effect of a single layer to that of the overall conductivity. The table summarizes the changed variable in each plot and the capture onset potential obtained from the modeling (d).

The ability to separate live and dead cells with dielectrophoresis has been attributed to the difference in cell conductivity. When a cell dies, especially through heat treatment, the membrane becomes more permeable, resulting in an increase in conductivity of about four orders of magnitude, from about $10^{-7}$ S/m to about $10^{-3}$ S/m [78]. This also allows an efflux of cytoplasmic ions, resulting in a decrease of cytoplasmic conductivity, from 0.44 S/m for live cells to 0.9 S/m for dead cells [79]. Modeling this interesting case shows a similar result to Figure 3.3a and c, with the dead cells requiring a higher potential for capture. This is consistent with what was shown by Lapizco-Encinas et al. [8], where dead *Escherichia coli* cells are captured at locations of higher field gradient than live *E. coli*.

**3.4.3.2 Zeta Potential**

The zeta potential for a cell is a defining property reflecting the interplay between surface charge and the ionic solution surrounding the cell. This variable appears in a linear relationship to electrokinetic mobility in equations (equations 1 and 3). As such, a difference in zeta potential will cause a difference in both the slope and the capture onset potential (equation 34). Even a small difference in zeta potential will give a noticeable difference in both the capture onset potential and the slope of the dielectrophoretic data (Figure 3.4). The literature shows that the zeta potential can vary between strains of a single species, as demonstrated by *Streptococcus mutans*. At pH 7, the zeta potential for this species can range from about -20 to -35 mV [80]. It is unsurprising, then, that different species have even larger differences in their zeta potentials. For example, the zeta potential of *Rhodococcus erythropolis* is -102 mV [81], while *Pasteurella multocida*

has a zeta potential of -25 mV [82] with an in-tact capsule. The non-capsulated derivative of *P. multocida* has a zeta potential of -15 mV at the same pH of 7 (Figure 3.4) [82].




c

| | | a | b |
|---|---|---|---|
| Zeta Potential | Blue Solid | -25 mV | -25 mV |
| | Red Dashed | -102 mV | -15 mV |
| Onset Potential | Blue Solid | 714 V | 714 V |
| | Red Dashed | 1150 V | 657 V |
| Slope | Blue Solid | $1.95 \cdot 10^{-5}$ | $1.95 \cdot 10^{-5}$ |
| | Red Dashed | $3.14 \cdot 10^{-5}$ | $1.79 \cdot 10^{-5}$ |

Figure 3.4 Calculated biophysical data of modeled cells of varying zeta potential in a dielectrophoretic system. Zeta potentials corresponding to those of *Rhodococcus erythropolis* (-102 mV, red dashed line) and *Pasteurella multocida* (-25 mV, blue solid line) were plotted (a). Within a single species of bacteria, capsulation can make a difference in zeta potential: zeta potentials corresponding to capsulated (-25 mV, blue solid line) and non-capsulated (-15 mV, red dashed line) strains of *P. multocida* (b) were plotted. The table shows the different zeta potentials used in each plot and the calculated capture onset potentials and slopes (c).

These real values for zeta potential found in the literature can be used in the mathematical model to show how such differences will affect dielectrophoretic behavior. Small differences in the zeta potential of the cell, such as that arising from the presence vs. absence of the capsule, will give a notable difference in the capture onset potential. Larger zeta potential variations logically result in even larger variations in the capture onset potential. From this, disparities in capture onset potential up to about 450 V, and perhaps larger, which accompany a small change in slope could be assigned to a difference in zeta potential. However, as noted, differences in conductivity could also contribute to differences in capture onset potential.

Varying properties of the system such as the concentration of particles, the zeta potential of the channel wall, the conductivity of the medium, or the permittivity of the medium will have little to no effect on the difference of capture onset potentials between two species. It does, in the case of zeta potential of the wall, shift the forces required for capture. However, both the concentration and the permittivity of the medium have a large impact on the difference in slopes between two species. Without knowing these parameters accurately for a specific system, it would be difficult to attribute a difference in slope to any one property, including zeta potential differences.

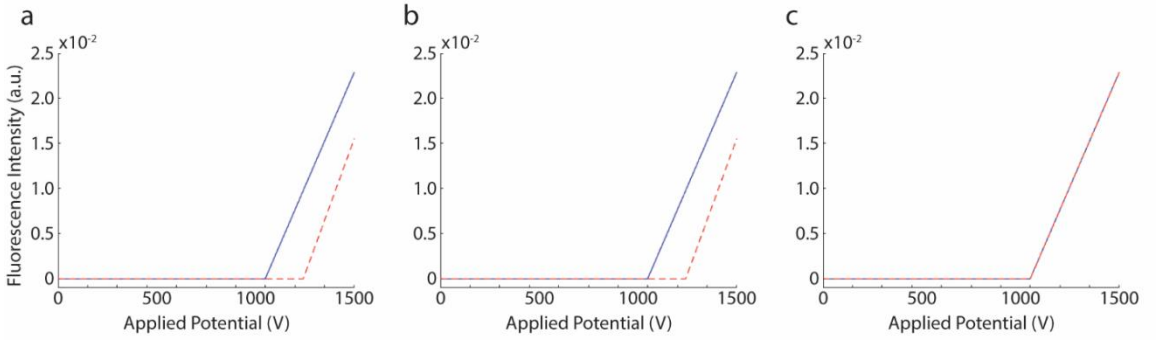
#### 3.4.3.3 Surface Charge Density

Surface charge density and surface viscosity have analytical solutions for their electrophysical effects. Surface viscosity is approximated with so-called surface softness ($\lambda^{-1}$). This softness parameter arises as the inverse of a measure of the friction of a liquid flowing through the surface layer of the cell [47]. Cells characteristically have

some number of polymers on the surface, and as such the inclusion of the softness parameter gives a more accurate description of cells. Both the surface charge density and the softness can vary in bacteria due to differences in the lipids forming the membrane, the amount and type of glycosylation in the capsule and/or peptidoglycan layer, and the presence of proteins at the surface of the cell. An increase in the surface charge density ($N_c$) or a decrease in surface viscosity (η), represented by the softness parameter (λ), will increase electrokinetic mobility (equation 17). This increase in $\mu_{EK}$ will cause an increase in the slope of the line (Figure 3.5, equation 34), and an increase in the capture onset potential.

Both the density of charged groups and the $\lambda$ factor have been found for various bacterial species. Example gram-negative (*Escherichia coli*) and gram-positive (*Staphylococcus aureus*) species, for which $N_c$ and $\lambda$ are found in the literature, are used to demonstrate typical behaviors. For *E. coli*, the surface charge density at a pH of 7 is 0.145 M (or $1.74 \cdot 10^{-5}$ mmol/m$^2$), while for *S. aureus*, it is 0.025 M (or $3.00 \cdot 10^{-6}$ mmol/m$^2$). The $\lambda$ factor for *E. coli* is 1.5 nm$^{-1}$, while for *S. aureus*, it is 0.53 nm$^{-1}$ [46]. Using these values, the electrophoretic mobility is affected (equation 17), and thus the capture onset potential and the slope of the data (equation 34). The capture onset potential and slope of the data for the modeled particles are summarized in Figure 3.5d. These two populations are representative of a large range of surface charge densities that will be found on bacterial cells; however, there may be other species or strains with much larger or smaller surface charge densities. Considered separately, the surface charge density has a noticeable impact on the electrokinetic mobility, and thus both the capture

onset potential and the slope (equation 34), while a difference in the $\lambda$ factor gives little to no discernable change (Figure 3.5).




d

| | | a | b | c |
|---|---|---|---|---|
| Surface Charge Density | Blue Solid | 0.025 M | 0.025 M | 0.025 M |
| | Red Dashed | 0.145 M | 0.145 M | 0.025 M |
| Surface Softness | Blue Solid | 0.53 $nm^{-1}$ | 0.53 $nm^{-1}$ | 0.53 $nm^{-1}$ |
| | Red Dashed | 1.5 $nm^{-1}$ | 0.53 $nm^{-1}$ | 1.5 $nm^{-1}$ |
| Onset Potential | Blue Solid | 1400 V | 1400 V | 1400 V |
| | Red Dashed | 1660 V | 1660 V | 1400 V |
| Slope | Blue Solid | $3.81 \cdot 10^{-5}$ | $3.81 \cdot 10^{-5}$ | $3.81 \cdot 10^{-5}$ |
| | Red Dashed | $4.51 \cdot 10^{-5}$ | $4.51 \cdot 10^{-5}$ | $3.81 \cdot 10^{-5}$ |

Figure 3.5 Calculated biophysical data of modeled cells in a dielectrophoretic system influenced by changes in surface charge density, $N_c$, and the softness parameter, $\lambda$. Representative values found in the literature for common bacteria are plotted: *Staphylococcus aureus* (solid blue line, $N_c$ = 0.025 M, $\lambda$ = 0.53 $nm^{-1}$) and *Escherichia coli* (dashed red line, $N_c$ = 0.145 M, $\lambda$ = 1.5 $nm^{-1}$) (a). With $\lambda$ held constant at the *S. aureus* value (0.53 $nm^{-1}$), only $N_c$ is varied (b). With $N_c$ held constant at the *S. aureus* value (0.025 M), only $\lambda$ is varied (c). The table summarizes the values for surface charge density and surface softness used in each plot, and the calculated capture onset potentials and slopes (d).

The magnitude of the change in both capture onset potential and slope, when two differing species are considered, is smaller for the surface charge density than for zeta

potential. Larger variations in capture onset potential, as well as in slope, could more likely be ascribed to zeta potential alone than to surface charge density alone. However, these two parameters are very closely related, and likely will change together. As discussed above, variation solely in overall conductivity will only result in a difference in the capture onset potential and will leave the slope unchanged.

As with population differences in zeta potential, varying system properties, including particle concentration, medium permittivity, or medium viscosity, will not cause much of an effect on the difference in capture onset potential of two populations with differing surface charge densities. The concentration, medium permittivity, and medium viscosity, however, do appear to affect the difference in slopes. As discussed above, this makes it difficult to attribute a change in slope to any one specific property.

Experimental dielectrophoretic data for a strain of *S. epidermidis* (ATCC 35983) [29] can be compared to the results from the model using the surface charge density from that strain that was determined by Kiers et al. [83]. The capture onset potential for this strain, using the same channel that is used for the modeling presented here, was determined experimentally to be $443 \pm 51$ V. Kiers at al. found the surface charge density of this strain to be 0.028 M (or $3.36 \cdot 10^{-6}$ mmol/m$^2$), with a $\lambda$ of 1.9 nm$^{-1}$. Setting the surface softness and surface charge density as that found by Kiers et al., and other parameters as in that experiment, results in a calculated capture onset potential of 416 V. This is within the standard deviation of the experimentally-determined capture onset potential, showing that this model accurately reflects experiment.

#### 3.4.3.4 Charge Distribution/Multipoles and Dipoles

The presence of permanent dipoles can affect both the electrophoretic and dielectrophoretic mobilities. Altering the dipole will cause a difference in both the slope and the capture onset potential. A distribution of charges in a sphere is well represented as the potential distribution of a system of multipoles [19]. The shape and deformability of a cell, as well as the mobility of surface charges, all will affect that system of multipoles.

Typical DEP relationships, such as equation 6, consider only the dipole approximation of all multipoles in a particle. While using the equations that include the higher-order multipoles can provide a refined value, it does not add any new information for most systems [84]. Nevertheless, exceptions to the assumption of the dipole as a good approximation do exist [19, 40]. In general, the dipole force dominates for small particles relative to the size of the electric field inhomogeneity, but the multipole force terms become important as particles become larger relative to the field variations [19, 40, 85, 86]. One such case is described by Washizu [86, 87], where a particle is located near the center of quadrupole electrodes, and another is when the particle is larger than one-tenth of the electrode spacing [84].

### 3.5 Conclusion

Very subtle cellular differences have allowed differentiation and separation in dielectrophoretic systems, but it is difficult to connect this with known biological structures. The mathematical model of the data presented here provides a starting point to discover this needed connectivity. The bracketing of literature-based high and low

real-world values of conductivity, zeta potential, and surface charge density allow for an understanding of likely and unlikely possibilities within these systems.

The biophysical properties of a cell are a summation of many values, and DEP gives a single value. Thus, many properties are collapsed and will appear similar in such a system. Furthermore, a single change in the makeup of a cell may change multiple parameters. When the type or extent of the cellular difference is unknown, this work can help in assigning the origin of the differences. For a well-vetted system where likely differences are known, this model can indicate the extent of a dissimilarity between two populations, or perhaps the expression of a specific protein.

### 3.6 References


1. H. A. Pohl, *Journal of Applied Physics*, 1951, *22*, 869-871.
2. R. Pethig, *Journal of The Electrochemical Society*, 2016, *164*, B3049-B3055.
3. C. Asbury, L., A. H. Dierks and G. van den Engh, *Electrophoresis*, 2002, *23*, 2658-2666.
4. C.-F. Chou, J. O. Tegenfeldt, O. Bakajin, S. S. Chan, E. C. Cox, N. Darnton, T. Duke and R. H. Austin, *Biophysical Journal*, 2002, *83*, 2170-2179.
5. P. R. C. Gascoyne, J. Noshari, T. J. Anderson and F. F. Becker, *Electrophoresis*, 2009, *30*, 1388-1398.
6. P. V. Jones, A. F. DeMichele, L. Kemp and M. A. Hayes, *Analytical and Bioanalytical Chemistry*, 2014, *406*, 183-192.
7. B. H. Lapizco-Encinas, S. Ozuna-Chacon and M. Rito-Palomares, *Journal of Chromatography A*, 2008, *1206*, 45-51.
8. B. H. Lapizco-Encinas, B. A. Simmons, E. B. Cummings and Y. Fintschenko, *Analytical Chemistry*, 2004, *76*, 1571-1579.
9. G. H. Markx, Y. Huang, X.-F. Zhou and R. Pethig, *Microbiology*, 1994, *140*, 585-591.

10. S. Otto, U. Kaletta, F. F. Bier, C. Wenger and R. Holzel, *Lab on a Chip*, 2014, *14*, 998-1004.

11. J. Regtmeier, T. T. Duong, R. Eichhorn, D. Anselmetti and A. Ros, *Analytical Chemistry*, 2007, *79*, 3925-3932.

12. S. J. R. Staton, P. V. Jones, G. Ku, S. D. Gilman, I. Kheterpal and M. A. Hayes, *Analyst*, 2012, *137*, 3227-3229.

13. X.-B. Wang, Y. Huang, J. P. H. Burt, G. H. Markx and R. Pethig, *Journal of Physics D: Applied Physics*, 1993, *26*, 1276-1285.

14. M. Washizu, S. Suzuki, O. Kurosawa, T. Nishizaka and T. Shinohara, *IEEE Transactions on Industry Applications*, 1994, *30*, 835-843.

15. T. N. G. Adams, K. M. Leonard and A. R. Minerick, *Biomicrofluidics*, 2013, *7*, 64114.

16. P. V. Jones, S. J. R. Staton and M. A. Hayes, *Analytical and Bioanalytical Chemistry*, 2011, *401*, 2103-2111.

17. Y. Huang, R. Holzel, R. Pethig and X.-B. Wang, *Physics in Medicine and Biology*, 1992, *37*, 1499-1517.

18. T. B. Jones, *Electromechanics of Particles*, Cambridge University Press, New York, 1995.

19. R. Pethig, *Biomicrofluidics*, 2010, *4*, 022811.

20. H. A. Pohl, *Dielectrophoresis The behavior of neutral matter in nonuniform electric fields*, Cambridge University Press, New York, 1978.

21. M. Washizu and T. B. Jones, *Journal of Electrostatics*, 1994, *33*, 187-198.

22. J. S. Crane and H. A. Pohl, *Journal of Electrostatics*, 1978, *5*, 11-19.

23. Z. R. Gagnon, *Electrophoresis*, 2011, *32*, 2466-2487.

24. E. B. Cummings and A. K. Singh, *Analytical Chemistry*, 2003, *75*, 4724-4731.

25. F. F. Becker, X.-B. Wang, Y. Huang, R. Pethig, J. Vykoukal and P. R. C. Gascoyne, *Proceedings of the National Academy of Sciences of the United States of America*, 1995, *92*, 860-864.

26. A. Rohani, J. H. Moore, J. A. Kashatus, H. Sesaki, D. F. Kashatus and N. S. Swami, *Analytical Chemistry*, 2017, *89*, 5757-5764.

27. T. N. G. Adams, A. Y. L. Jiang, P. D. Vyas and L. A. Flanagan, *Methods*, 2018, *133*, 91-103.

28. S. K. Srivastava, P. R. Daggolu, S. C. Burgess and A. R. Minerick, *Electrophoresis*, 2008, *29*, 5033-5046.

29. P. V. Jones, S. Huey, P. Davis, R. Yanashima, R. McLemore, A. McLaren and M. A. Hayes, *Analyst*, 2015, *140*, 5152-5161.

30. W. A. Braff, D. Willner, P. Hugenholtz, K. Rabaey and C. R. Buie, *PLoS One*, 2013, *8*, e76751.

31. P. V. Jones and M. A. Hayes, *Electrophoresis*, 2015, *36*, 1098-1106.

32. A. LaLonde, M. F. Romero-Creel, M. A. Saucedo-Espinosa and B. H. Lapizco-Encinas, *Biomicrofluidics*, 2015, *9*, 064113.

33. A. R. Minerick, *AIChE Journal*, 2008, *54*, 2230-2237.

34. M. A. Saucedo-Espinosa and B. H. Lapizco-Encinas, *Electrophoresis*, 2015, *36*, 1086-1097.

35. S. J. R. Staton, K. P. Chen, T. J. Taylor, J. R. Pacheco and M. A. Hayes, *Electrophoresis*, 2010, *31*, 3634-3641.

36. J. T. Davies and E. K. Rideal, *Interfacial Phenomena*, Academic Press, New York, 1961.

37. N.-T. Nguyen and S. T. Wereley, *Fundamentals and Applications of Microfluidics*, Artech House, Boston, 2nd edn., 2006.

38. P. Tabeling, *Introduction to Microfluidics*, Oxford University Press, New York, 2005.

39. R. W. Clarke, J. D. Piper, L. Ying and D. Klenerman, *Physical Review Letters*, 2007, *98*, 198102.

40. H. Nili and N. G. Green, *Physical Review E: Statistical, Nonlinear, and Soft Matter Physics*, 2014, *89*, 063302.

41. A. Irimajiri, T. Hanai and A. Inoyue, *Journal of Theoretical Biology*, 1979, *78*, 251-269.

42. W. Bai, K. Zhao and K. Asami, *Colloids and Surfaces, B: Biointerfaces*, 2007, *58*, 105-115.

43. T. Kakutani, S. Shibatani and M. Sugai, *Bioelectrochemistry and Bioenergetics*, 1993, *31*, 131-145.

44. H. Ohshima and T. Kondo, *Journal of Colloid and Interface Science*, 1987, *116*, 305-311.

45. H. Ohshima and T. Kondo, *Journal of Colloid and Interface Science*, 1989, *130*, 281-282.

46. R. Sonohara, N. Muramatsu, H. Ohshima and T. Kondo, *Biophysical Chemistry*, 1995, *55*, 273-277.

47. E. Daly and B. R. Saunders, *Physical Chemistry Chemical Physics*, 2000, *2*, 3187-3193.

48. J. L. Ortega-Vinuesa, R. Hidalgo-Alvarez, F. J. de las Nieves, C. L. Davey, D. J. Newman and C. P. Price, *Journal of Colloid and Interface Science*, 1998, *204*, 300-311.

49. S. Takashima and H. Morisaki, *Colloids and Surfaces, B: Biointerfaces*, 1997, *9*, 205-212.

50. M. Torimura, S. Ito, K. Kano, T. Ikeda, Y. Esaka and T. Ueda, *Journal of Chromatography B*, 1999, *721*, 31-37.

51. J. L. Anderson, *Journal of Colloid and Interface Science*, 1985, *105*, 45-54.

52. M. C. Fair and J. L. Anderson, *Journal of Colloid and Interface Science*, 1989, *127*, 388-400.

53. M. D. Pysher and M. A. Hayes, *Langmuir*, 2005, *21*, 3572-3577.

54. M. Dinpajooh and D. V. Matyushov, *Journal of Chemical Physics*, 2016, *145*, 014504.

55. M. Dinpajooh and D. V. Matyushov, *Physica A: Statistical Mechanics and its Applications*, 2016, *463*, 366-375.

56. D. V. Matyushov, *Journal of Chemical Physics*, 2004, *120*, 1375-1382.

57. D. V. Matyushov, *Journal of Chemical Physics*, 2012, *136*, 085102.

58. D. V. Matyushov, *Molecular Physics*, 2014, *112*, 2029-2039.

59. S. Seyedi and D. V. Matyushov, *Chemical Physics Letters*, 2018, *712*, accepted (preprint available from corresponding author).

60. C. V. Crowther and M. A. Hayes, *Analyst*, 2017, *142*, 1608-1618.

61. W. A. Braff, A. Pignier and C. R. Buie, *Lab on a Chip*, 2012, *12*, 1327-1331.

62. F. Camacho-Alanis, L. Gan and A. Ros, *Sensors and Actuators B: Chemical*, 2012, *173*, 668-675.

63. J. Ding, R. M. Lawrence, P. V. Jones, B. G. Hogue and M. A. Hayes, *Analyst*, 2016, *141*, 1997-2008.

64. J. Ding, C. Woolley and M. A. Hayes, *Analytical and Bioanalytical Chemistry*, 2017, *409*, 6405-6414.

65. A. Nakano, F. Camacho-Alanis and A. Ros, *Analyst*, 2015, *140*, 860-868.

66. D. V. Polniak, E. Goodrich, N. Hill and B. H. Lapizco-Encinas, *Journal of Chromatography A*, 2018, *1545*, 84-92.

67. M. T. Rabbani, C. F. Schmidt and A. Ros, *Analytical Chemistry*, 2017, *89*, 13235-13244.

68. M. A. Saucedo-Espinosa, A. LaLonde, A. Gencoglu, M. F. Romero-Creel, J. R. Dolas and B. H. Lapizco-Encinas, *Electrophoresis*, 2016, *37*, 282-290.

69. B. Brazey, J. Cottet, A. Bolopion, H. Van Lintel, P. Renaud and M. Gauthier, *Lab on a Chip*, 2018, *18*, 818-831.

70. C.-H. Chuang and Y.-W. Huang, *Microelectronic Engineering*, 2012, *97*, 317-323.

71. B. H. Lapizco-Encinas, B. A. Simmons, E. B. Cummings and Y. Fintschenko, *Electrophoresis*, 2004, *25*, 1695-1704.

72. H. Moncada-Hernandez, J. L. Baylon-Cardiel, V. H. Perez-Gonzalez and B. H. Lapizco-Encinas, *Electrophoresis*, 2011, *32*, 2502-2511.

73. S. Ozuna-Chacon, B. H. Lapizco-Encinas, M. Rito-Palomares, S. O. Martinez-Chapa and C. Reyes-Betanzo, *Electrophoresis*, 2008, *29*, 3115-3122.

74. Z. Wang, T. Han, T.-J. Jeon, S. Park and S. M. Kim, *Sensors and Actuators B: Chemical*, 2013, *178*, 683-688.

75. Y. Tomizawa, E. Tamiya and Y. Takamura, *Physical Review E: Statistical, Nonlinear, and Soft Matter Physics*, 2009, *79*, 051902.

76. R. Pethig, *Dielectrophoresis : theory, methodology and biological applications*, Hoboken, NJ : John Wiley & Sons, Ltd, 1st edn., 2017.

77. G. H. Markx and C. L. Davey, *Enzyme and Microbial Technology*, 1999, *25*, 161-171.

78. R. Pethig and G. H. Markx, *Trends in Biotechnology*, 1997, *15*, 426-432.

79. R. Holzel, *Biochimica et Biophysica Acta*, 1999, *1450*, 53-60.

80. J. Olsson and P.-O. Glantz, *Archives of Oral Biology*, 1977, *22*, 461-466.

81. A. van der Wal, M. Minor, W. Norde, A. J. B. Zehnder and J. Lyklema, *Journal of Colloid and Interface Science*, 1997, *186*, 71-79.

82. W. W. Wilson, M. M. Wade, S. C. Holman and F. R. Champlin, *Journal of Microbiological Methods*, 2001, *43*, 153-164.

83. P. J. M. Kiers, R. Bos, H. C. van der Mei and H. J. Busscher, *Microbiology*, 2001, *147*, 757-762.

84. T. Schnelle, T. Muller, S. Fiedler and G. Fuhr, *Journal of Electrostatics*, 1999, *46*, 13-28.

85. E. Liang, R. L. Smith and D. S. Clague, *Physical Review E: Statistical, Nonlinear, and Soft Matter Physics*, 2004, *70*, 066617.

86. M. Washizu, T. B. Jones and K. V. I. S. Kaler, *Biochimica et Biophysica Acta*, 1993, *1158*, 40-46.

87. M. Washizu, *Journal of Electrostatics*, 1992, *29*, 177-188.

# CHAPTER 4

# BIOPHYSICAL DIFFERENTIATION OF SUSCEPTIBILITY AND CHEMICAL DIFFERENCES IN *STAPHYLOCOCCUS AUREUS*

## 4.1 Introduction

*Staphylococcus aureus* colonizes approximately 30-50% of adults, with 10-20% persistently colonized [1-3]. This colonization may not cause disease or infection, but it does increase the risk for infection, especially for postoperative wound (surgical site) infections [4, 5]. *S. aureus* has been shown to cause skin and soft tissue infections, bone, joint and implant related infections, pneumonia, bacteremia (blood poisoning), endocarditis, and gastroenteritis (food poisoning) [6, 7].

Treatment of such infections was made possible by the discovery and use of antimicrobials, beginning in the 1940s. However, resistance to antimicrobials emerged soon after their introduction [8]. In 1959, methicillin was introduced to treat *S. aureus* infections resistant to the commonly-used penicillin. To cause cell death, methicillin and other $\beta$-lactam antimicrobials bind to the penicillin binding proteins (PBPs). Methicillin resistance in *S. aureus* is conferred by the presence of a penicillin binding protein, PBP2a, that has a less-accessible binding site than other PBPs which doesn't allow methicillin to bind [9, 10]. This enzyme is expressed in addition to other PBPs found in the bacteria [11].

Methicillin-resistant *S. aureus* causes hundreds of thousands of hospitalizations each year in the United States [9]. Antimicrobial resistance, including methicillin

resistance, causes the death of approximately 700,000 people around the world each year. This number is expected to rise if the problem of resistance is not addressed [12].

Treating infections caused by resistant pathogens requires using the proper antimicrobials, ones to which the microorganism is known to be susceptible. Traditional methods of bacterial identification and susceptibility testing are time-consuming, taking up to 14 days, often requiring multiple rounds of culture. During this time, empiric treatment is begun based on clinical judgement to give the patients the best possible outcome given the limitations of current methods. A broad-spectrum antimicrobial is required at this stage to cover the most likely microorganisms that may be causing the infection. This leads to a broader disruption of the host biome than would occur with focused treatment for the specific pathogen and a greater risk for the emergence of organisms resistant to the broad antimicrobials used, perpetuating the problem [13].

A rapid detection method for antimicrobial resistance would improve patient outcomes by allowing for proper treatment as well as decrease the unnecessary use of broad-spectrum antimicrobials. Most dramatically, initially choosing the correct antimicrobial to treat an infection increases survival [14]. Many methods are being developed to decrease time-to-result in susceptibility testing. Genotyping methods include pulsed field gel electrophoresis, multilocus sequence typing, random amplification polymorphism DNA typing, and the use of PCR, among others [7]. Phenotypic approaches for testing susceptibility to various antimicrobials include microcalorimetry, colorimetric pH tests, fluorescence in situ hybridization with time lapse microscopy, ultra-high-resolution bacterial mass measurement, and various mass

spectrometry methods [13, 15-17]. Each of these methods have their advantages and disadvantages. The genotypic methods indicate the potential of bacteria to be antimicrobial resistant, but does not indicate the extent to which the gene is expressed or the level of susceptibility [13]. Many phenotypic methods test for a single type of resistance, and thus would have to be performed in tandem with other methods to give a complete picture.

Bacteria are a common target of dielectrophoresis (DEP) research towards determining the biophysical behavior of specific species and strains under a variety of circumstances. This knowledge has been employed in many applications, including the separation of live and dead bacteria [18]. Bacteria can be distinguished based on small biophysical differences, exemplified by study of *E. coli* serotypes [19]. DEP has been used to distinguish antimicrobial resistant and susceptible bacteria, specifically gentamicin resistant and susceptible *Staphylococcus epidermidis* [20]. Dielectrophoretic methods, including those to discern antimicrobial susceptibility, typically take minutes, which is much faster than methods requiring multiple cultures. This phenomenon uses electric field gradients to probe the properties of polarizable particles. First described by Pohl in 1951 [21], DEP has since been used with a variety of analytes, from viruses and proteins to bacteria and stem cells [18-20, 22-33].

Originally, electrode-based dielectrophoresis was used, where patterned electrodes created the electric field gradients necessary for DEP. The technique was used to separate analytes using AC fields and depended on differences in the conductivity or permittivity of the particle [21, 34, 35]. In 2003, insulator-based dielectrophoresis

(iDEP) was introduced, where insulators instead of electrodes were used to create the electric field gradients [36]. With iDEP, DC fields are used, and therefore electroosmosis and electrophoresis can be utilized for analyte transport. This also provides other physical properties that can be investigated [37].

Here, two strains of *Staphylococcus aureus* are studied, one methicillin-resistant (MRSA) and one methicillin-susceptible (MSSA), to determine whether they can be distinguished with DEP when tagged with a fluorescent label. The same strains were studied without the fluorescent label to demonstrate whether the differentiation can be label-free. Finally, the same populations with and without the fluorescent label are compared. This chapter shows the differentiation of MRSA and MSSA both with and without a chemical label, as well as the differentiation based on biophysical differences introduced by the label itself.

**4.2 Theory**

The three main effects that cause motion of particles in a microchannel when an electric field is applied are electroosmosis, electrophoresis, and dielectrophoresis. These phenomena have been described in detail previously [35, 36, 38-41]. Each will be briefly described here, as well as the phenomenon of dielectrophoretic capture.

Electroosmosis is the bulk motion of a fluid in response to charges at the walls of the microchannel. The electroosmotic velocity is given by [38, 41]

$$\boldsymbol{v}_{EOF} = \mu_{EOF}\boldsymbol{E} = -\frac{\varepsilon\zeta_w}{\eta}\boldsymbol{E} \qquad (1)$$

where $\mu_{EOF}$ is the electroosmotic mobility, $E$ is the applied electric field, $\varepsilon$ is the permittivity of the medium, $\zeta_w$ is the zeta potential of the wall, and $\eta$ is the viscosity of the medium.

Electrophoresis is the motion of a charged particle in response to an electric field. The electrophoretic velocity, much like the electroosmotic velocity, is given by the equation [38, 41]

$$\boldsymbol{v}_{EP} = \mu_{EP}\boldsymbol{E} = -\frac{\varepsilon\zeta_p}{\eta}\boldsymbol{E} \tag{2}$$

where $\mu_{EP}$ is the electrophoretic mobility and $\zeta_p$ is the zeta potential of the particle. Electroosmosis and electrophoresis are both directly proportional to the electric field, and are considered together to give the electrokinetic velocity of the particle

$$\boldsymbol{v}_{EK} = \boldsymbol{v}_{EOF} + \boldsymbol{v}_{EP} \tag{3}$$

The electrokinetic mobility, $\mu_{EK}$, describes the forward flow of the analyte down the microchannel.

Dielectrophoresis describes the motion of a polarizable particle in the presence of an electric field gradient. Rather than relying on the charge of the analyte, DEP requires only that a particle be polarizable, or have an inducible dipole moment. The dielectrophoretic velocity experienced by a spherical particle is

$$\boldsymbol{v}_{DEP} = \mu_{DEP}\nabla|\boldsymbol{E}|^2 = \frac{\varepsilon_m r^2 f_{CM}}{3\eta}\nabla|\boldsymbol{E}|^2 \tag{4}$$

where $\mu_{DEP}$ is the dielectrophoretic mobility, $r$ is the radius of the particle, and $f_{CM}$ is the Clausius-Mossotti factor. In DC fields, the Clausius-Mossotti factor is [18]

$$f_{CM} = \frac{\sigma_p - \sigma_m}{\sigma_p + 2\sigma_m} \tag{5}$$

where $\sigma_p$ is the conductivity of the particle and $\sigma_m$ is the conductivity of the medium. The sign of this factor indicates whether a particle will experience positive DEP (attracted to regions of high field gradient) or negative DEP (repelled from regions of high field gradient).

Capture in dielectrophoretic systems occurs when the flux, $\boldsymbol{j} \cdot \boldsymbol{E}$, of a given particle past a particular point in the channel is zero. The flow of particles ($j$) in a microchannel is [18, 42]

$$\boldsymbol{j} = D\nabla \mathrm{C} + \mathrm{C}(v_{bulk} + v_{EK} + v_{DEP}) \tag{6}$$

where $D$ is the diffusion coefficient, $C$ is particle concentration, and $v_{bulk}$ is the motion due to pressure-driven flow. In many dielectrophoretic systems, $D$ is relatively negligible and is considered to be zero here. Likewise, in systems where the pressure is balanced, $v_{bulk}$ is also zero. As a result, and substituting equations 2 and 4 for EK and DEP velocities respectively, equation 6 becomes

$$\boldsymbol{j} = \mu_{EK} E + \mu_{DEP} \nabla |\boldsymbol{E}|^2 \tag{7}$$

Trapping then occurs when

$$(\mu_{EK} E + \mu_{DEP} \nabla |\boldsymbol{E}|^2) \cdot \boldsymbol{E} \geq 0 \tag{8}$$

Rearranging this gives the condition for capture:

$$\frac{\mu_{EK}}{\mu_{DEP}} \leq \frac{\nabla E^2}{E} \tag{9}$$

This ratio of mobilities, $\frac{\mu_{EK}}{\mu_{DEP}}$, is dependent on the properties of the particles and is related to the conditions under which they will be captured. The lowest potential at which

capture will occur (the capture onset potential) is related to the ratio of mobilities, according to

$$\frac{\mu_{EK}}{\mu_{DEP}} = \frac{\nabla E^2}{E} \tag{10}$$

Using a multiphysics software such as COMSOL, the potential applied in a microchannel can be related to the value of $\frac{\nabla E^2}{E}$ at that location, which has the same value as the ratio of mobilities when this potential is the capture onset potential. Thus, the potential at which capture begins to occur for a specific analyte can be correlated to a ratio of mobilities for that analyte.

## 4.3 Materials and Methods

### 4.3.1 Microdevice Fabrication

All experiments were carried out on a microchannel previously described [19, 20, 31, 43, 44]. The microchannel geometry consists of equilateral triangles along the channel walls, with opposing tips forming a constriction, termed a gate. The size of the triangles increases from inlet to outlet, with six of each size repeating consecutively. This increase in triangle size causes the gate width, or the distance between opposing points of the triangles, to decrease from inlet to outlet. The channel used in these experiments has a length of 4.1 cm, a width of 1000 $\mu$m, and an average depth of 16.8 $\mu$m. The largest gate width, nearest the inlet, is 945 $\mu$m, while the smallest, nearest the outlet, is 27 $\mu$m.

Template wafers were fabricated using soft-lithography techniques. Four-inch Si wafers were coated with AZ 4330 photoresist (AZ Electronic Materials, Branchberg, NJ).

To expose the photoresist, a glass chrome mask (JD Photo-Tools, United Kingdom) with the channel pattern was used. After exposure, the wafers were developed then etched using reactive ion etching (ICP etcher, SPTS, San Jose, CA) with $SF_6$ and $C_4F_8$ gases. Any leftover photoresist was then removed.

To make the devices used in experiments, polydimethylsiloxane (PDMS) (Sylgard 184, Dow/Corning, Midland, MI) was poured onto the wafers and cured for one hour at 70°C. The PDMS casts were then peeled from the wafer, trimmed to size, and punched with 3.0 mm diameter holes to allow access to the inlet and outlet reservoirs at each end. These PDMS casts were stored in the freezer for up to one month prior to use.

For dielectrophoretic experiments, the trimmed and punched PDMS casts were bonded to a glass microscope slide. After cleaning with acetone and isopropyl alcohol (glass) or isopropyl alcohol only (PDMS) and rinsing with water, both the PDMS and glass were treated with oxygen plasma using a plasma cleaner (PDC-32G, Harrick Plasma, Ithaca, NY) for 60 seconds at 18 W. The PDMS and glass were then sealed upon contact. The resulting microchannel had three walls of PDMS and one wall of glass, with access holes through the PDMS at each end. The microdevices were used on the same day as they were bonded.

### 4.3.2 Bacterial Preparation and Labeling

Four bacterial suspensions, unlabeled MRSA, unlabeled MSSA, labeled MRSA, and labeled MSSA were prepared. Two strains of *Staphylococcus aureus*, methicillin-resistant ATCC 43300 (MRSA) and methicillin-sensitive ATCC 29213 (MSSA), were obtained. Seed stock was stored in tryptic soy broth (TSB) with 10% glycerol at -80°C.

This seed stock was streaked onto TSB agar plates and incubated overnight at 37°C. To grow a liquid culture, aliquots of 10 mL sterile TSB were placed in culture tubes, which were then inoculated with a single colony of one strain, resulting in a monoclonal culture. These were then placed in a shaker/incubator overnight at 37°C and 250 RPM. The culture was allowed to reach late log phase, where the concentration of bacteria was approximately $10^9$ CFU/mL. A 1:10 dilution of the resulting culture was made using 2 mM phosphate buffer (PB) at pH 7.4. The bacteria were then either labeled with NHS-rhodamine (Thermo Scientific, Rockford, IL) or left unlabeled.

The bacteria to be left unlabeled were centrifuged twice at 1677 × g for 5 minutes. Following the first centrifugation, the supernatant was removed and the pellet resuspended in 2 mM PB. After the final centrifugation, the supernatant was removed and the pellet was resuspended in 2 mM PB with 4 mg/mL bovine serum albumin (BSA) (Sigma, St. Louis, MO).

Other bacteria were labeled with NHS-rhodamine (excitation wavelength 552 nm, emission wavelength 575 nm) dye. A 10 mg/mL solution of NHS-rhodamine in DMSO was made and 20 $\mu$L of that solution were added to 1 mL of the 1:10 dilution of cells. This was then incubated in a 37°C water bath for 20 minutes. The cells were then washed as described above for the unlabeled cells, with three total centrifugations.

Cells were washed and/or labeled on the day they were used. Two separate plates grown from seed stock were used in these experiments, and at least three separate liquid cultures were used for each population studied.

### 4.3.3 DEP Experiments

A completed microdevice was filled with 15 μL 2 mM PB at pH 7.4 in both the inlet and outlet reservoirs using the punched access holes. The buffer in the reservoirs was then removed, and the channel was conditioned by filling the inlet with 15 μL PB with 4 mg/mL BSA [45]. After allowing the PB with BSA to stand in the microchannel for 15 minutes, the buffer was again removed from the reservoirs. The bacterial sample was then introduced into the channel by pipetting 15 μL of the labeled or unlabeled washed culture into the inlet reservoir, allowed to stand for 5 minutes to fill the channel, and then 15 μL 2 mM PB with BSA was placed in the outlet reservoir to create a pressure balance between the two reservoirs.

The microchannel was placed on the stage of an Olympus IX70 inverted microscope (Center Valley, PA) with a 4x objective. Hydrodynamic flow was balanced by observing particle motion in the microchannel and pipetting 2 mM PB with BSA buffer into the necessary reservoir to equalize the pressure. A mercury short arc lamp (H30 102 w/2, OSRAM) was used as a light source for fluorescence microscopy, with an Olympus DAPI, FITC, and Texas Red triple band pass filter. For the unlabeled experiments, bright field illumination with an incandescent lamp was used to directly illuminate the channel. Platinum electrodes with diameter 0.404 mm (Alfa Aesar, Ward Hill, MA) were inserted into the inlet and outlet reservoirs using the punched access holes. These electrodes were connected to a HVS448 3000D high voltage sequencer (Labsmith, Inc., Livermore, CA). DC potentials of 100 V to 1200 V, for labeled bacteria, and 100 V to 1000 V, for unlabeled bacteria, were applied across the microchannel in 100

V increments to find the potential at which capture begins to occur. The 27 μm gate nearest the inlet, and the particle motion and capture at this location, was observed. Images and video of the particle motion in the microchannel were obtained with a monochrome QICAM cooled CCD camera (QImaging, Inc., Surrey, BC) and Streampix V image capture software (Norpix, Inc., Montreal, QC). Image J software (National Institutes of Health, Bethesda, Maryland) was used for image analysis.

### 4.3.4 Data Modeling

The mathematical model described by Hilton and Hayes is used to analyze the data obtained from these iDEP experiments [37]. Briefly, the number of cells that can reach the gate, and therefore capture, is determined based on the particle velocity (equation 3), the concentration of particles ($n$), the time potential is applied ($t$), and the dimensions of the microchannel, according to

$$N = n\mu_{EK}twhE_{ave} \tag{11}$$

where $w$ is the average width of the channel, $h$ is the height of the channel, and $E_{ave}$ is the average magnitude of the electric field in the microchannel. The total signal intensity from the region of interest is then determined by accounting for the nominal signal intensity ($\gamma$) and the variable fluorescence intensity per particle due to the vertical stacking of particles in the channel with a correction factor ($s$). The fluorescence intensity for a given region of interest, with a specific applied potential, is then

$$FI = \frac{\gamma n\mu_{EK}twhE_{ave}}{s} \tag{12}$$

The time can be varied, resulting in a time-based model, or the applied potential varied, resulting in a voltage-based model (Figure 4.1). The voltage-based model includes a

term accounting for the capture onset potential. This term ($c$) is found when the two sides of equation 9 are equal. For the specific dimensions of the channel used in this study, COMSOL modeling (version 5.1 with AC/DC module) was used to determine the distribution of the electric field. Values of $E_{ave}(V)$, $E_{max}$, and $\nabla|E|^2{}_{max}$ along the centerline were used to find an equation for the magnitude of the electric field (in units of V/cm) as a function of the applied potential, $V$

$$E_{ave}(V) = 0.24 * V \tag{13}$$

as well as an equation for $c$

$$\left[\frac{\nabla|E|^2{}_{max}}{E_{max}}(c)\right] = [1.4 * 10^7] * c = \frac{\mu_{EK}}{\mu_{DEP}} \tag{14}$$

$$c = \frac{1}{1.4 * 10^7}\left(\frac{\mu_{EK}}{\mu_{DEP}}\right) \tag{15}$$

The voltage-based model is best described by a piecewise function, with the discontinuity at the capture onset potential:

$$FI(V) = \begin{cases} 0 & if\ V < \frac{1}{1.4 * 10^7}\left(\frac{\mu_{EK}}{\mu_{DEP}}\right) \\ 0.24 * \frac{\gamma n \mu_{EK} twh}{s}\left[V - \frac{1}{1.4 * 10^7}\left(\frac{\mu_{EK}}{\mu_{DEP}}\right)\right] & if\ V \geq \frac{1}{1.4 * 10^7}\left(\frac{\mu_{EK}}{\mu_{DEP}}\right) \end{cases} \tag{16}$$

From this equation, two features of the data can be compared between various strains studied: the slope and the capture onset potential, which is the potential at which the junction occurs between the two pieces of the function. The slope of the data in the second part of the piecewise function can be related to the velocity, and therefore the electrokinetic mobility, of the analyte. The capture onset potential can be used to determine the ratio of mobilities for the analyte (Figure 4.1).

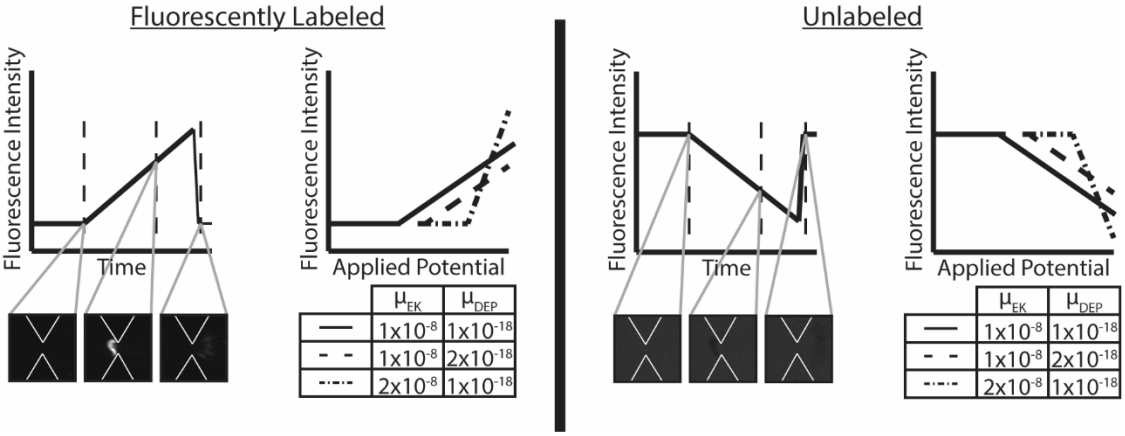



Figure 4.1 Dielectrophoretic data features, such as the slope and the *x*-intercept, signal important differences in populations. For fluorescently labeled cells (left), the signal intensity will increase as time increases while the potential is applied. The plot of fluorescence intensity at a given time of applied potential vs. applied potential shows how varying $\mu_{EK}$ and/or $\mu_{DEP}$ will result in an altered slope and/or *x*-intercept. For unlabeled cells (right), the signal intensity will decrease with time while the potential is applied, as the capture appears as a dark band in the channel. Similar variations in capture onset potential and slope will occur with varying $\mu_{EK}$ and/or $\mu_{DEP}$.

### 4.3.5 Safety Considerations

All bacteria used in this study are Biosafety Level II. Experiments were performed in an approved Biosafety Level II laboratory, within accordance with the current version of the CDC/NIH BMBL publication.

## 4.4 Results

Rhodamine-labeled MRSA, rhodamine-labeled MSSA, unlabeled MRSA, and unlabeled MSSA were studied with dielectrophoresis. The fluorescence or optical intensity at the capture location was measured after 15 s of applied potential for varying potentials (Figure 4.2). In each case, the data sets were well-behaved, and information about the populations, such as the ratio of mobilities or the electrokinetic mobility, could be determined. For the rhodamine-labeled bacteria, an increase in capture resulted in an

increase of signal intensity. For the unlabeled bacteria, the capture appeared as a darkened band where the signal decreased with an increasing amount of capture.

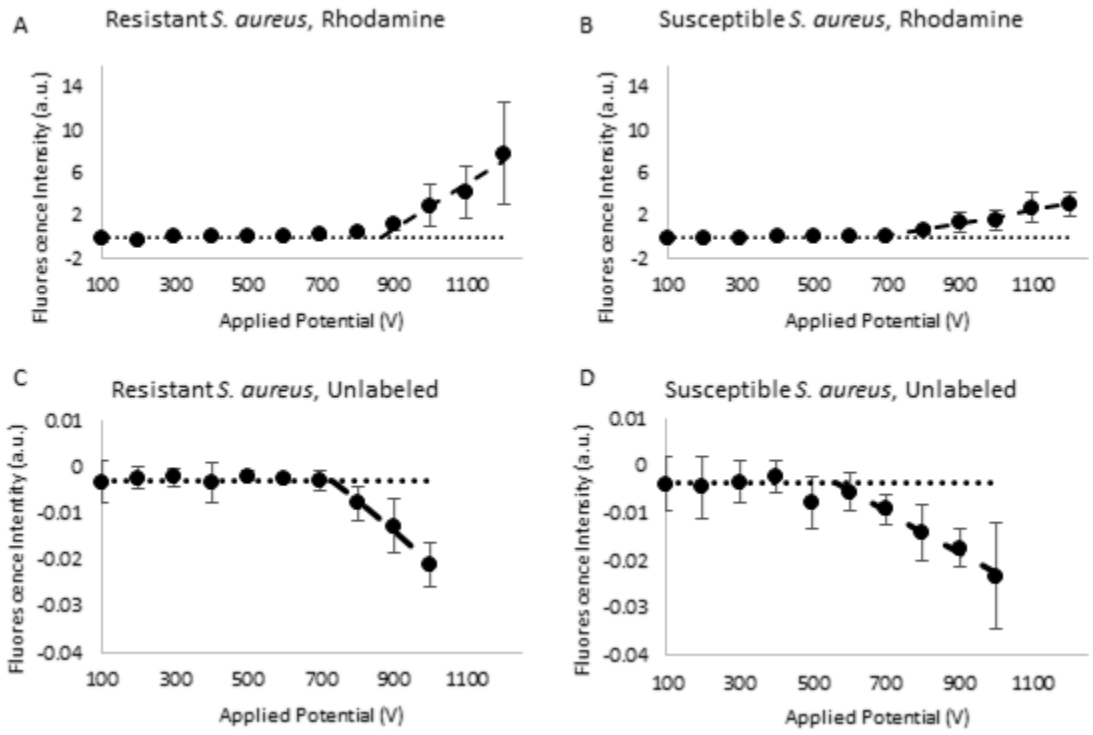



Figure 4.2 Dielectrophoretic capture data from MRSA (A and C) and MSSA (B and D) when labeled with rhodamine (A and B) or unlabeled (C and D), after 15 s of applied potential. The dotted line represents the baseline. The capture onset potential for each strain was 732 $\pm$ 44 V (A), 562 $\pm$ 59 V (B), 865 $\pm$ 71 V (C), and 685 $\pm$ 61 V (D). Each of these capture onset potentials are correlated to the ratio of the electrokinetic and dielectrophoretic mobilities of the bacteria. In the case of the labeled bacteria, the slope for the MRSA and MSSA strains are 21.3 $\pm$ 7.0·10$^{-3}$ a.u. (A) and 6.1 $\pm$ 1.2·10$^{-3}$ a.u. (B), respectively. For the unlabeled bacteria, the slopes are -6.6 $\pm$ 1.6·10$^{-5}$ a.u. (C) and -4.4 $\pm$ 0.9·10$^{-5}$ a.u. (D). Error bars are 95% confidence intervals, while reported error values are the standard deviation.

From the onset capture potential and equation 14, the ratio of mobilities for each population studied was found. Rhodamine-labeled MRSA had a ratio of mobilities, $\frac{\mu_{EK}}{\mu_{DEP}}$, of 1.24 $\pm$ 0.10·10$^{10}$ V/m$^2$. Unlabeled MRSA had a ratio of mobilities of 1.05 $\pm$ 0.06·10$^{10}$ V/m$^2$.

Similar to the MRSA strain, rhodamine-labeled MSSA was found to have an onset capture potential higher than that of the unlabeled bacteria. For the labeled MSSA strain, a ratio of mobilities of $9.86 \pm 0.89 \cdot 10^{9}$ V/m$^2$ was found. The ratio of mobilities for unlabeled MSSA was found to be $8.09 \pm 0.85 \cdot 10^{9}$ V/m$^2$.

The slopes of the voltage-dependent data for the MRSA and MSSA strains also give insight into the differences between them. For rhodamine-labeled MRSA, the slope of the voltage-dependent data was $21.3 \pm 7.0 \cdot 10^{-3}$ a.u. In contrast, the slope of the data for the rhodamine-labeled MSSA strain was $6.1 \pm 1.2 \cdot 10^{-3}$ a.u.

While the rhodamine-labeled bacteria are fluorescent and as such cause an increase in signal upon capture, the unlabeled bacteria appear as a dark band. As capture of unlabeled bacteria occurs, the size and intensity of the dark band change and a decrease in the signal intensity is observed. Unlabeled MRSA had a slope of $-6.6 \pm 1.6 \cdot 10^{-5}$ a.u., while unlabeled MSSA had a slope of $-4.4 \pm 0.9 \cdot 10^{-5}$ a.u.

**4.5 Discussion**

Significant differences between the ratio of mobilities of the MRSA and MSSA strains studied were found for both labeled and unlabeled bacteria, with a significance of $p < 0.05$ in each case. While only one methicillin-resistant and one methicillin-susceptible strain were studied, this shows the potential of this technique to differentiate between resistant and susceptible strains, although further testing would be needed to extend this to other bacterial strains. The onset capture potential is higher for the MRSA strain than the MSSA strain for both the labeled and the unlabeled bacteria. For the labeled bacteria, there is a difference of $180 \pm 21$ V in the capture onset potential, or a

$2.5 \pm 0.30 \cdot 10^9$ V/m$^2$ for difference in $\frac{\mu_{EK}}{\mu_{DEP}}$ between the MRSA and MSSA strains. For the unlabeled bacteria, this difference is 170 $\pm$ 20 V, or $2.4 \pm 0.29 \cdot 10^9$ V/m$^2$.

This work expands upon the biophysical differentiation of gentamicin resistant and susceptible *S. epidermidis* labeled with a fluorophore [20]. This is a demonstration that another antimicrobial resistance mechanism can be differentiated using dielectrophoretic capture. This work also shows that the label is not responsible for, or necessary for, distinguishing between these bacterial strains. The differentiation is based on the inherent differences in biophysical properties between the strains that is detectable by DEP, rather than a small difference undetectable by DEP, magnified by a label.

The slopes between the MRSA and MSSA bacteria also vary between strains and can be compared. In the case of both the labeled and unlabeled bacteria, the magnitude of the slope for MRSA was larger than that of MSSA. This indicates a difference in the electrokinetic mobilities between the two strains, with the mobility of the MRSA strain higher than that of the MSSA (equation 16). As with the capture onset potential, this difference in slope for the unlabeled bacteria eliminates potential variables added by the process of labeling or the presence of the label, showing that a difference occurs because of intrinsic properties of the two strains studied.

Using the mathematical model of dielectrophoretic data [37], an approximation of the electrokinetic mobility can be determined for the fluorescently-labeled particles. Assuming an average channel width of 0.3 mm and an $s$ factor of 15 to account for stacking and the depth-of-field, $\mu_{EK}$ for the labeled MRSA is $1.25 \pm 0.51 \cdot 10^{-8}$ m$^2$/V·s. With the same assumptions, $\mu_{EK}$ for the labeled MSSA is $7.01 \pm 1.6 \cdot 10^{-9}$ m$^2$/V·s. The

difference in the electrokinetic mobility of these two strains is $5.49 \pm 2.6 \cdot 10^{-9}$ $m^2/V \cdot s$. This effect size is large compared to the theoretical limit, which states that the minimum resolvable difference in electrokinetic mobility is $2 \cdot 10^{-12}$ $m^2/V \cdot s$ [46].

From these values for $\mu_{EK}$ and the ratio of mobilities, $\mu_{DEP}$ can be determined. For the labeled MRSA, $\mu_{DEP}$ is $1.01 \pm 0.42 \cdot 10^{-18}$ $m^4/V^2s$, while for the labeled MSSA $\mu_{DEP}$ is $7.1 \pm 1.7 \cdot 10^{-19}$ $m^4/V^2s$. Between these two strains, the difference in electrokinetic mobility is $3.0 \pm 1.4 \cdot 10^{-19}$ $m^4/V^2s$, while the theoretical minimum resolvable difference in dielectrophoretic mobility is $1 \cdot 10^{-23}$ $m^4/V^2s$ [46]. The dielectrophoretic mobilities of the MRSA and MSSA strains studied are significantly different at a 95% confidence level, which shows that the difference between the two populations does not affect only the electrokinetic mobility, but also the dielectrophoretic mobility. The values for electrokinetic and dielectrophoretic mobilities are similar to what have been previously reported for similar microorganisms [47, 48].

The electrophoretic response of cells has been shown to differ based on some specific cellular properties. Differing growth mediums result in variations in the properties of a population, giving measurable differences in the electrophoretic mobility. However, some properties, such as a specific antigen found in *Escherichia coli* cells, do not have a significant effect on electrophoresis [49]. Here, the difference in both the slope (the electrokinetic mobility) and the capture onset potential (the electrokinetic and/or dielectrophoretic mobilities) may be attributable to the presence of the PBP2a enzyme in the resistant population.

PBP2a is a membrane-anchored protein and has regions of both high and low charge (Figure 4.3). Beyond a surface charge change due to the presence of PBP2a enzymes, additions of membrane-anchored proteins could also cause changes in the fluidity of the membrane lipids or deformability of the cell, each of which would affect the dielectrophoretic behavior.

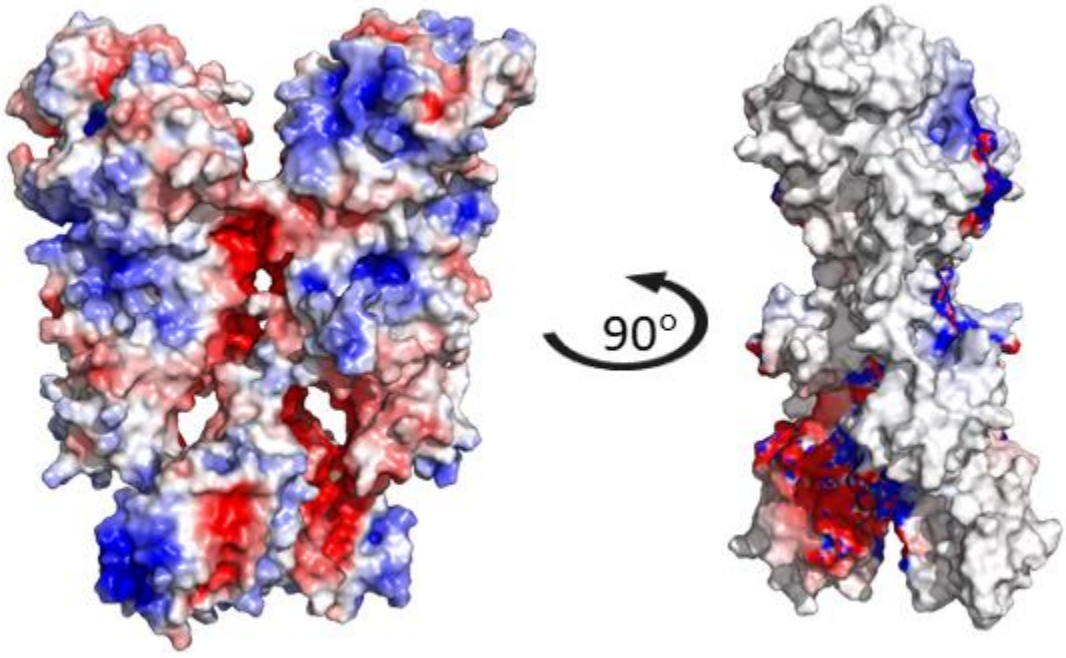



Figure 4.3 Structure and surface charge density map of PBP2a. This enzyme has areas of both positive (blue) and negative (red) charge. The protein is anchored to the cytoplasmic membrane at the N-terminus. Image generated using PyMOL(Protein Data Bank entry 5M18).

The complicated nature of proteins and the myriad of possible changes in cell properties that can occur in response to the addition of the enzyme make it difficult to assign the difference to a specific property. However, the known connections between DEP results and cellular properties allow for some categorization in their relationship, and the mathematical model [37] gives some insight into the nature of the difference

(Figure 4.1). Since both the slope and the capture onset potential differ between the two strains, the difference between the MRSA and MSSA strains will arise from dissimilar electrokinetic mobilities. From these to values, it was determined that the dielectrophoretic mobilities vary as well. While one dissimilarity between the MRSA and MSSA strains is a function of the addition of the mecA plasmid and the expression of the PBP2a enzyme, other differences between these two strains may exist.

Beyond biological differences, chemical changes to a cell can be made in the laboratory to cause a well-defined source of change for DEP behavior. Thus, another interesting comparison is between the labeled and unlabeled populations of each strain, as the label and the method of attachment is known. In the MRSA, the ratio of mobilities was found to be higher for the labeled bacteria than the unlabeled bacteria, with a difference of $1.9 \pm 0.19 \cdot 10^9$ V/m$^2$. The ratio of mobilities is also higher for the labeled than the unlabeled MSSA, by $1.7 \pm 0.23 \cdot 10^9$ V/m$^2$.

Since the identity and attachment chemistry of the label is established, the physical source of changes in DEP behavior is known. However, additional biophysical changes could also be present due to the addition of the label. The NHS-group on the rhodamine dye reacts with primary amines on the surface of the cell. Primary amines have a $pK_a$ of 10.6; therefore, they will have a positive charge under the experimental condition of pH 7.4. Reaction of a cell with NHS-rhodamine replaces a singly-positively charged functional group on the cell surface with an always-positive amine and a carboxylate, which is negatively charged at pH 7.4 (Figure 4.4). Thus, there is an overall decrease in surface charge upon labeling the cells.

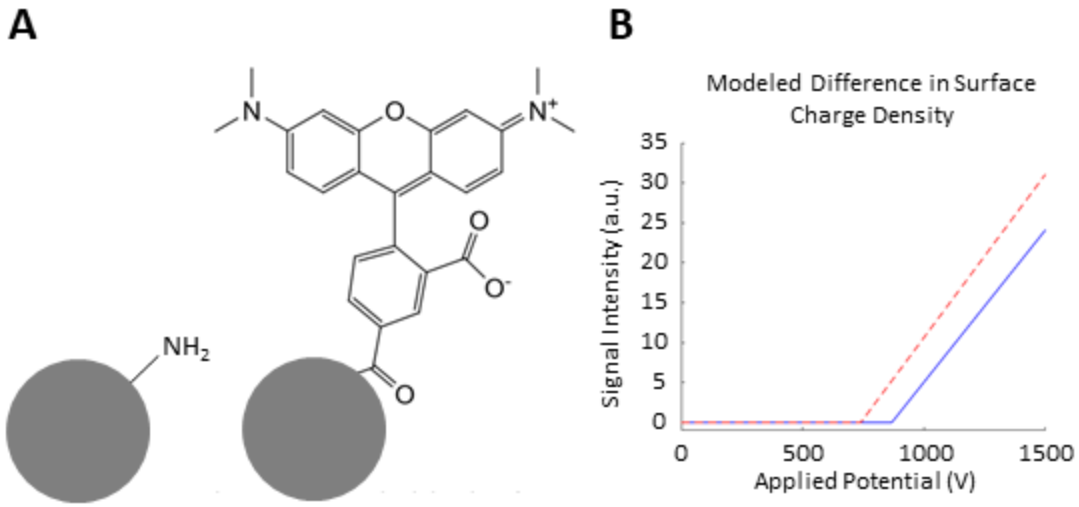



Figure 4.4 Structure of NHS-rhodamine, used to fluorescently label cells (A, right). The rhodamine attaches to primary amines on the surface of the cell (A, left). At pH 7.4, a primary amine will have a positive charge, while the NHS-rhodamine will be a neutral zwitterion. The difference in surface charge density required to give the variation in onset capture potential seen between the labeled and unlabeled cells is modeled (B). The dashed red line represents a rhodamine-labeled population, while the solid blue line represents an unlabeled population where the absolute value of the slope is depicted.

An increase in the surface charge density will result in an increase of capture onset potential. Assuming that only the surface charge density, and no other cell properties, changes with the addition of the label, an approximate value for the increase in surface charge density can be determined. Using the ratio of mobilities determined above for each population, it was found that an increase of surface charge density of approximately two times over the lower density would give a capture onset potential difference between the two populations of about 128 V. Thus, it appears that the addition of the label increases the surface charge density by double the original total charge. As the overall cellular charge is negative, and the addition of the label causes the charge to be less positive and therefore more negative, the surface charge is increasing. As the

addition of the label causes the capture onset potential to increase as well, this correlates with the determination that an increase in surface charge should increase the capture onset potential. However, there may be other factors involved that are affected by the label, either in the electrokinetic or dielectrophoretic mobilities. Some possibilities include zeta potential, conductivity, or multipole moments. Further, the addition of a label could also cause changes in the phenotype of the bacteria themselves, affecting their dielectrophoretic behavior.

### 4.6 Conclusion

Subtle biological differences can be sensed with DEP. Rhodamine-labeled methicillin-resistant and -susceptible *Staphylococcus aureus* were distinguished, with the MRSA strain requiring a higher potential for capture than the MSSA strain. This was correlated to a higher ratio of mobilities being discerned with this method. Further, the higher slope of the voltage-dependent data showed evidence of a higher electrokinetic mobility for the MRSA strain. From the ratio of mobilities and the electrokinetic mobilities, the dielectrophoretic mobility of both the MRSA and MSSA strains were determined and found to be different. These two strains were also differentiated when unlabeled.

Differences in dielectrophoretic behavior due to a chemical alteration, the addition of the fluorescent label, were also observed. For each strain, the unlabeled population was found to have a higher ratio of mobilities than the corresponding labeled population of that strain.

Differences in bacterial populations, such as the presence of antimicrobial resistance or of a label, result in different dielectrophoretic behavior. This behavior can be quantified using a mathematical model, leading to an understanding of what is being detected by DEP. The DEP behavior of clinically relevant strains must be unique and reproducible for this technique to be used to identify bacteria, determine antimicrobial susceptibility, and be used in patient care. The data presented here establish that DEP can distinguish between methicillin-resistant and -susceptible *S. aureus*, one bacterial strain with clinical importance known to confer loss of susceptibility to this antimicrobial.

**4.7 References**


1. K. Loewen, Y. Schreiber, M. Kirlew, N. Bocking and L. Kelly, *Canadian Family Physician*, 2017, *63*, 512-520.
2. F. D. Lowy, *The New England Journal of Medicine*, 1998, *339*, 520-532.
3. W. C. Noble, H. A. Valkenburg and C. H. L. Wolters, *Journal of Hygiene*, 1967, *65*, 567-573.
4. A. Hassoun, P. K. Linden and B. Friedman, *Critical Care*, 2017, *21*, 211.
5. R. P. Wenzel and T. M. Perl, *Journal of Hospital Infection*, 1995, *31*, 13-24.
6. D. J. Diekema, M. A. Pfaller, F. J. Schmitz, J. Smayevsky, J. Bell, R. N. Jones, M. Beach and S. P. Group, *Clinical Infectious Diseases*, 2001, *32*, S114-S132.
7. J. Miao, L. Chen, J. Wang, W. Wang, D. Chen, L. Li, B. Li, Y. Deng and Z. Xu, *Microbial Pathogenesis*, 2017, *107*, 17-28.
8. National Institute of Allergy and Infectious Diseases, History, Methicillin-Resistant Staphylococcus aureus, Antimicrobial Resistance, https://www.niaid.nih.gov/research/mrsa-antimicrobial-resistance-history, (accessed 4 October, 2018).
9. T. J. Foster, *FEMS Microbiology Reviews*, 2017, *41*, 430-449.
10. D. Lim and N. C. J. Strynadka, *Nature Structural Biology*, 2002, *9*, 870-876.

11. M. J. Pucci and T. J. Dougherty, *Journal of Bacteriology*, 2002, *184*, 588-591.

12. P. Sarkar, V. Yarlagadda, C. Ghosh and J. Haldar, *Medchemcomm*, 2017, *8*, 516-533.

13. F. P. Maurer, M. Christner, M. Hentschke and H. Rohde, *Infectious Disease Reports*, 2017, *9*, 18-27.

14. A. Kumar, D. Roberts, K. E. Wood, B. Light, J. E. Parrillo, S. Sharma, R. Suppes, D. Feinstein, S. Zanotti, L. Taiberg, D. Gurka, A. Kumar and M. Cheang, *Critical Care Medicine*, 2006, *34*, 1589-1596.

15. J. M. Entenza, B. Betrisey, O. Manuel, M. Giddey, O. Sakwinska, F. Laurent and A. Bizzini, *Journal of Clinical Microbiology*, 2014, *52*, 180-186.

16. A. Novais, M. Brilhante, J. Pires and L. Peixe, *Journal of Clinical Microbiology*, 2015, *53*, 3105-3107.

17. L. Poirel and P. Nordmann, *Journal of Clinical Microbiology*, 2015, *53*, 3003-3008.

18. B. H. Lapizco-Encinas, B. A. Simmons, E. B. Cummings and Y. Fintschenko, *Analytical Chemistry*, 2004, *76*, 1571-1579.

19. P. V. Jones, A. F. DeMichele, L. Kemp and M. A. Hayes, *Analytical and Bioanalytical Chemistry*, 2014, *406*, 183-192.

20. P. V. Jones, S. Huey, P. Davis, R. Yanashima, R. McLemore, A. McLaren and M. A. Hayes, *Analyst*, 2015, *140*, 5152-5161.

21. H. A. Pohl, *Journal of Applied Physics*, 1951, *22*, 869-871.

22. T. N. G. Adams, A. Y. L. Jiang, P. D. Vyas and L. A. Flanagan, *Methods*, 2018, *133*, 91-103.

23. J. Ding, R. M. Lawrence, P. V. Jones, B. G. Hogue and M. A. Hayes, *Analyst*, 2016, *141*, 1997-2008.

24. M. P. Hughes, H. Morgan, F. J. Rixon, J. P. H. Burt and R. Pethig, *Biochimica et Biophysica Acta*, 1998, *1425*, 119-126.

25. F. H. Labeed, J. Lu, H. J. Mulhall, S. A. Marchenko, K. F. Hoettges, L. C. Estrada, A. P. Lee, M. P. Hughes and L. A. Flanagan, *PLoS One*, 2011, *6*, e25458.

26. B. H. Lapizco-Encinas, S. Ozuna-Chacon and M. Rito-Palomares, *Journal of Chromatography A*, 2008, *1206*, 45-51.

27. G. H. Markx, Y. Huang, X.-F. Zhou and R. Pethig, *Microbiology*, 1994, *140*, 585-591.

28. H. Morgan and N. G. Green, *Journal of Electrostatics*, 1997, *42*, 279-293.

29. S. Otto, U. Kaletta, F. F. Bier, C. Wenger and R. Holzel, *Lab on a Chip*, 2014, *14*, 998-1004.

30. H. Song, J. M. Rosano, Y. Wang, C. J. Garson, B. Prabhakarpandian, K. Pant, G. J. Klarmann, A. Perantoni, L. M. Alvarez and E. Lai, *Lab on a Chip*, 2015, *15*, 1320-1328.

31. S. J. R. Staton, P. V. Jones, G. Ku, S. D. Gilman, I. Kheterpal and M. A. Hayes, *Analyst*, 2012, *137*, 3227-3229.

32. S. Velugotla, S. Pells, H. K. Mjoseng, C. R. E. Duffy, S. Smith, P. De Sousa and R. Pethig, *Biomicrofluidics*, 2012, *6*, 44113.

33. M. Washizu, S. Suzuki, O. Kurosawa, T. Nishizaka and T. Shinohara, *IEEE Transactions on Industry Applications*, 1994, *30*, 835-843.

34. T. B. Jones, *Electromechanics of Particles*, Cambridge University Press, New York, 1995.

35. H. A. Pohl, *Dielectrophoresis The behavior of neutral matter in nonuniform electric fields*, Cambridge University Press, New York, 1978.

36. E. B. Cummings and A. K. Singh, *Analytical Chemistry*, 2003, *75*, 4724-4731.

37. S. H. Hilton and M. A. Hayes, *Analytical and Bioanalytical Chemistry*, 2019, DOI: 10.1007/s00216-019-01757-7.

38. N.-T. Nguyen and S. T. Wereley, *Fundamentals and Applications of Microfluidics*, Artech House, Boston, 2nd edn., 2006.

39. R. Pethig, *Biomicrofluidics*, 2010, *4*, 022811.

40. R. Pethig, *Dielectrophoresis : theory, methodology and biological applications*, Hoboken, NJ : John Wiley & Sons, Ltd, 1st edn., 2017.

41. P. Tabeling, *Introduction to Microfluidics*, Oxford University Press, New York, 2005.

42. A. Lalonde, A. Gencoglu, M. F. Romero-Creel, K. S. Koppula and B. H. Lapizco-Encinas, *Journal of Chromatography A*, 2014, *1344*, 99-108.

43. P. V. Jones, S. J. R. Staton and M. A. Hayes, *Analytical and Bioanalytical Chemistry*, 2011, *401*, 2103-2111.

44. S. J. R. Staton, K. P. Chen, T. J. Taylor, J. R. Pacheco and M. A. Hayes, *Electrophoresis*, 2010, *31*, 3634-3641.

45. W. Schrott, Z. Slouka, P. Cervenka, J. Ston, M. Nebyla, M. Pribyl and D. Snita, *Biomicrofluidics*, 2009, *3*, 44101.

46. P. V. Jones and M. A. Hayes, *Electrophoresis*, 2015, *36*, 1098-1106.

47. L. D. Garza-García, V. H. Pérez-González, O. A. Pérez-Sánchez and B. H. Lapizco-Encinas, *Chemical Engineering & Technology*, 2011, *34*, 371-378.

48. H. Moncada-Hernandez, J. L. Baylon-Cardiel, V. H. Perez-Gonzalez and B. H. Lapizco-Encinas, *Electrophoresis*, 2011, *32*, 2502-2511.

49. M. E. Bayer and J. L. Sloyer Jr., *Journal of General Microbiology*, 1990, *136*, 867-874.

# CHAPTER 5

# DIELECTROPHORESIS OF KPC-POSITIVE AND -NEGATIVE *KLEBSIELLA PNEUMONIAE* AND POST-HOC ASSESSMENT OF DIFFERENCES

## 5.1 Introduction

*Klebsiella pneumoniae* are rod-shaped bacteria most commonly found in clinical settings. Infections caused by *K. pneumoniae* include pneumonia, meningitis, and bacteremia [1]. One of the last-resort antibiotics used for hospital-acquired infections, including those caused by *K. pneumoniae*, are carbapenems [2-4]. It is no wonder, then, that *Klebsiella pneumoniae* carbapenemases (KPCs), enzymes that render carbapenems ineffective, are of growing concern. KPCs are part of a class of enzymes, the carbapenemases, that confer resistance to $\beta$-lactam antibiotics [5]. Carbapenemases hydrolyze $\beta$-lactams, making them unable to bind to their target and thus ineffective [6-8]. Infections of bacteria producing KPCs are associated with worse patient outcomes, including longer hospital stays, failure of treatment, and an increased risk of death [9-12].

The ability to determine susceptibility to KPC and other antibiotics allows for proper treatment to be administered. Rapid methods of susceptibility testing allow for faster treatment, resulting in better patient outcomes. The location of carbapenemase genes on mobile genetic elements allows resistance to spread between organisms [13], and KPCs are not always detected by routine susceptibility testing [14-17]. This makes an accurate method of detection for carbapenem resistance and the presence of KPCs necessary.

Dielectrophoresis (DEP) has previously been shown to distinguish between antibiotic resistant and susceptible bacteria, specifically gentamicin-resistant and -susceptible *Staphylococcus epidermidis* and methicillin-resistant and susceptible *Staphylococcus aureus* [18, 19]. This technique, described and named by Pohl in 1951 [20], has since seen applications with a wide range of analytes, from viruses and DNA to bacteria and blood cells [18, 21-34].

DEP relies on the presence of an electric field gradient. The dielectrophoretic force, $\boldsymbol{F}_{DEP}$, is given by

$$\boldsymbol{F} = 2\pi r^3 \varepsilon_m f_{CM} \nabla |\boldsymbol{E}|^2 \quad (1)$$

where $r$ is the radius of the analyte, $\varepsilon_m$ is the permittivity of the medium, $\nabla|E|^2$ is the gradient of the electric field squared, and $f_{CM}$ is the Clausius-Mossotti factor [35, 36]. This factor, in DC fields, is dependent on the conductivity, such that

$$f_{CM} = \frac{\sigma_p - \sigma_m}{\sigma_p + 2\sigma_m} \quad (2)$$

where $\sigma_p$ and $\sigma_m$ are the conductivity of the particle and of the medium, respectively.

The gradients necessary for DEP can be formed using patterned electrodes (electrode-based DEP, eDEP) or patterned insulators in a microchannel with electrodes at the beginning and end (insulator-based DEP, iDEP) [20, 30, 31, 37]. While eDEP uses AC fields, iDEP can use either AC or DC fields. When DC fields are applied, electrophoresis and electroosmosis can be used for transport of analytes. These fields are used to manipulate the particles in various ways, including repelling, trapping, and streaming [21, 26, 31, 34, 37-48]. Capture will be the main phenomenon investigated in this study.

Here, two KPC-positive and one KPC-negative *K. pneumoniae* strains were analyzed using dielectrophoresis. Differences in the conditions required for capture for each of these three strains were observed. Variations in multiple growths of a single strain were also seen where any difference was unknown prior to analysis. The two populations of this strain were analyzed for differences in the presence of the KPC gene.

**5.2 Theory**

Three main effects govern the motion of a particle in a microchannel: electroosmosis, electrophoresis, and dielectrophoresis. In uniform fields, or in areas of low electric field gradient, electroosmosis and electrophoresis dictate the movement. Electroosmosis is the flow of the bulk fluid when an electric field is present. The flow brings the analytes in the fluid along with it, moving them down the microchannel. The electroosmotic velocity, $\boldsymbol{v}_{EOF}$, is given by the equation

$$\boldsymbol{v}_{EOF} = \frac{\varepsilon \zeta_m}{\eta} \boldsymbol{E} = \mu_{EOF} \boldsymbol{E} \tag{3}$$

where $\varepsilon$ is the permittivity, $\zeta_m$ is the zeta potential of the wall, $\eta$ is the viscosity of the medium, $\mu_{EOF}$ is the electroosmotic mobility, and $\boldsymbol{E}$ is the electric field [49]. Electrophoresis is the motion of charged particles when in an electric field. The electrophoretic velocity is given by the equation

$$\boldsymbol{v}_{EP} = \frac{\varepsilon \zeta_p}{\eta} \boldsymbol{E} = \mu_{EP} \boldsymbol{E} \tag{4}$$

where $\zeta_p$ is the zeta potential of the particle and $\mu_{EP}$ is the electrophoretic mobility [49]. The velocity of an analyte in a microchannel will be the sum of the electroosmotic and electrophoretic velocities, called the electrokinetic velocity, $\boldsymbol{v}_{EK}$

$$\boldsymbol{v}_{EK} = \boldsymbol{v}_{EOF} + \boldsymbol{v}_{EP} = \mu_{EK}\boldsymbol{E} \tag{5}$$

and the electrokinetic mobility, $\mu_{EK}$, is similarly the sum of the electroosmotic and the electrophoretic mobilities.

In the system presented here, electroosmosis and electrophoresis are used to transport the analytes down the microchannel to arrive at locations of high field gradient, where dielectrophoresis becomes important to the motion of the analyte. The dielectrophoretic velocity is

$$\boldsymbol{v}_{DEP} = \frac{\varepsilon_m r^2 f_{CM}}{3\eta}\nabla|\boldsymbol{E}|^2 = \mu_{DEP}\nabla|\boldsymbol{E}|^2 \tag{6}$$

When the flux of particles past a given point in the microchannel is zero, capture occurs and the particles stop their forward motion along the microchannel [35]. This happens when

$$\frac{\mu_{EK}}{\mu_{DEP}} \leq \frac{\nabla|E|^2}{E} \tag{7}$$

The lowest applied potential at which this condition can be true is when

$$\frac{\mu_{EK}}{\mu_{DEP}} = \frac{\nabla|E|^2}{E} \tag{8}$$

and is termed the capture onset potential, while at lower potentials the inequality in equation 7 will not hold true and capture will not occur.

## 5.3 Materials and Methods

### 5.3.1 Fabrication of the Microdevice

Experiments were performed using a microchannel previously described in-depth [18, 28, 48, 50, 51]. Briefly, the microchannel is approximately 1000 µm wide and 4.1 cm long, including an inlet or outlet reservoir at either end, and an average depth of 16.8

μm. The channel geometry has equilateral triangles along each wall of the channel, with opposing points at the same lateral distance in the channel, forming a constriction termed a "gate". The distance between opposing triangle tips decreases from inlet to outlet down the channel as triangle size increases. The gate nearest the inlet is the largest at 945 μm, while the gate nearest the outlet is the smallest at 27 μm.

Template wafers of the microchannel geometry were fabricated with soft lithography methods. To pattern four-inch silicon wafers, they were first coated with AZ 4330 photoresist (AZ Electronic Materials, Branchburg, NJ), then exposed through a glass chrome mask with the channel geometry (JD Photo-Tools, United Kingdom), then developed. Following this, the wafers were etched using reactive ion etching (ICP etcher, STPS, San Jose, CA) with $SF_6$ and $C_4F_8$ gases. Any remaining photoresist was removed.

The devices used to perform experiments were made using these template wafers. Polydimethyl siloxane (PDMS) (Sylgard 184, Dow/Corning, Midland, MI) was poured on to the wafer and then cured at 70°C for one hour. The resulting PDMS cast was peeled from the wafer and trimmed. Access holes 3 mm in diameter were punched in both the inlet and outlet at each end. The casts were stored at -20°C for up to one month before use.

To complete the device for experiments, the PDMS casts were washed with isopropyl alcohol, then water. Glass microscope slides (VWR Radnor, PA) were washed with acetone, then isopropyl alcohol, then water. Both the PDMS casts and the glass slides were treated with oxygen plasma with a plasma cleaner (PDC-32G, Harrick-Plasma, Ithaca, NY) at 18 W for 60 seconds, following which they were allowed to seal

upon contact. The resulting completed microchannel had one wall of glass and three of PDMS, as well as access holes to the inlet and outlet in either end. The devices were used on the same day as bonding.

### 5.3.2 Cell Culture

Three strains of *Klebsiella pneumoniae* (KPC-positive TG60131 and TG40855, and KPC-negative TG93473) were obtained from TGen (TGen North, Flagstaff, AZ). Liquid cultures were grown by placing 10 mL aliquots of sterile Luria broth into culture tubes. These were then inoculated with a single colony of one strain. This was then incubated overnight at 37°C while shaking at 250 RPM and allowed to reach late log phase. This culture was used for an experimental sample, as well as to make a seed stock. The seed stock was made by mixing the liquid culture with glycerol to make a 16.7% glycerol stock solution and stored at -80°C. To grow a new plate, seed stock was streaked onto LB agar plates, which were then incubated overnight at 37°C.

For experiments, a 1:10 dilution of the liquid culture was made with 2 mM phosphate buffer at pH 7.4. This mixture was centrifuged at 1677 × g for 5 minutes. The supernatant was then removed, and the pellet resuspended in 2 mM phosphate buffer. The solution was centrifuged once more under the same conditions and the supernatant removed. The final resuspension was 2 mM phosphate buffer with 4 mg/mL bovine serum albumin (BSA) (Sigma, St. Louis, MO). Cells were used on the same day as dilution and washing, and up to three days after culture.

### 5.3.3 Dielectrophoresis Experiments

A completed and bonded microchannel was filled with 15 µL 2 mM phosphate buffer, pH 7.4, in both the inlet and the outlet. The buffer was then removed from the reservoirs. The inlet was again filled with 15 µL 2 mM phosphate buffer with BSA, and the device was allowed to sit for 15 minutes. This solution was then removed from the reservoirs. Following this, 15 µL of the bacteria solution in BSA was placed in the inlet reservoir and allowed to sit for 5 minutes. The outlet was then filled with 15 µL 2 mM phosphate buffer with BSA.

The filled microdevice was placed on the stage of an inverted microscope (Olympus IX70, Center Valley, PA) with a 4x objective. To balance hydrodynamic flow, 2 mM phosphate buffer with BSA was pipetted into the appropriate reservoir. Platinum electrodes were placed into the inlet and outlet reservoirs and connected to an HVS448 3000D high voltage sequencer (Labsmith, Inc., Livermore, CA). DC potentials of 200 V to 1400 V were applied across the microchannel. Images and video were collected using a monochrome QICAM cooled CCD camera (QImaging, Inc., Surrey, UK) and Streampix V image capture software (Norpix, Inc., Montreal, QC). For image analysis, ImageJ software was used (National Institutes of Health, Bethesda, Maryland).

### 5.3.4 Data Modeling

The mathematical model of dielectrophoretic data from Hilton and Hayes was used to interpret the data presented below has been discussed in-depth previously [52]. Briefly, dielectrophoretic data can be described by a piecewise function. This shows the signal intensity as a function of the applied potential. One piece of this function

represents the data before capture begins to occur, while the other piece represents data at potentials higher than the capture onset potential, once capture is occurring. The potential at which capture begins to occur is related to equation 8. The signal intensity increases linearly with increasing potential after this. As the analyte particles arrive at the capture location and are trapped, each will increase the signal intensity a given amount. The rate at which the particles arrive is determined by their velocity and their concentration. As the channel used in the present study is the same as that discussed by Hilton and Hayes, the values relating the electric field to the applied potential are the same. The piecewise function describing the signal intensity, $SI$, as a function of applied potential, $V$, is

$$SI(V) = \begin{cases} 0 & if\ V < \frac{1}{1.4 \cdot 10^7}\left(\frac{\mu_{EK}}{\mu_{DEP}}\right) \\ 0.24\gamma n \mu_{EK} twhs\left[V - \frac{1}{1.4 \cdot 10^7}\left(\frac{\mu_{EK}}{\mu_{DEP}}\right)\right] & if\ V \geq \frac{1}{1.4 \cdot 10^7}\left(\frac{\mu_{EK}}{\mu_{DEP}}\right) \end{cases} \quad (10)$$

where $\gamma$ is the signal intensity per particle, $n$ is the concentration of the particles in the microchannel, $\mu_{EK}$ is the electrokinetic mobility, $t$ is the time of potential applied, and $w$ and $h$ are the width and height of the channel, respectively. The correction factor, $s$, accounts for other factors that may affect the signal, including stacking of the analyte or saturation of the detector (Figure 5.1).

### 5.3.5 Polymerase Chain Reaction (PCR) Methods

To prepare the bacterial sample for PCR, a colony from a plate or bacteria from a centrifuged, pelleted sample was placed in 10 µL water. This was heated at 100°C for 10 minutes. Primers were synthesized by Sigma (St. Louis, MO). Forward primer sequence was CGTCTAGTTCTGCTGTCTTGT and reverse primer sequence was

ACCGTCATGCCTGTTGTC, with an expected 338 base pair product. A control reaction with an expected product size of 389 base pairs was also run. Primer stocks at 200 mM were prepared in water. The stocks were diluted to 10 mM for use. A 20 µL polymerase chain reaction was prepared with 0.2 mM dNTPs (New England BioLabs, Ipswich, MA), 0.5 mM each forward and reverse primers (New England BioLabs, Ipswich, MA), 1x Phusion HF buffer (New England BioLabs, Ipswich, MA), 0.4 U Phusion polymerase (New England BioLabs, Ipswich, MA), and 5 µL of previously prepared bacterial sample. PCR was performed with initial denaturation at 98°C for 30 seconds, followed by 20 cycles of denaturation at 98°C for 20 seconds, annealing at 64°C, and extension at 72°C for 30 seconds. A final extension was performed at 72°C for 1 minute, after which the reaction was held at 8°C. PCR products were run on a 1% agarose gel stained with GelRed (Biotium, Fremont, CA) with a 1 kilobase ladder (New England BioLabs, Ipswich, MA) to confirm size of the product.

### 5.3.6 Safety Considerations

All organisms used here were Biosafety Level I or II organisms. All experiments were performed in an approved Biosafety Level II laboratory, within accordance to the current version of the CDC/NIH BMBL publication.

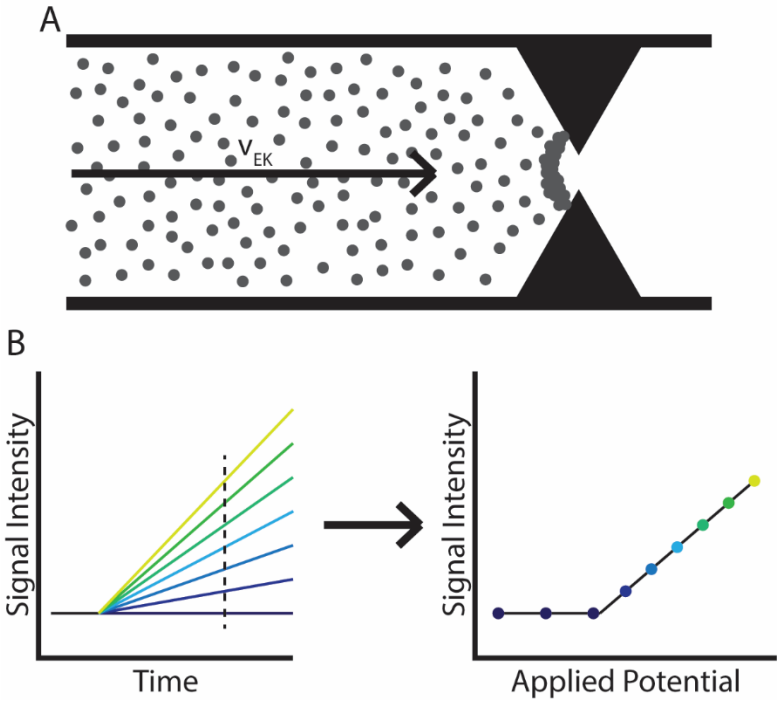



Figure 5.1 Dielectrophoresis captures particles in a microchannel which reach the capture region using the electrokinetic force for transport (A). The signal intensity increases with time (B, left), with the rate of increase correlated to the applied potential (low potential indicated by black, high potential indicated by yellow-green). A single time point can be assessed for a range of voltages, and the signal intensity plotted vs. the applied potential (B, right).

**5.4 Results and Discussion**

The capture onset potentials between the susceptible and each resistant strain can be compared. These each show a different condition required for capture. The resistant 60313 strain has a capture onset potential of 859 $\pm$ 77 V, or a $\frac{\nabla E^2}{E}$ of 1.24 $\pm$ 0.11·$10^{10}$ V/$m^2$ required for capture. The resistant 40855 strain shows capture beginning around 1200 V applied, corresponding to a $\frac{\nabla E^2}{E}$ of 1.73·$10^{10}$ V/$m^2$, but a slope could not be established to determine a more precise capture onset potential. The susceptible 93473 strain of *K. pneumoniae*, however, does not capture below 1400 V applied. A $\frac{\nabla E^2}{E}$ of

greater than $2.02 \cdot 10^{10}$ V/m$^2$ is required for capture of this strain. Each of these three strains show clear differences in the conditions required for capture (Figure 5.2).

An interesting observation was made with the resistant 40855 strain. The onset capture potential described above is for liquid cultures from the original plate of the bacteria. However, a second plate was grown, and the capture onset potential of the samples grown from this plate differed from the 1200 V; the capture onset potential for the "new" plate was found to be $726 \pm 64$ V, corresponding to a $\frac{\nabla E^2}{E}$ of $1.05 \pm 0.09 \cdot 10^{10}$ V/m$^2$ required for capture (Figure 5.3).

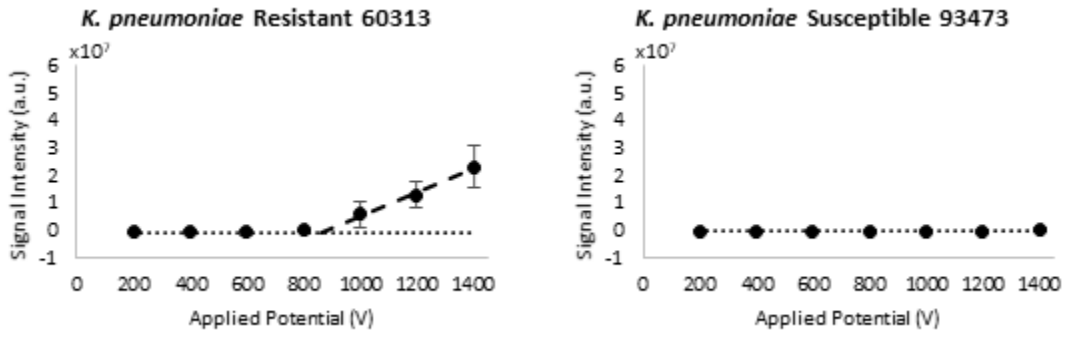



Figure 5.2 Dielectrophoretic data of KPC-negative (left) and -positive (right) *K. pneumoniae*. The KPC-negative strain did not capture at the potentials applied in these experiments (up to 1400 V), while the KPC-positive strain had a capture onset potential of $859 \pm 77$ V. Error bars are 95% confidence intervals, while reported error is the standard deviation.

The populations from the old and new plates of the resistant 40855 strain of *K. pneumoniae* clearly show different dielectrophoretic signatures. This must be attributed to a physical difference somewhere in the cell. Although the fact that something changed between these two populations was not known prior to analysis, it was able to be detected.

A method that detects a change or difference in the analyte without prior knowledge of the basis for the difference, or even that a difference might occur, has great impact in the detection and analysis of bioparticles.

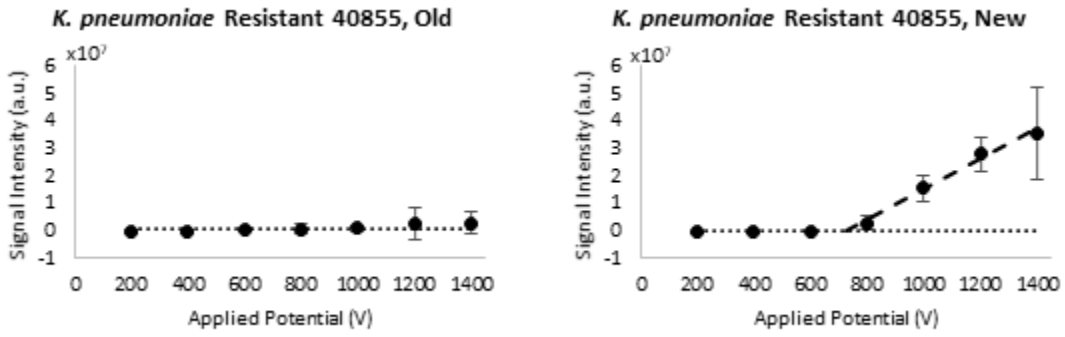



Figure 5.3 Dielectrophoretic data of two different populations of a KPC-positive *K. pneumoniae* strain. The original population began to capture at about 1200 V applied (left). Bacteria cultured from a second plate of the strain had a lower capture onset potential, 726 $\pm$ 64 V (right). Error bars are 95% confidence intervals, while reported error is the standard deviation.

One of the likely sources of this difference is the loss of the KPC gene. Antibiotic resistance genes, or the expression of those genes, are known to be lost when the cell is under stress and not in the presence of the antibiotics. PCR was used to determine if the KPC gene was present in the colonies on the new plate, as well as in the liquid culture from the new plate. PCR of three colonies from the new plate showed the presence of the KPC gene, while the PCR of the liquid culture did not (Figure 5.4). However, this is not conclusive for the absence of the KPC gene in the liquid culture, as there are many possible reasons for the lack of band in the lane from the culture, including uncertainty in whether any bacteria were placed into the reaction tube or if the cells were washed off when moving from the culture tube to the PCR tube.

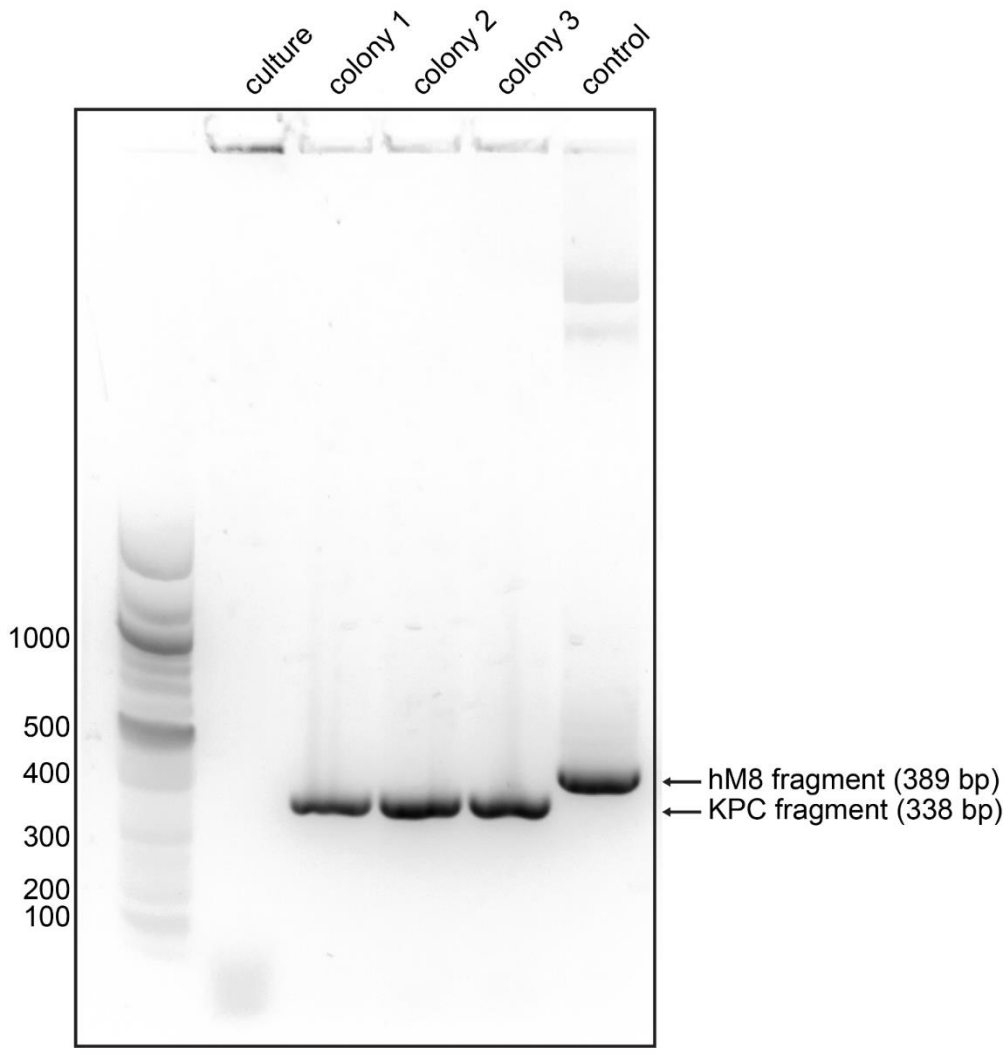



Figure 5.4 Results of PCR to determine the KPC-gene in the re-plated population of TG40855 *K. pneumoniae*. Three colonies showed the presence of the KPC gene in the population, while the liquid culture did not. A fragment of the TRPM8 protein was used as a control. Whether this is from the loss of the gene or lack of bacterial in the culture tube remains an open question.

Another possibility is that the growth in the liquid culture is not the *K. pneumoniae* but rather contamination. A negative control was used each time a liquid culture was grown to eliminate this possibility. The PCR genetic testing confirms the presence of the KPC gene in the colonies on the plate, providing confirmation that the colonies are in fact the KPC+ *K. pneumoniae* expected. No growth was seen in the

negative controls when growing a liquid culture from the plates, indicating that the growth in the inoculated liquid is *K. pneumoniae*. However, to confirm the presence or absence of the KPC+ gene and determine the reason for variation in the capture conditions, further analysis is needed for confirmation.

## 5.5 Conclusion

Dielectrophoresis of *Klebsiella pneumoniae* showed differences in the behavior of three strains: one KPC-negative and two KPC-positive strains. Each of these strains was found to have a different capture onset potential, and thus different ratios of mobilities.

Further, changes in the strain that were not known prior to analysis were detected in one of the KPC-positive strains. PCR revealed that the KPC gene was indeed still present in the changed population of this strain. This difference between the two populations of the strain must arise from another source. Further testing would be needed to determine the physical difference causing the variation in dielectrophoretic behavior.

## 5.6 References


1. T. A. de Campos, L. F. Goncalves, K. G. Magalhaes, V. de Paulo Martins, G. J. Pappas Junior, G. Peirano, J. D. D. Pitout, G. B. Goncalves, J. P. R. Furlan, E. G. Stehling and A. Pitondo-Silva, *Frontiers in Medicine*, 2018, *5*, 265.

2. I. Galdadas, S. Lovera, G. Perez-Hernandez, M. D. Barnes, J. Healy, H. Afsharikho, N. Woodford, R. A. Bonomo, F. L. Gervasio and S. Haider, *Scientific Reports*, 2018, *8*, 12916.

3. D. M. Livermore, *Journal of Antimicrobial Chemotherapy*, 2009, *64 Suppl 1*, i29-i36.

4. D. M. Livermore, R. Hope, G. Brick, M. Lillie and R. Reynolds, *Journal of Antimicrobial Chemotherapy*, 2008, *62 Suppl 2*, ii41-ii54.

5. P. I. P. Ramos, R. C. Picao, L. G. P. de Almeida, N. C. B. Lima, R. Girardello, A. C. P. Vivan, D. E. Xavier, F. G. Barcellos, M. Pelisson, E. C. Vespero, C.

Medigue, A. T. R. de Vasconcelos, A. C. Gales and M. F. Nicolas, *BMC Genomics*, 2014, *15*.

6. A. M. Queenan and K. Bush, *Clinical Microbiology Reviews*, 2007, *20*, 440-458.

7. D. Z. Rechenchoski, A. M. L. Dambrozio, A. C. P. Vivan, P. A. Schuroff, T. d. N. Burgos, M. Pelisson, M. R. E. Perugini and E. C. Vespero, *Brazilian Journal of Microbiology*, 2017, *48*, 509-514.

8. D. J. Wolter, P. M. Kurpiel, N. Woodford, M.-F. I. Palepou, R. V. Goering and N. D. Hanson, *Antimicrobial Agents and Chemotherapy*, 2009, *53*, 557-562.

9. R. S. Arnold, K. A. Thom, S. Sharma, M. Phillips, J. K. Johnson and D. J. Morgan, *Southern Medical Journal*, 2011, *104*, 40-45.

10. H. Khalili, S. Dashti-Khavidaki, M.-R. Shahidi, A. Abdollahi, S. Jafari, Z. Jahangard-Rafsanjani and A.-H. Talasaz, *DARU Journal of Pharmaceutical Sciences*, 2012, *20*.

11. Centers for Disease Control and Prevention, *Facility Guidance for Control of Carbapenem-resistant Enterobacteriaceae (CRE) November 2015 Update - CRE Toolkit*, 2015.

12. Centers for Disease Control and Prevention, *Morbidity and Mortality Weekly Report*, 2009, *58*, 256-260.

13. A. R. McMullen, M. L. Yarbrough, M. A. Wallace, A. Shupe and C.-A. D. Burnham, *Clinical Chemistry*, 2017, *63*, 723-730.

14. S. Bratu, D. Landman, R. Haag, R. Recco, A. Eramo, M. Alam and J. Quale, *Archives of Internal Medicine*, 2005, *165*, 1430-1435.

15. S. Bratu, M. Mooty, S. Nichani, D. Landman, C. Gullans, B. Pettinato, U. Karumudi, P. Tolaney and J. Quale, *Antimicrobial Agents and Chemotherapy*, 2005, *49*, 3018-3020.

16. B. M. Lomaestro, E. Tobin, H., W. Shang and T. Gootz, *Clinical Infectious Diseases*, 2006, *43*, e26-e28.

17. P. Nordmann, G. Cuzon and T. Naas, *The Lancet Infectious Diseases*, 2009, *9*, 228-236.

18. P. V. Jones, S. Huey, P. Davis, R. Yanashima, R. McLemore, A. McLaren and M. A. Hayes, *Analyst*, 2015, *140*, 5152-5161.

19. S. H. Hilton, C. V. Crowther, A. McLaren and M. A. Hayes, *Analyst*, 2019, Submitted.

20. H. A. Pohl, *Journal of Applied Physics*, 1951, *22*, 869-871.

21. C. Asbury, L., A. H. Dierks and G. van den Engh, *Electrophoresis*, 2002, *23*, 2658-2666.

22. F. F. Becker, X.-B. Wang, Y. Huang, R. Pethig, J. Vykoukal and P. R. C. Gascoyne, *Proceedings of the National Academy of Sciences of the United States of America*, 1995, *92*, 860-864.

23. K. L. Chan, H. Morgan, E. Morgan, I. T. Cameron and M. R. Thomas, *Biochimica et Biophysica Acta*, 2000, *1500*, 313-322.

24. C.-F. Chou, J. O. Tegenfeldt, O. Bakajin, S. S. Chan, E. C. Cox, N. Darnton, T. Duke and R. H. Austin, *Biophysical Journal*, 2002, *83*, 2170-2179.

25. J. Ding, R. M. Lawrence, P. V. Jones, B. G. Hogue and M. A. Hayes, *Analyst*, 2016, *141*, 1997-2008.

26. J. Ding, C. Woolley and M. A. Hayes, *Analytical and Bioanalytical Chemistry*, 2017, *409*, 6405-6414.

27. M. P. Hughes, H. Morgan, F. J. Rixon, J. P. H. Burt and R. Pethig, *Biochimica et Biophysica Acta*, 1998, *1425*, 119-126.

28. P. V. Jones, S. J. R. Staton and M. A. Hayes, *Analytical and Bioanalytical Chemistry*, 2011, *401*, 2103-2111.

29. B. H. Lapizco-Encinas, B. A. Simmons, E. B. Cummings and Y. Fintschenko, *Electrophoresis*, 2004, *25*, 1695-1704.

30. B. H. Lapizco-Encinas, B. A. Simmons, E. B. Cummings and Y. Fintschenko, *Analytical Chemistry*, 2004, *76*, 1571-1579.

31. G. H. Markx, Y. Huang, X.-F. Zhou and R. Pethig, *Microbiology*, 1994, *140*, 585-591.

32. H. Morgan and N. G. Green, *Journal of Electrostatics*, 1997, *42*, 279-293.

33. J. Regtmeier, T. T. Duong, R. Eichhorn, D. Anselmetti and A. Ros, *Analytical Chemistry*, 2007, *79*, 3925-3932.

34. S. K. Srivastava, P. R. Daggolu, S. C. Burgess and A. R. Minerick, *Electrophoresis*, 2008, *29*, 5033-5046.

35. A. Lalonde, A. Gencoglu, M. F. Romero-Creel, K. S. Koppula and B. H. Lapizco-Encinas, *Journal of Chromatography A*, 2014, *1344*, 99-108.

36. H. A. Pohl, *Dielectrophoresis The behavior of neutral matter in nonuniform electric fields*, Cambridge University Press, New York, 1978.

37. E. B. Cummings and A. K. Singh, *Analytical Chemistry*, 2003, *75*, 4724-4731.

38. W. A. Braff, A. Pignier and C. R. Buie, *Lab on a Chip*, 2012, *12*, 1327-1331.

39. F. Camacho-Alanis, L. Gan and A. Ros, *Sensors and Actuators B: Chemical*, 2012, *173*, 668-675.

40. D. Chen and H. Du, *Microfluidics and Nanofluidics*, 2010, *9*, 281-291.

41. P. R. C. Gascoyne, J. Noshari, T. J. Anderson and F. F. Becker, *Electrophoresis*, 2009, *30*, 1388-1398.

42. B. H. Lapizco-Encinas, S. Ozuna-Chacon and M. Rito-Palomares, *Journal of Chromatography A*, 2008, *1206*, 45-51.

43. H. Moncada-Hernandez, J. L. Baylon-Cardiel, V. H. Perez-Gonzalez and B. H. Lapizco-Encinas, *Electrophoresis*, 2011, *32*, 2502-2511.

44. A. Nakano, F. Camacho-Alanis and A. Ros, *Analyst*, 2015, *140*, 860-868.

45. S. Ozuna-Chacon, B. H. Lapizco-Encinas, M. Rito-Palomares, S. O. Martinez-Chapa and C. Reyes-Betanzo, *Electrophoresis*, 2008, *29*, 3115-3122.

46. M. A. Saucedo-Espinosa, A. LaLonde, A. Gencoglu, M. F. Romero-Creel, J. R. Dolas and B. H. Lapizco-Encinas, *Electrophoresis*, 2016, *37*, 282-290.

47. H. Song, J. M. Rosano, Y. Wang, C. J. Garson, B. Prabhakarpandian, K. Pant, G. J. Klarmann, A. Perantoni, L. M. Alvarez and E. Lai, *Lab on a Chip*, 2015, *15*, 1320-1328.

48. S. J. R. Staton, K. P. Chen, T. J. Taylor, J. R. Pacheco and M. A. Hayes, *Electrophoresis*, 2010, *31*, 3634-3641.

49. P. Tabeling, *Introduction to Microfluidics*, Oxford University Press, New York, 2005.

50. P. V. Jones, A. F. DeMichele, L. Kemp and M. A. Hayes, *Analytical and Bioanalytical Chemistry*, 2014, *406*, 183-192.

51. S. J. R. Staton, P. V. Jones, G. Ku, S. D. Gilman, I. Kheterpal and M. A. Hayes, *Analyst*, 2012, *137*, 3227-3229.

52. S. H. Hilton and M. A. Hayes, *Analytical and Bioanalytical Chemistry*, 2019, DOI: 10.1007/s00216-019-01757-7.

# CHAPTER 6

# DIELECTROPHORETIC SEPARATION OF GENTAMICIN-RESISTANT AND -SUSCEPTIBLE *STAPHYLOCOCCUS EPIDERMIDIS*

## 6.1 Introduction

The ability to separate particles and have a pure sample is a necessary part of many analytical methods. Similarly, the purification of a species is also a part of clinical analysis, including antibiotic resistance determination; pure cultures are required for testing of susceptibility [1, 2]. A method that separates based on antibiotic resistance could be used either as a step in existing diagnostic schemes or on its own to determine susceptibility. Dielectrophoresis (DEP) shows promise as such a method.

### 6.1.1 Antibiotic Resistance

One of the growing problems facing healthcare today is antibiotic resistance. Both the World Health Organization and the Centers for Disease Control and Prevention have indicated the seriousness of this problem, and the importance of curtailing the development of more resistance [3, 4]. Resistance, of course, is problematic for a patient, making infections more difficult to treat and reducing the probability of finding an effective antibiotic for treatment.

An important tool for slowing the furthering of resistance is the development of diagnostics, particularly rapid diagnostics. Currently, infection identification and susceptibility testing can take up to four days. Initial treatment during this time is empiric and so the antibiotic used may not be effective against the bacteria causing the infection. A delay in effective treatment, including initially using an inappropriate

antibiotic, has been associated with increased mortality [5, 6]. Rapid diagnostics would enable the susceptibility profile of an infection to be determined quickly, allowing proper treatment to be administered earlier in the course of the infection. Aside from the effect on patient care, treatment with inappropriate antibiotics has been associated with increasing resistance; thus, treatment with appropriate antibiotics could help curtail the spread of resistance [7-10].

Here, gentamicin-resistant and -susceptible *Staphylococcus epidermidis* are studied. *Staphylococcus epidermidis* is a gram-positive bacteria commonly found on human skin and mucous [11, 12]. It is also one of the causes of infections in hospital and other healthcare settings [13]. In fact, it is one of the most common causes of infections associated with medical devices [14]. One antibiotic used for treatment of *S. epidermidis* infections is gentamicin, an aminoglycoside antibiotic. These antibiotics cause cell death by disrupting the protein-proofreading function after binding to the 16S subunit of bacteria's ribosomal RNA [15]. Resistance to gentamicin in *Staphylococcus* species is conferred by aminoglycoside-modifying enzymes which modify the antibiotic, leaving it unable to interact with its target [16]. While the enzymes responsible for this can vary a bit, this resistance is often linked to the AAC(6')-APH(2'') enzyme. AAC(6') is an acetyltransferase, while APH(2'') is a phosphotransforase [17].

### 6.1.2 Dielectrophoresis

Dielectrophoresis (DEP) has been utilized in numerous applications with a range of analytes, and has been used to separate and/or differentiate between similar analytes [18-37]. It has been shown to be sensitive to small differences in bacterial strains,

including in the ability to distinguish between three specific strains of *E. coli* [23]. Dielectrophoretic experiments take minutes, rather than the hours many susceptibility testing methods require. The ability to distinguish antibiotic susceptibility and separate bacteria based on their susceptibility profile could allow DEP to find application as a diagnostic.

DEP utilizes electric field gradients to influence the motion of particles. Historically, patterned electrodes were used to create these field gradients [38-41]. While this method is still used, electrodeless DEP was developed by Chou et al, and insulator-based dielectrophoresis was developed by Cummings and Singh, both in the early 2000s [20, 42]. Instead of patterned electrodes, patterned insulators are used to create the electric field gradients in a microchannel with the electrodes placed at the ends. This technique has since been used for a variety of analytes [23, 25, 26, 33, 43-48]. In electrode-based DEP, AC fields must be used. In insulator-based DEP, either AC or DC fields may be utilized. Both electrode-based and insulator-based DEP continue to be used today [18, 37, 49-53].

### 6.1.3 DEP Separations

Most dielectrophoretic separations are simple bifurcations, the separation of a particle mixture into two populations. Some of these methods only separate the particles while the potential is applied [26, 27]. In these methods, the two populations are held separately but near one another. Once the potential is released, the particles disperse back into the microchannel and again mix together. Where there is no ability to shuttle particles off to separate chambers before they are mixed, separations which quickly re-

mix populations show the possibilities of dielectrophoresis, but are not as applicable in real-world separations.

Other separations trap one type of particle while allowing others to pass through the microchannel [18, 21, 48, 53, 54]. These separations are useful for removing a specific analyte from a solution, but do not apply to allow for the separation of multiple analytes without multiple instances of the separation occurring. To extend the separation to remove two or more analytes from a solution, the time required increases with each additional analyte.

Gradient-based insulator dielectrophoresis (g-iDEP) provides a solution to some of these separation-bifurcation problems. This technique uses insulating features, specifically triangles, down each side of a rectangular microchannel with opposing triangle points from each side directed toward each other. These features increase in size down the channel, and thus the distance between opposing points decreases. This causes a variation, or gradient, in the intensity of the local electric field gradient formed at the constrictions. Such a device has been used for the capture of single analytes to determine the conditions necessary for their capture [23, 33, 55]. Here, it is used to separate a mixture of gentamicin resistant and susceptible strains of *Staphylococcus epidermidis*, with the ability for the separation of a larger number of analytes. The separation is done with each of the strains labeled with differing fluorescent dyes. The order in which the strains are found separated in the microchannel remains the same even after switching which strain is labeled with which dye.

## 6.2 Theory

Dielectrophoresis in DC fields relies on three effects influencing the motion of particles in a microchannel: electroosmosis, electrophoresis, and dielectrophoresis. These effects have all been previously described in-depth but will be briefly discussed here [41, 56-60]. Electroosmosis and electrophoresis are both proportional to the magnitude of the applied electric field, and thus are considered together as the electrokinetic force. The velocity due to this force, $\boldsymbol{v}_{EK}$, is

$$\boldsymbol{v}_{EK} = \mu_{EK}\boldsymbol{E} \tag{1}$$

where $\mu_{EK}$ is the electrokinetic mobility and $\boldsymbol{E}$ is the electric field. The dielectrophoretic force is prominent in areas of high electric field gradient. The dielectrophoretic velocity of a particle, $\boldsymbol{v}_{DEP}$, is

$$\boldsymbol{v}_{DEP} = \mu_{DEP}\nabla|\boldsymbol{E}|^2 \tag{2}$$

where $\mu_{DEP}$ is the dielectrophoretic mobility and $\nabla|\boldsymbol{E}|^2$ is the gradient of the electric field squared.

The electrokinetic force is used to transport the particles down the microchannel, while dielectrophoresis becomes important for the motion of the particles where the electric field gradient is high. When the flux of the particles past a point in the channel is zero, the particles have stopped, or become captured, at that location. The flux of particles is given by

$$\boldsymbol{j} \cdot \boldsymbol{E} = (\mu_{EK}\boldsymbol{E} + \mu_{DEP}\nabla|\boldsymbol{E}|^2) \cdot \boldsymbol{E} \tag{3}$$

where $\boldsymbol{j}$ is the flow of particles [54]. Setting the flux greater than or equal to zero and rearranging gives the condition that must be met for capture to occur

$$\frac{\mu_{EK}}{\mu_{DEP}} \leq \frac{\nabla E^2}{E} \tag{4}$$

which is dependent on both properties of the particles and the electric field. Particles with a higher electrokinetic or lower dielectrophoretic mobility will require a greater ratio of $\frac{\nabla E^2}{E}$ in order to be captured.

In a typical experiment with a single strain, particles have filled the microchannel prior to beginning the experiment. The signal intensity is monitored over time of potential applied for a range of applied potentials. At potentials lower than that required for the capture condition (equation 4) to be met, no capture will occur and the signal intensity will remain consistent. At potentials higher than that required for capture, the signal increases over time as particles reach the gate and are captured, traveling down the microchannel as a result of the electrokinetic velocity. When the signal from a given time point is compared over a range of applied potentials, the signal will increase with increasing potential, as the electrokinetic velocity increases with increasing field strength (Figure 6.1).

In a separation experiment, the potential is applied before the particles are allowed to reach the gates. The particles travel down the microchannel until they reach a gate at which their capture conditions are met.

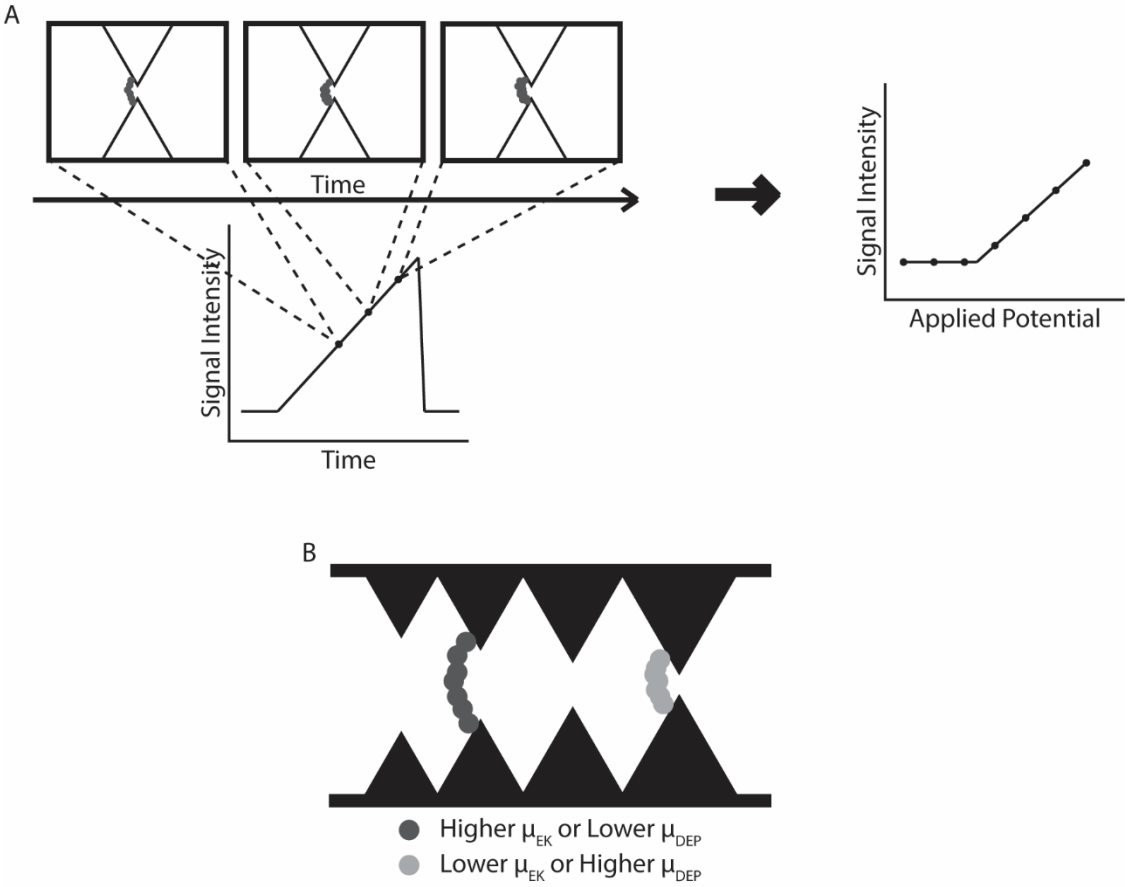



Figure 6.1 Dielectrophoretic signal intensity increases with increasing time as more particles reach the capture location (A). The signal from a given time point at a range of voltages can be plotted and the conditions for capture assessed through the potential at which capture begins to occur. These conditions can be met by varying the gate size (B). Analytes which require a lower ratio for capture will be captured at larger gates, while those which require a higher ratio will be captured at smaller gates.

## 6.3 Materials and Methods

### 6.3.1 Device Fabrication and Assembly

Two separate microchannel designs were used. The first has been previously described in-depth [23, 33, 55]. They both have many elements in common. Each microchannel is made from insulating material, with insulating equilateral triangle shapes along each wall to form a sawtooth pattern. Opposing points of these triangles come

together to form a constriction. The successive triangles increase in size from the inlet to the outlet, resulting in a decrease in the distance between opposing points. The first pattern, termed version 1 (V1), is 4.1 cm long, 1000 μm wide at the widest locations, and an average of 14 μm deep, with an inlet and an outlet reservoir at either end. Constrictions formed by opposing triangle points range from 945 μm nearest the inlet to 27 μm nearest the outlet. Each gate size repeats six times (Figure 6.2, top).

The second microchannel design, version 2 (V2), is 4.2 cm long, 1000 μm wide, and an average of 20 μm deep, again with an inlet and an outlet reservoir at either end. The constrictions formed in this microchannel range from 73 μm nearest the inlet to 25 μm nearest the outlet. Each gate size repeats three times (Figure 6.2, bottom).

Master silicon wafers with each channel pattern were created using soft lithography techniques. To make a wafer, it was first coated with AZ4330 photoresist (AZ Electronic Materials, Branchburg, NJ), then exposed through a chrome mask (JD Photo-Tools, United Kingdom) in the pattern of the microchannel. The wafer was then developed, leaving the channel pattern raised on the wafer in photoresist. The wafer was then etched using $SF_6$ and $C_4F_8$ gases with reactive ion etching (ICP etcher, SPTS, San Jose, CA). The resulting wafer is a negative of the microchannel, with the pattern raised.

To create the device used in dielectrophoresis experiments, polydimethyl siloxane (PDMS) (Sylgard 184, Dow/Corning, Midland, MI) casts were made of the silicon wafers. PDMS was poured over the wafer, then allowed to cure at 70°C for 1 hour. Following curing, the PDMS was peeled from the wafer and trimmed. Reservoir access

holes 3 mm in diameter were punched in either end. Casts were stored in the freezer for a maximum of one month before use.

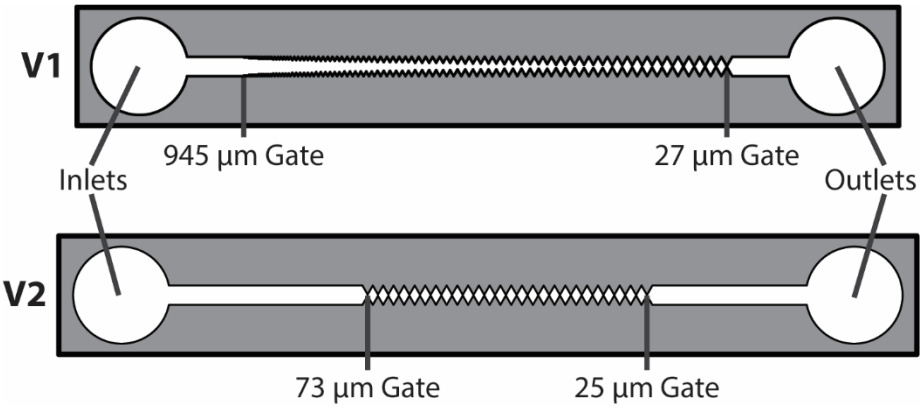



Figure 6.2 Patterns of the two channels used here, V1 (top) and V2 (bottom). The inlets are located on the left-hand side of the image, while the outlets are on the right. The sizes of the largest and smallest gates are indicated.

The device was assembled on the day experiments were performed. PDMS casts of the channel were cleaned with isopropanol, followed by water. Glass microscope slides (VWR, Radnor, PA) were cleaned with acetone, then isopropanol, then water. The PDMS and glass slide were treated with oxygen plasma (PDC-32G, Harrick-Plasma, Ithaca, NY), at 18 W for 60 seconds. Following plasma treatment, the PDMS and glass were allowed to seal upon contact, resulting in a microchannel with one wall of glass and three walls of PDMS.

### 6.3.2 Bacterial Culture

Two strains of *Staphylococcus epidermidis*, gentamicin-resistant ATCC 35983 and gentamicin-susceptible ATCC 14990, were obtained. Seed stock of each *S. epidermidis* strain was made in tryptic soy broth (TSB) with 10% glycerol, and stored at -80°C. To create liquid cultures, 8 mL sterile TSB was placed in culture tubes. The

broth was then inoculated with one strain of *S. epidermidis* and placed in a shaker/incubator overnight at 37°C.

### 6.3.3 Labeling

For single strain experiments, each strain was labeled with Vybrant DiO fluorescent dye (Invitrogen, Carlsbad, CA) (excitation 484 nm, emission 501 nm). The liquid culture of the bacteria was diluted 1:10 with 2 mM phosphate buffer. A 1 mL aliquot of diluted bacteria solution was mixed with 5 µL dye, mixed with agitation, and incubated at 37°C in a water bath for 20 minutes. Following incubation, the bacteria solution was centrifuged, the supernatant removed, and the bacteria resuspended in 2 mM phosphate buffer. This was repeated twice more for a total of three washes. The final resuspension was in 2 mM phosphate buffer with 4 mg/mL bovine serum albumin (BSA) (Sigma, St. Louis, MO).

For dual strain experiments, resistant and susceptible bacteria were labeled with either NHS-rhodamine or NHS-fluorescein. The process for labeling with either of the two dyes was the same. In each case, the liquid culture of the strain to be labeled was diluted 1:10 with phosphate buffer. A 10 mg/mL solution of NHS-rhodamine or NHS-fluorescein was made in DMSO. To label the bacteria, 1.0 mL bacteria dilution was incubated with 20 µL dye in DMSO solution at 37°C for 20 minutes. As before, the solution was centrifuged following incubation. The supernatant was removed and the pellet resuspended in 2 mM phosphate buffer at pH 7.4. This was repeated two more times, for a total of three centrifugations. Following the final centrifugation, the pellet was resuspended in 2 mM phosphate buffer with 4 mg/mL BSA. A mixture of resistant

and susceptible bacteria with opposite labels was made by combining equal volumes of each labeled strain (rhodamine-labeled resistant *S. epidermidis* and fluorescein-labeled susceptible *S. epidermidis*, or the opposite dyes).

### 6.3.4 Experimental

The V1 microchannel was used for single-strain experiments while the V2 microchannel was used for dual-strain experiments. In each case, the completed microchannel was filled with 15 µL 2 mM phosphate buffer at pH 7.4 in both the inlet and the outlet. The buffer was removed and the channel was conditioned with 15 µL 2 mM phosphate buffer with BSA placed in the inlet, which then was allowed to stand for 15 minutes.

For single strain experiments, the buffer was removed and 15 µL fluorescently-labeled bacteria solution was placed into the inlet, let stand for 5 minutes, followed by 15 µL 2 mM phosphate buffer with BSA placed into the outlet to balance pressure. Any further hydrodynamic flow was balanced with 2 mM phosphate buffer with BSA placed into the appropriate reservoir.

For dual strain experiments, the buffer was removed and 15 µL of the mixture of bacteria was placed in the inlet. Immediately after, 15 µL 2 mM phosphate buffer with BSA was placed into the outlet to balance pressure and stop the bacteria from reaching the gate area prior to application of potential. Hydrodynamic flow was again balanced with 2 mM phosphate buffer with BSA placed into the appropriate reservoir.

Completed microdevices were placed on an Olympus IX70 inverted microscope with a 4x objective. Potential was applied to the microchannel with platinum electrodes

placed in the inlet and outlet reservoirs. In single strain experiments, DC potentials from 100 V to 3000 V were applied across the microchannel. A single gate (27 μm) was monitored and video captured with a monochrome QICAM cooled CCD camera (QImaging, Inc., Surrey, UK), using Streampix V image capture software (Norpix, Inc., Montreal, QC). In dual strain experiments, a potential of 1000 V was applied across the microchannel. A range of gates was monitored and color video captured with an iPhone 5S camera (Apple, Cupertino, CA). Apple iPhoto (Apple, Cupertino, CA) was used to retrieve the images from the camera.

For both single strain and dual strain experiments, ImageJ (National Institutes of Health, Bethesda, Maryland) was used to analyze the image data.

### 6.3.5 Safety Considerations

All organisms used in this work are Biosafety Level I or II. All experiments were performed in an approved Biosafety Level II laboratory in accordance to the current version of the CDC/NIH BMBL publication.

## 6.4 Results and Discussion

Differences between the capture behavior of gentamicin-resistant and -susceptible *Staphylococcus epidermidis* were determined [61]. The susceptible strain requires a higher ratio of the gradient of the electric field squared to the magnitude of the electric field, $\frac{\nabla E^2}{E}$, than the resistant strain (Figure 6.3). The ratios determined are $5.7 \pm 3.3 \cdot 10^9$ V/m$^2$ and $1.15 \pm 0.17 \cdot 10^{10}$ V/m$^2$ for the resistant and susceptible strains, respectively.

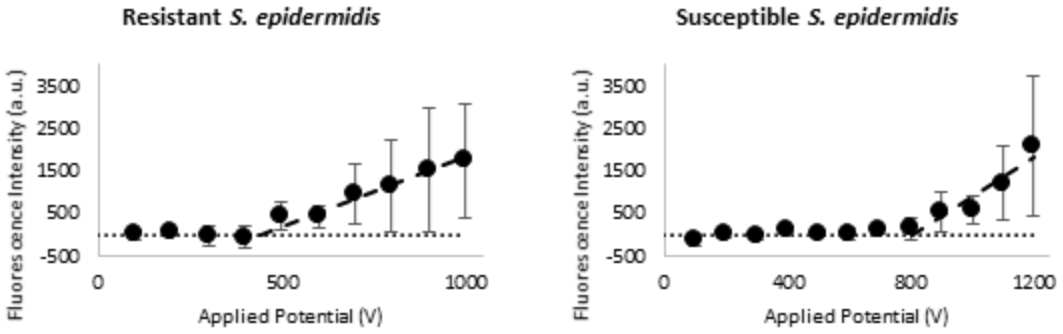



Figure 6.3 Dielectrophoresis data from gentamicin-resistant (left) and -susceptible (right) *Staphylococcus epidermidis*. Capture onset potentials for the two strains are 402 $\pm$ 230 V (resistant) and 800 $\pm$ 120 V (susceptible). Error bars are standard deviations. This data was previously published in [61].

There are two ways to achieve an increased $\frac{\nabla E^2}{E}$ ratio in a microchannel. First, the applied potential can be increased. This will increase both the gradient of the electric field as well as the magnitude of the applied field, but the gradient will increase at a faster rate. Increasing the applied potential will then result in an increase of $\frac{\nabla E^2}{E}$ ratio. This method of varying the applied potential was used in single strain experiments when a single gate was monitored in the V1 microchannel (Figure 6.2, top). Second, the size of the constriction, or gate, can be altered. The gate size will affect the magnitude of the gradient, with smaller constrictions having greater field gradients and therefore a greater $\frac{\nabla E^2}{E}$ ratio than areas with larger constrictions. This provides differing $\frac{\nabla E^2}{E}$ ratios within a microchannel when a single potential is applied. The V2 microchannel (Figure 6.2, bottom) was designed with nine different gate sizes. This provides nine possible different capture locations, each with its own properties and $\frac{\nabla E^2}{E}$ ratio with a single applied potential. The size of the gates in this channel were designed to give $\frac{\nabla E^2}{E}$ ratios that

would be useful for capturing bacteria and other like-sized analytes with achievable potentials.

Varying of gate sizes in the V2 microchannel was used to separate a mixture of gentamicin-resistant and -susceptible *S. epidermidis* in the microchannel in dual strain experiments. From the prior knowledge of *S. epidermidis* (Figure 6.3), the resistant strain is predicted to capture at larger gates, while the susceptible strain will require a higher $\frac{\nabla E^2}{E}$ ratio (smaller gate size). Instead, the susceptible bacteria will pass by the larger gates and be captured at locations with smaller constrictions and a higher $\frac{\nabla E^2}{E}$ ratio. This prediction based on single strain experiments was verified by separating a mixture of rhodamine-labeled resistant *S. epidermidis* and fluorescein-labeled susceptible *S. epidermidis* in a single V2 microchannel. The resistant strain captured at larger gates than the susceptible strain as expected (Figure 6.4).

In order to verify that this separation was not due entirely to differences between the two labels, the dyes were switched and the experiment repeated. A mixture of fluorescein-labeled resistant *S. epidermidis* and rhodamine-labeled susceptible *S. epidermidis* was separated. While the capture location of each strain shifted, signaling that the dye does have an effect on the capture of the bacteria, the susceptible strain still required a higher $\frac{\nabla E^2}{E}$ ratio for capture to occur than the resistant strain, and thus captured later in the microchannel as seen before (Figure 6.5).

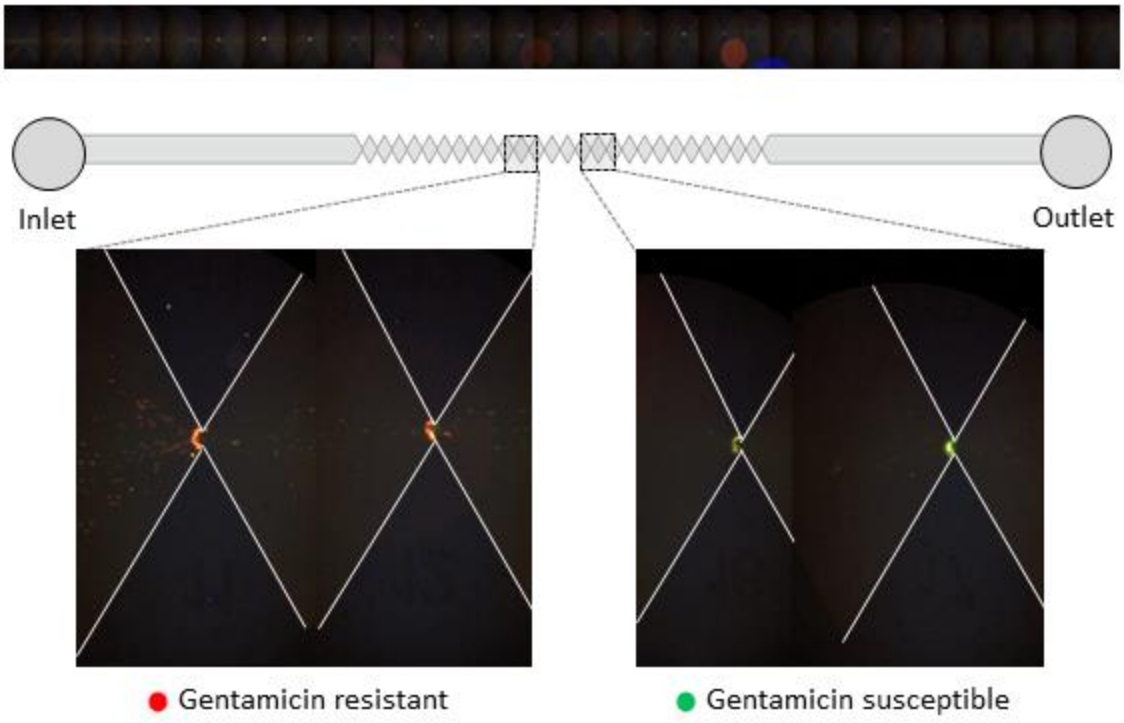



Figure 6.4 The separation of rhodamine-labeled resistant (red) and fluorescein-labeled susceptible (green) *Staphylococcus epidermidis*. A compilation of images of all gates (gate 1, left, to gate 27, right) in the microchannel, from various time points (top) shows the areas in which each strain captured. Larger images (bottom) show distinct red and green captured particles. This separation was originally published in [61].

This shift does bring in an interesting component. Since the identity and structure of each dye is known (Figure 6.6), and the attachment chemistry of the two dyes are similar, the conditions required for capture in each case can be compared. For the resistant strain, the rhodamine-labeled population captured at a smaller gate size than the fluorescein-labeled population. For the susceptible strain, the opposite occurred. The fluorescein-labeled population captured at a smaller gate size than the rhodamine-labeled population. Further analysis could shed more light on this difference, including determining whether the addition of the dye affecting electrokinetic mobility only,

dielectrophoretic mobility only, or both is responsible for the difference in capture conditions.

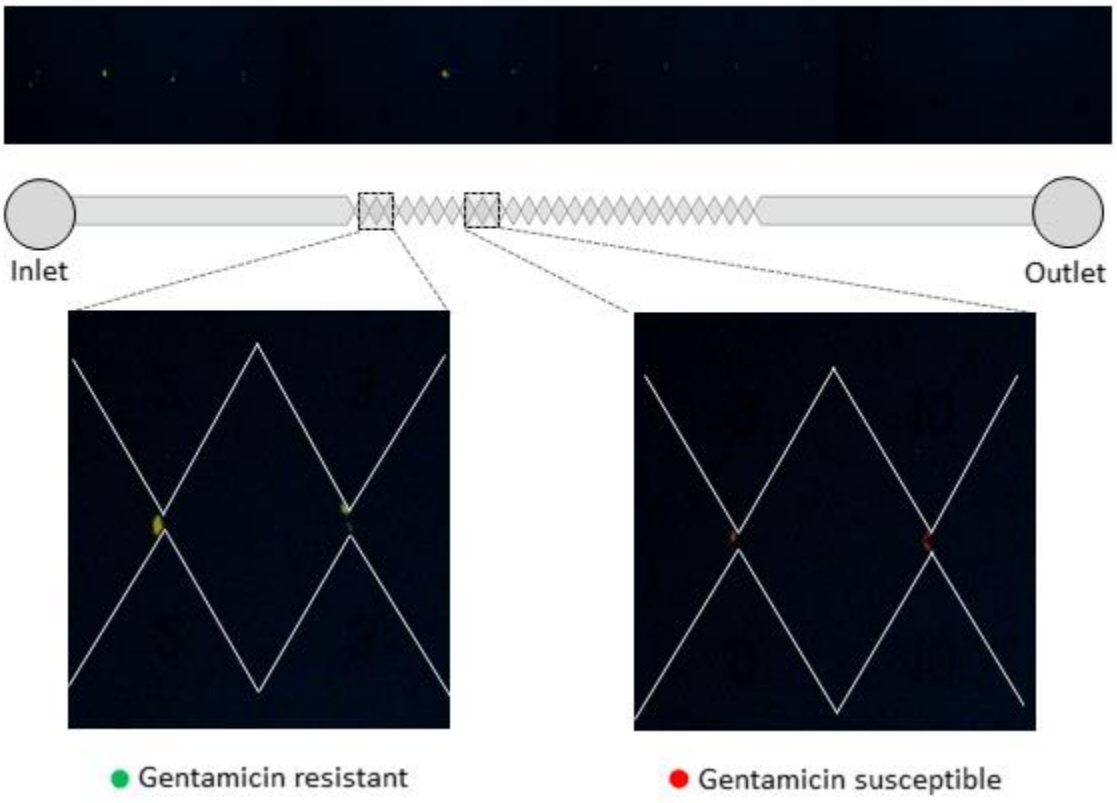



Figure 6.5 The separation of fluorescein-labeled resistant (green) and rhodamine-labeled susceptible (red) *Staphylococcus epidermidis*. A compilation of images of gates 1 (left) to 16 (right) in the microchannel, from various time points (top) shows the areas in which each strain captured. Larger images (bottom) show distinct red and green captured particles.

The gradient design of the insulator-based DEP device gives rise to the opportunity to separate more than two populations. The separations presented here have locations in the microchannel where no capture is occurring. Species or populations with the correct $\frac{\mu_{EK}}{\mu_{DEP}}$ ratio to capture at those locations could also be separated out of this mixture. The concentrations of the bacteria in the separations presented here were high,

resulting in overloading of the capture locations and all of the bacteria unable to capture at a single gate size. A lower concentration could allow for the capture to be even less spread down the channel as bacteria capture at the first gate which meets the capture conditions rather than being forced to a further gate. By capturing at fewer gates, there are more locations available for other populations to capture.

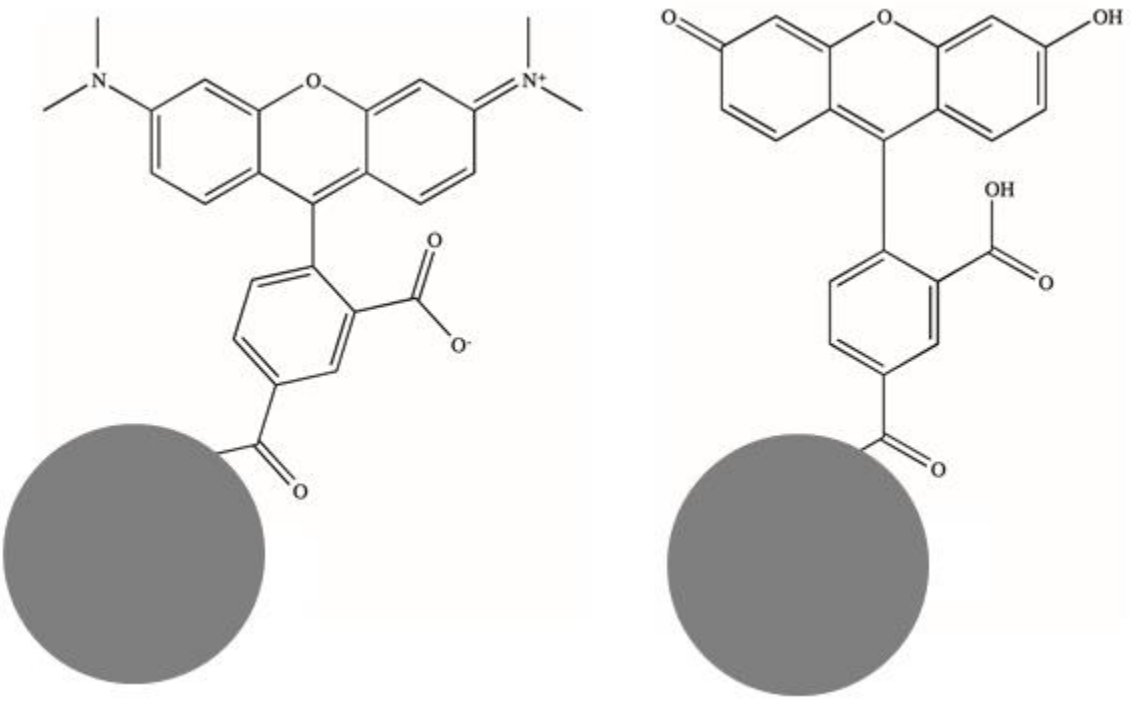



Figure 6.6 The structure of rhodamine (left) and fluorescein (right), as attached to a cell. These two dye molecules were used in the separation of resistant and susceptible *Staphylococcus epidermidis* (see Figures 6.4 and 6.5), and affect the capture conditions of each strain.

Three total dyes were used in this study: Vybrant DiO, NHS-rhodamine, and NHS-fluorescein. Vybrant DiO is an intercalating dye, inserting itself into the membrane, while the NHS dyes each attach to primary amine groups on the surface of the cell. In each case, the susceptible strain required a higher $\frac{\nabla E^2}{E}$ ratio for capture. By using three different dyes with two different mechanisms of attachment to the bacterial cell, it

shows that the difference in dielectrophoretic behavior is not tied to the dye itself or the number of dye molecules that can attach to the cellular surface, but rather is likely a function of the biophysical differences between the antibiotic resistant and susceptible strains.

## 6.5 Conclusions

Gentamicin-resistant and -susceptible strains of *Staphylococcus epidermidis* were studied with dielectrophoresis. The initial study showed that the susceptible strain required a higher $\frac{\nabla E^2}{E}$ ratio than the resistant strain for the capture to occur. This difference was exploited to successfully separate a mixture of the two strains in a gradient insulator-based dielectrophoresis device when labeled with two different dyes for identification. The resistant strain captured at larger gates than the susceptible strain. When the label on each strain was switched, the mixture continued to separate in the same order as before. With the gradient design of the device, mixtures of more than two populations could be separated in space in a single device.

## 6.6 References


1. European Committee on Antimicrobial Susceptibility Testing, *Reading guide: EUCAST disk diffusion method for antimicrobial susceptibility testing, version 6.0*, 2019.
2. European Committee on Antimicrobial Susceptibility Testing, *EUCAST reading guide for broth microdilution, version 1.0*, 2019.
3. World Health Organization, *Global Action Plan on Antimicrobial Resistance*, World Health Organizaion, Geneva, Switzerland, 2015.
4. Centers for Disease Control and Prevention, Antibiotic Resistance: A Global Threat, https://www.cdc.gov/features/antibiotic-resistance-global/index.html, (accessed February 11, 2019).

5. E. H. Ibrahim, G. Sherman, S. Ward, V. J. Fraser and M. H. Kollef, *CHEST*, 2000, *118*, 146-155.

6. C.-I. Kang, S.-H. Kim, W. B. Park, K.-D. Lee, H.-B. Kim, E.-C. Kim, M.-d. Oh and K.-W. Choe, *Antimicrobial Agents and Chemotherapy*, 2005, *49*, 760-766.

7. World Health Organization, Antimicrobial resistance, https://www.who.int/en/news-room/fact-sheets/detail/antimicrobial-resistance, (accessed February 13, 2019).

8. Centers for Disease Control and Prevention, *Antibiotic Resistance Threats in the United States, 2013*, 2013.

9. H. Goossens, M. Ferech, R. Vander Stichele and M. Elseviers, *The Lancet*, 2005, *365*, 579-587.

10. S. Riedel, S. E. Beekmann, K. P. Heilmann, S. S. Richter, J. Garcia-de-Lomas, M. Ferech, H. Goosens and G. V. Doern, *European Journal of Clinical Microbiology and Infectious Diseases*, 2007, *26*, 485-490.

11. E. A. Grice and J. A. Segre, *Nature Reviews Microbiology*, 2011, *9*, 244-253.

12. W. E. Kloos and M. S. Musselwhite, *Applied Microbiology*, 1975, *30*, 381-395.

13. C. Vuong and M. Otto, *Microbes and Infection*, 2002, *4*, 481-489.

14. M. Otto, *Nature Reviews Microbiology*, 2009, *7*, 555-567.

15. T. Hermann, *Cellular and Molecular Life Sciences*, 2007, *64*, 1841-1852.

16. G. D. Wright, *Chemical Communications*, 2011, *47*, 4055-4061.

17. G. H. Miller, F. J. Sabatelli, R. S. Hare, Y. Glupczynski, P. Mackey, D. Shales, K. Shimizu and K. J. Shaw, *Clinical Infectious Diseases*, 1997, *24*, S46-S62.

18. T. N. G. Adams, A. Y. L. Jiang, P. D. Vyas and L. A. Flanagan, *Methods*, 2018, *133*, 91-103.

19. C. Asbury, L., A. H. Dierks and G. van den Engh, *Electrophoresis*, 2002, *23*, 2658-2666.

20. C.-F. Chou, J. O. Tegenfeldt, O. Bakajin, S. S. Chan, E. C. Cox, N. Darnton, T. Duke and R. H. Austin, *Biophysical Journal*, 2002, *83*, 2170-2179.

21. P. R. C. Gascoyne, J. Noshari, T. J. Anderson and F. F. Becker, *Electrophoresis*, 2009, *30*, 1388-1398.

22. M. P. Hughes, H. Morgan, F. J. Rixon, J. P. H. Burt and R. Pethig, *Biochimica et Biophysica Acta*, 1998, *1425*, 119-126.

23. P. V. Jones, A. F. DeMichele, L. Kemp and M. A. Hayes, *Analytical and Bioanalytical Chemistry*, 2014, *406*, 183-192.

24. F. H. Labeed, J. Lu, H. J. Mulhall, S. A. Marchenko, K. F. Hoettges, L. C. Estrada, A. P. Lee, M. P. Hughes and L. A. Flanagan, *PLoS One*, 2011, *6*, e25458.

25. B. H. Lapizco-Encinas, S. Ozuna-Chacon and M. Rito-Palomares, *Journal of Chromatography A*, 2008, *1206*, 45-51.

26. B. H. Lapizco-Encinas, B. A. Simmons, E. B. Cummings and Y. Fintschenko, *Electrophoresis*, 2004, *25*, 1695-1704.

27. B. H. Lapizco-Encinas, B. A. Simmons, E. B. Cummings and Y. Fintschenko, *Analytical Chemistry*, 2004, *76*, 1571-1579.

28. G. H. Markx, Y. Huang, X.-F. Zhou and R. Pethig, *Microbiology*, 1994, *140*, 585-591.

29. H. Morgan and N. G. Green, *Journal of Electrostatics*, 1997, *42*, 279-293.

30. S. Otto, U. Kaletta, F. F. Bier, C. Wenger and R. Holzel, *Lab on a Chip*, 2014, *14*, 998-1004.

31. J. Regtmeier, T. T. Duong, R. Eichhorn, D. Anselmetti and A. Ros, *Analytical Chemistry*, 2007, *79*, 3925-3932.

32. H. Song, J. M. Rosano, Y. Wang, C. J. Garson, B. Prabhakarpandian, K. Pant, G. J. Klarmann, A. Perantoni, L. M. Alvarez and E. Lai, *Lab on a Chip*, 2015, *15*, 1320-1328.

33. S. J. R. Staton, P. V. Jones, G. Ku, S. D. Gilman, I. Kheterpal and M. A. Hayes, *Analyst*, 2012, *137*, 3227-3229.

34. S. Velugotla, S. Pells, H. K. Mjoseng, C. R. E. Duffy, S. Smith, P. De Sousa and R. Pethig, *Biomicrofluidics*, 2012, *6*, 44113.

35. X.-B. Wang, Y. Huang, J. P. H. Burt, G. H. Markx and R. Pethig, *Journal of Physics D: Applied Physics*, 1993, *26*, 1276-1285.

36. M. Washizu, S. Suzuki, O. Kurosawa, T. Nishizaka and T. Shinohara, *IEEE Transactions on Industry Applications*, 1994, *30*, 835-843.

37. J. Ding, C. Woolley and M. A. Hayes, *Analytical and Bioanalytical Chemistry*, 2017, *409*, 6405-6414.

38. J. S. Crane and H. A. Pohl, *Journal of The Electrochemical Society*, 1968, *115*, 584-586.

39. J. S. Crane and H. A. Pohl, *Journal of Electrostatics*, 1978, *5*, 11-19.

40. H. A. Pohl, *Journal of Applied Physics*, 1951, *22*, 869-871.

41. H. A. Pohl, *Dielectrophoresis The behavior of neutral matter in nonuniform electric fields*, Cambridge University Press, New York, 1978.

42. E. B. Cummings and A. K. Singh, *Analytical Chemistry*, 2003, *75*, 4724-4731.

43. J. Ding, R. M. Lawrence, P. V. Jones, B. G. Hogue and M. A. Hayes, *Analyst*, 2016, *141*, 1997-2008.

44. P. V. Jones, S. J. R. Staton and M. A. Hayes, *Analytical and Bioanalytical Chemistry*, 2011, *401*, 2103-2111.

45. A. LaLonde, M. F. Romero-Creel, M. A. Saucedo-Espinosa and B. H. Lapizco-Encinas, *Biomicrofluidics*, 2015, *9*, 064113.

46. H. Moncada-Hernandez, J. L. Baylon-Cardiel, V. H. Perez-Gonzalez and B. H. Lapizco-Encinas, *Electrophoresis*, 2011, *32*, 2502-2511.

47. A. Nakano, F. Camacho-Alanis and A. Ros, *Analyst*, 2015, *140*, 860-868.

48. M. A. Saucedo-Espinosa, A. LaLonde, A. Gencoglu, M. F. Romero-Creel, J. R. Dolas and B. H. Lapizco-Encinas, *Electrophoresis*, 2016, *37*, 282-290.

49. Q. Jin, C. Cui, H. Chen, J. Wu, J. Hu, X. Xing, J. Geng and Y. Wu, *Frontiers of Environmental Science & Engineering*, 2019, *13*, 16.

50. M. Elitas, Y. Yildizhan, M. Islam, R. Martinez-Duarte and D. Ozkazanc, *Electrophoresis*, 2019, *40*, 315-321.

51. M. T. Rabbani, C. F. Schmidt and A. Ros, *Analytical Chemistry*, 2017, *89*, 13235-13244.

52. A. Rohani, J. H. Moore, J. A. Kashatus, H. Sesaki, D. F. Kashatus and N. S. Swami, *Analytical Chemistry*, 2017, *89*, 5757-5764.

53. D. V. Polniak, E. Goodrich, N. Hill and B. H. Lapizco-Encinas, *Journal of Chromatography A*, 2018, *1545*, 84-92.

54. A. Lalonde, A. Gencoglu, M. F. Romero-Creel, K. S. Koppula and B. H. Lapizco-Encinas, *Journal of Chromatography A*, 2014, *1344*, 99-108.

55. S. J. R. Staton, K. P. Chen, T. J. Taylor, J. R. Pacheco and M. A. Hayes, *Electrophoresis*, 2010, *31*, 3634-3641.

56. J. T. Davies and E. K. Rideal, *Interfacial Phenomena*, Academic Press, New York, 1961.

57. N.-T. Nguyen and S. T. Wereley, *Fundamentals and Applications of Microfluidics*, Artech House, Boston, 2nd edn., 2006.

58. R. Pethig, *Biomicrofluidics*, 2010, *4*, 022811.

59. R. Pethig, *Dielectrophoresis : theory, methodology and biological applications*, Hoboken, NJ : John Wiley & Sons, Ltd, 1st edn., 2017.

60. P. Tabeling, *Introduction to Microfluidics*, Oxford University Press, New York, 2005.

61. P. V. Jones, S. Huey, P. Davis, R. Yanashima, R. McLemore, A. McLaren and M. A. Hayes, *Analyst*, 2015, *140*, 5152-5161.

# CHAPTER 7

# SUMMARY AND CONCLUSIONS

## 7.1 Summary

This dissertation has shown the differentiation and separation of bacteria with small biophysical differences using dielectrophoresis. The mathematical model of dielectrophoretic data presented in Chapter 3 connects biophysical properties to the features of dielectrophoretic data. This was demonstrated with features such as conductivity, zeta potential, and surface charge density. The degree to which each of these properties affect the features of the data (capture onset potential and slope) was assessed. Such a connection between physical properties of analytes and the features of the data allows for dielectrophoresis to begin to be used as a tool to assess these properties in subtly-different populations.

The differentiation of methicillin-resistant and -susceptible *Staphylococcus aureus* in Chapter 4 demonstrates the potential of dielectrophoresis to be used as a diagnostic tool. However, much more work would need to be done to establish the feasibility of this application. Performing this differentiation without a label shows that a label is not necessary for the distinction between the two strains. Assessment of the difference between the labeled and unlabeled population of a single strain allowed for the differentiation based on a known, chemical difference.

Chapter 5 demonstrates the extension of antibiotic resistance differentiation with dielectrophoresis to another genus of bacteria and mechanism of resistance. Two KPC-positive strains and one KPC-negative strain of *Klebsiella pneumoniae* were

differentiated. In addition, a change in one of the strains that occurred when re-plating was detected in differences in dielectrophoretic data. The ability to detect previously unknown differences in populations is a valuable property of this device. When unknown analytes are detected, further analysis could be undertaken to assess that unknown particle.

The separation of gentamicin-resistant and -susceptible *Staphylococcus epidermidis* is presented in Chapter 6. This separation took advantage of differences in dielectrophoretic response between the two strains detected with experiments on each strain individually to allow for their capture in two separate locations in the microchannel. The result was the separation and concentration of the analytes in space. With proper microchannel design, this separation could be extended to a larger number of analytes in a single channel.

**7.2 Future Outlook**

Dielectrophoresis shows promise as a high-resolution separation technique. The incorporation of features such as valves, pumps, and side channels could enable dielectrophoresis to be used in conjunction with other miniaturized analytical methods in a lab-on-a-chip configuration. Such a device could incorporate sample pre-treatment steps, separations, and a post separation analysis. In such a system, dielectrophoresis could be used in diagnostics, and specifically in rapid antimicrobial susceptibility testing.

For dielectrophoresis to be used as a diagnostic tool, or for it to be useful as a bioparticle analysis technique, more must be done to test the dielectrophoretic response of known biophysical differences. The variation in dielectrophoretic response of more

known, characterized population differences will allow for the characterization of the DEP response based on specific population changes that affect multiple properties. Combining multiple methods of dielectrophoresis, such as using AC fields with a DC offset, gives a larger number of features which can be assessed and properties of the analytes which can be tested.

### 7.3 Antimicrobial Susceptibility Testing

Current antimicrobial susceptibility testing is done via disk diffusion, broth dilution, and the E-test. Each of these methods requires multiple culturing steps. A pure sample must be obtained to grow again in the presence of antibiotics to determine the minimum inhibitory concentration of various antimicrobial agents. This method generally requires multiple days, and when complicating factors arise, can take up to a week or more. Studies have shown that a delay in proper treatment, such as an antimicrobial to which an infection is susceptible, by as little as one hour can have adverse effects on patient outcomes and survival [1] so a rapid test for susceptibility would be desirable.

Beyond the need for rapid tests in current healthcare schemes, point-of-care diagnostic devices have a place in many healthcare situations. Methods that meet the World Health Organization's ASSURED criteria (methods that are Affordable, Sensitive, Specific, User-friendly, Rapid and robust, Equipment-free, and Deliverable to end users) are useful in low-resource settings where common medical laboratory tests including disk diffusion and broth dilution discussed above cannot be performed. These tests could also find a place in rural areas where patients can travel to a hospital where these tests and the necessary infrastructure are available, but it would be a burden and so the journey is not

undertaken unless absolutely necessary. ASSURED-type devices could be used as in indicator if more serious medical intervention is needed and a trip should be taken to a hospital or if proper treatment can be administered from a local clinic.

### 7.4 Dielectrophoresis As A Point-Of-Care Device

Dielectrophoresis has many of the qualities required for these ASSURED diagnostic devices. Each individual device could be made inexpensively, likely at less than $1 per test if production of a specific device design was scaled up. The microchannels themselves are small, about 4.1 cm in length, 1 mm wide, and 20 μm deep, making them much easier to transport to the usage site. A single test takes on the order of minutes, indicating the speed of the test. The work presented in this dissertation shows the incredible sensitivity and specificity of DEP, and theory shows the resolution can be much greater than has been achieved here [2]. Further efforts in engineering would need to be made to enable the proper adaptation of dielectrophoresis to a device that can take advantage of these features of dielectrophoresis that lend it to a point-of-care device. Further, endeavors to make the technique more user-friendly, perhaps by becoming more automated, would be necessary for this method to find a place among such diagnostics.

The work presented in this dissertation contributes to the body of work necessary to enable DEP as a technique for such point-of-care devices. Connecting dielectrophoretic data to properties of particles, as shown in Chapter 3, is essential in understanding how small differences in analyte populations will affect dielectrophoresis and how those differences can be detected. Without a basis for understanding the

meaning of dielectrophoretic data, this technique is an interesting tool but less useful in real-world application involving identification of pathogens.

The investigations in Chapters 4, 5, and 6 illustrate real-world examples of small biophysical differences between populations distinguished with DEP. Specifically, antimicrobial susceptible and resistant strains of the same species of bacteria were shown to be able to be distinguished with this method. While prior work had shown that resistant and susceptible strains show differing dielectrophoretic behavior after treatment with antibiotics [3-10], this work shows that the difference in these strains is distinguishable in the native, untreated form. This enables the possibility of DEP used as a much more rapid diagnostic device, as time does not need to be taken to treat the pathogen. This supports the establishment of DEP as a rapid technique.

The separations from Chapter 6 demonstrate that DEP may be used with a mixed sample. If two analytes have different ratios of mobilities, which relates to their capture conditions, they can be separated in space while being concentrated at the capture location. While the range of pathogens used with this device up to this time is limited, they are spread out over a range of possible capture conditions, with a strain of *Listeria monocytogenes* having a ratio of mobilities of $2.2 \times 10^9 \frac{V}{m^2}$ and a *Klebsiella pneumoniae* strain with a ratio of greater than $2.0 \times 10^{10} \frac{V}{m^2}$. It is expected that while the capture conditions of some pathogens will overlap, they will likely group together in like-pathogens. By studying more analytes, a more complete picture of capture conditions of various pathogens can be formed. Knowledge of the capture conditions of a specific pathogen allow for the absence of that pathogen to be confirmed, as well as the

possibility of the presence of the pathogen to be assessed. In diagnostic devices, such negative results are important. The ability of dielectrophoresis to concentrate the particles would also facilitate the further analysis of collected analytes in a multiplexed system.

To present a fuller picture of the impact DEP may have on point-of-care devices, the work presented in Chapter 5 is highlighted. Imagine that a point-of-care diagnostic device has been employed in a low-resource setting. This device gives a yes/no answer to the presence of specific pathogens. Patients get the treatment they need. However, a minor mutation in one of the pathogens may induce a change that renders this treatment ineffective. This mutation may not appear in the diagnostic, which still indicates the presence of the same pathogen, suggesting the original treatment should be administered. This treatment stops working for the few individuals with this new form of the pathogen. A diagnostic device which can indicate small, unknown changes in a pathogen, such as those described in Chapter 5 of this dissertation, could prove useful in this case. The presence of a new health threat could be identified, the pathogen isolated, and a new response to this infection administered.

### 7.5 Other Applications of Dielectrophoresis

Dielectrophoresis could also find place in other pathogen detection schemes. These usages could be detection of foodborne pathogens and disease epidemiology. Small differences between strains indicates whether outbreaks are of the different origins. Detecting these small differences is difficult and time-consuming, but important for identifying and controlling outbreaks. Connecting disease related to foodborne

pathogens allows for the contaminated food to be located and removed from shelves and consumption stopped. If there are two different sources of similar pathogens, this must be identified so that the outbreak can be controlled.

While the work presented in this dissertation focuses on the analysis of bacteria, other microbes and non-living analytes can be studied with dielectrophoresis. These analyses would follow many of the same principles. The analysis of bacteria and other bioparticles enables the study of the living world, impacting medical treatment and human health.

### 7.6 References


1. A. Kumar, D. Roberts, K. E. Wood, B. Light, J. E. Parrillo, S. Sharma, R. Suppes, D. Feinstein, S. Zanotti, L. Taiberg, D. Gurka, A. Kumar and M. Cheang, *Critical Care Medicine*, 2006, *34*, 1589-1596.

2. P. V. Jones and M. A. Hayes, *Electrophoresis*, 2015, *36*, 1098-1106.

3. C.-C. Chung, I.-F. Cheng, H.-M. Chen, H.-C. Kan, W.-H. Yang and H.-C. Chang, *Analytical Chemistry*, 2012, *84*, 3347-3354.

4. K. F. Hoettges, Y. Hubner, L. M. Broche, S. L. Ogin, G. E. N. Kass and M. P. Hughes, *Analytical Chemistry*, 2008, *80*, 2063-2068.

5. S. Inoue, H.-B. Lee, A. L. Becker, K. M. Weigel, J.-H. Kim, K.-H. Lee, G. A. Cangelosi and J.-H. Chung, *Analytical and Bioanalytical Chemistry*, 2015, *407*, 7673-7680.

6. J. Kirchhoff, U. Glaser, J. A. Bohnert, M. W. Pletz, J. Popp and U. Neugebauer, *Analytical Chemistry*, 2018, *90*, 1811-1818.

7. A. Rohani, J. H. Moore, Y.-H. Su, V. Stagnaro, C. Warren and N. S. Swami, *Sensors and Actuators B: Chemical*, 2018, *276*, 472-480.

8. U.-C. Schroder, J. Kirchhoff, U. Hubner, G. Mayer, U. Glaser, T. Henkel, W. Pfister, W. Fritzsche, J. Popp and U. Neugebauer, *Journal of Biophotonics*, 2017, *10*, 1547-1557.

9. I.-H. Su, W.-C. Ko, C.-H. Shih, F.-H. Yeh, Y.-N. Sun, J.-C. Chen, P.-L. Chen and H.-C. Chang, *Analytical Chemistry*, 2017, *89*, 4635-4641.

10. Y.-H. Su, C. A. Warren, R. L. Guerrant and N. S. Swami, *Analytical Chemistry*, 2014, *86*, 10855-10863.

REFERENCES

## CHAPTER 1


1. B. M. Davis, *Science*, 1897, *6*, 145-157.

2. P. W. Nugent, J. A. Shaw and M. Vollmer, *Applied Optics*, 2015, *54*, B128-B139.

3. G. Smit, B. A. Smit and W. J. M. Engels, *FEMS Microbiology Reviews*, 2005, *29*, 591-610.

4. A. Zourari, J. P. Accolas and M. J. Desmazeaud, *Lait*, 1992, *72*, 1-34.

5. R. C. Burns and R. W. F. Hardy, *Nitrogen fixation in bacteria and higher plants*, Springer-Verlag, Berlin, 1975.

6. L. V. Hooper and J. I. Gordon, *Science*, 2001, *292*, 1115-1118.

7. D. E. Chandler and R. W. Roberson, *Bioimaging: Current Concepts in Light and Electron Microscopy*, Jones and Bartlett Publishers, Sudbury, MA, 2009.

8. Y. Cheng, *Science*, 2018, *361*, 876-880.

9. D. L. Armstrong, C. Erxleben and J. A. White, in *Calcium in Living Cells*, ed. M. Whitaker, Academic Press, Burlington, MA, 2010, vol. 99.

10. B. Sakmann and E. Neher, *Annual Review of Physiology*, 1984, *46*, 455-472.

11. J. W. Dale and M. von Schantz, *From Genes to Genomes: Concepts and Applications of DNA Technology*, John Wiley & Sons, West Sussex, England, 2002.

12. J. A. Cooper, B. R. Mintz, S. L. Palumbo and W.-J. Li, in *Characterization of Biomaterials*, eds. M. Jaffe, W. Hammond, P. Tolias and T. Arinzeh, Woodhead Publishing, Cambridge, 2013, DOI: 10.1533/9780857093684.101, pp. 101-137.

13. R. Spillman, W. Kopaciewicz and A. J. Weiss, in *Encyclopedia of Separation Science*, ed. I. D. Wilson, Academic Press, 2007.

14. J. T. Watson and O. D. Sparkman, *Introduction to Mass Spectrometry: Instrumentation, Applications and Strategies for Data Interpretation*, John Wiley & Sons, Hoboken, NJ, 2007.

15. S. Nerli, A. C. McShan and N. G. Sgourakis, *Progress in Nuclear Magnetic Resonance Spectroscopy*, 2018, *106-107*, 1-25.

16. T. W. Ni, M. A. Tofanelli and C. J. Ackerson, in *Protected Metal Clusters - From Fundamentals to Applications*, eds. T. Tsukuda and H. Hakkinen, 2015, DOI: 10.1016/b978-0-08-100086-1.00005-1, pp. 103-125.

17. M. Kovermann, P. Rogne and M. Wolf-Watz, *Quarterly Reviews of Biophysics*, 2016, *49*.

18. J. C. Giddings, *Dynamics of Chromatography*, M. Dekker, New York, 1965.

19. D. C. Harris, *Quantitative Chemical Analysis*, W. H. Freeman, New York, 7th edn., 2007.

20. J. M. Miller, *Chromatography : Concepts and Contrasts*, Wiley, Hoboken, N.J., 2nd ed.. edn., 2005.

21. T. F. Bidleman, *Journal of Chemical Education*, 1979, *56*, 293.

22. Chemical Rubber Company, *CRC handbook of chemistry and physics*, CRC Press : Taylor & Francis, Boca Raton, Fla., Electronic ed.. edn., 1978.

23. R. Tijssen, in *Handbook of HPLC*, eds. E. Katz, R. Eksteen, P. Schoenmakers and N. Miller, Marcel Dekker, New York, 2011.

24. C. F. Poole, in *Encyclopedia of Separation Science*, ed. I. D. Wilson, Academic Press, 2000.

25. D. N. Taulbee and M. M. Maroto-Valer, in *Encyclopedia of Separation Science*, ed. I. D. Wilson, Academic Press, 2000.

26. N.-T. Nguyen and S. T. Wereley, *Fundamentals and Applications of Microfluidics*, Artech House, Boston, 2nd edn., 2006.

27. D. Perrett, in *Encyclopedia of Separation Science*, ed. I. D. Wilson, Academic Press, 2000.

28. P. Tabeling, *Introduction to Microfluidics*, Oxford University Press, New York, 2005.

29. R. Smith and M. Jobson, in *Encyclopedia of Separation Science*, ed. I. D. Wilson, Academic Press, 2000.

30. D. E. Raynie, in *Encyclopedia of Separation Science*, ed. I. D. Wilson, Academic Press, 2000.

31. C. D. Chin, V. Linder and S. K. Sia, *Lab on a Chip*, 2012, *12*, 2118-2134.

32. C. J. Easley, J. M. Karlinsey, J. M. Bienvenue, L. A. Legendre, M. G. Roper, S. H. Feldman, M. A. Hughes, E. L. Hewlett, T. J. Merkl, J. P. Ferrance and J. P. Landers, *PNAS*, 2006, *103*, 19272-19277.

33. F. Lan, B. Demaree, N. Ahmed and A. R. Abate, *Nature Biotechnology*, 2017, *35*, 640-646.

34. L. R. Volpatti and A. K. Yetisen, *Trends in Biotechnology*, 2014, *32*, 347-350.

35. L. Y. Yeo, H.-C. Chang, P. P. Y. Chan and J. R. Friend, *Small*, 2011, *7*, 12-48.

36. A. K. Yetisen, M. S. Akram and C. R. Lowe, *Lab on a Chip*, 2013, *13*, 2210-2251.

37. S. B. Cheng, C. D. Skinner, J. Taylor, S. Attiya, W. E. Lee, G. Picelli and D. J. Harrison, *Analytical Chemistry*, 2001, *73*, 1472-1479.

38. E. Eteshola and B. Michal, *Biomedical Microdevices*, 2004, *6*, 7-9.

39. A. Fernández-la-Villa, V. Bertrand-Serrador, D. F. Pozo-Ayuso and M. Castaño-Álvarez, *Analytical Methods*, 2013, *5*, 1494-1501.

40. D. Hoegger, P. Morier, C. Vollet, D. Heini, F. Reymond and J. S. Rossier, *Analytical and Bioanalytical Chemistry*, 2007, *387*, 267-275.

41. J. S. Mellors, V. Gorbounov, R. S. Ramsey and J. M. Ramsey, *Analytical Chemistry*, 2008, *80*, 6881-6887.

42. S. Park, Y. Zhang, S. Lin, T.-H. Wang and S. Yang, *Biotechnology Advances*, 2011, *29*, 830-839.

43. E. A. Redman, J. S. Mellors, J. A. Starkey and J. M. Ramsey, *Analytical Chemistry*, 2016, *88*, 2220-2226.

44. T. Wang, M. Zhang, D. D. Dreher and Y. Zeng, *Lab on a Chip*, 2013, *13*, 4190-4197.

45. E. B. Cummings and A. K. Singh, *Analytical Chemistry*, 2003, *75*, 4724-4731.

46. D. R. Gossett, W. M. Weaver, A. J. Mach, S. C. Hur, H. T. K. Tse, W. Lee, H. Amini and D. Di Carlo, *Analytical and Bioanalytical Chemistry*, 2010, *397*, 3249-3267.

47. P. V. Jones, S. J. R. Staton and M. A. Hayes, *Analytical and Bioanalytical Chemistry*, 2011, *401*, 2103-2111.

48. S. J. R. Staton, K. P. Chen, T. J. Taylor, J. R. Pacheco and M. A. Hayes, *Electrophoresis*, 2010, *31*, 3634-3641.

49. Y. Zheng, J. Nguyen, Y. Wei and Y. Sun, *Lab on a Chip*, 2013, *13*, 2464-2483.

50. H. Kettler, K. White and S. Hawkes, *Mapping the landscape of diagnostics for sexually transmitted infections*, World Health Organization, 2004.

51. A. E. Herr, A. V. Hatch, D. J. Throckmorton, H. M. Tran, J. S. Brennan, W. V. Giannobile and A. K. Singh, *PNAS*, 2007, *104*, 5268-5273.

52. X. Mao and T. J. Huang, *Lab on a Chip*, 2012, *12*, 1412-1416.

53. N. M. Myers, E. N. Kernisan and M. Lieberman, *Analytical Chemistry*, 2015, *87*, 3764-3770.

54. V. Srinivasan, V. K. Pamula and R. B. Fair, *Lab on a Chip*, 2004, *4*, 310-315.

55. W. Su, X. Gao, L. Jiang and J. Qin, *Journal of Chromatography A*, 2015, *1377*, 13-26.

56. A. A. Weaver, H. Reiser, T. Barstis, M. Benvenuti, D. Ghosh, M. Hunckler, B. Joy, L. Koenig, K. Raddell and M. Lieberman, *Analytical Chemistry*, 2013, *85*, 6453-6460.

57. C. Kaplan, in *Clinical Methods: The History, Physical, and Laboratory Examinations*, eds. H. K. Walker, W. D. Hall and J. W. Hurst, Butterworths, Boston, 3rd edn., 1990.

58. Clinical and Laboratory Standards Institute, Microbiology: Standards, https://clsi.org/standards/products/microbiology/documents/, (accessed February 22, 2019).

59. R. I. Aminov, *Frontiers in Microbiology*, 2010, *1*, 134.

60. J. Davies and D. Davies, *Microbiology and Molecular Biology Reviews*, 2010, *74*, 417-433.

61. A. Fleming, *British Journal of Experimental Pathology*, 1929, *10*, 226-236.

62. E. P. Abraham and E. Chain, *Reviews of Infectious Diseases*, 1988, *10*, 677-678.

63. K. Bush, *Clinical Microbiology and Infection*, 2004, *10 Suppl 4*, 10-17.

64. J. O'Neill, *Tackling Drug-Resistant Infections Globally: Final Report and Recommendations*, 2016.

65. Centers for Disease Control and Prevention, *Antibiotic Resistance Threats in the United States, 2013*, 2013.

66. F. C. Tenover, *American Journal of Infection Control*, 2006, *34*, S3-S10.

67. J. H. Jorgensen and J. D. Turnidge, in *Manual of Clinical Microbiology*, eds. J. H. Jorgensen and M. A. Pfaller, ASM Press, Washington, DC, 11th edn., 2015.

68. F. P. Maurer, M. Christner, M. Hentschke and H. Rohde, *Infectious Disease Reports*, 2017, *9*, 18-27.

69. J. D. Turnidge, in *Manual of Clinical Microbiology*, eds. J. H. Jorgensen and M. A. Pfaller, ASM Press, Washington, DC, 11th edn., 2015.

70. A. Kumar, D. Roberts, K. E. Wood, B. Light, J. E. Parrillo, S. Sharma, R. Suppes, D. Feinstein, S. Zanotti, L. Taiberg, D. Gurka, A. Kumar and M. Cheang, *Critical Care Medicine*, 2006, *34*, 1589-1596.

71. Centers for Disease Control and Prevention, Antibiotic/Antimicrobial Resistance: Combat Antimicrobial Resistance Globally, https://www.cdc.gov/drugresistance/intl-actvities.html, (accessed 25 February, 2019).

72. World Health Organization, Antimicrobial resistance, https://www.who.int/en/news-room/fact-sheets/detail/antimicrobial-resistance, (accessed February 13, 2019).

**CHAPTER 2**

1. N.-T. Nguyen and S. T. Wereley, *Fundamentals and Applications of Microfluidics*, Artech House, Boston, 2nd edn., 2006.

2. P. Tabeling, *Introduction to Microfluidics*, Oxford University Press, New York, 2005.

3. A. Lalonde, A. Gencoglu, M. F. Romero-Creel, K. S. Koppula and B. H. Lapizco-Encinas, *Journal of Chromatography A*, 2014, *1344*, 99-108.

4. H. Moncada-Hernandez, J. L. Baylon-Cardiel, V. H. Perez-Gonzalez and B. H. Lapizco-Encinas, *Electrophoresis*, 2011, *32*, 2502-2511.

5. H. A. Pohl, *Journal of Applied Physics*, 1951, *22*, 869-871.

6. H. A. Pohl, *Dielectrophoresis The behavior of neutral matter in nonuniform electric fields*, Cambridge University Press, New York, 1978.

7. A. Nakano, F. Camacho-Alanis and A. Ros, *Analyst*, 2015, *140*, 860-868.

8. C. V. Crowther and M. A. Hayes, *Analyst*, 2017, *142*, 1608-1618.

9. M. J. Beauchamp, H. Gong, A. T. Woolley and G. P. Nordin, *Micromachines*, 2018, *9*.

10. A. Enders, I. G. Siller, K. Urmann, M. R. Hoffmann and J. Bahnemann, *Small*, 2019, *15*, 1804326.

11. H. Gong, A. T. Woolley and G. P. Nordin, *Lab on a Chip*, 2016, *16*, 2450-2458.

12. A. Lambert, S. Valiulis and Q. Cheng, *ACS Sensors*, 2018, *3*, 2475-2491.

13. M. F. Santangelo, S. Libertino, A. P. F. Turner, D. Filippini and W. C. Mak, *Biosensors and Bioelectronics*, 2018, *99*, 464-470.

14. Y. Huang, S. Liu, W. Yang and C. Yu, *Applied Surface Science*, 2010, *256*, 1675-1678.

15. B. G. Hawkins, A. E. Smith, Y. A. Syed and B. J. Kirby, *Analytical Chemistry*, 2007, *79*, 7291-7300.

16. B. L. Thompson, Y. Ouyang, G. R. Duarte, E. Carrilho, S. T. Krauss and J. P. Landers, *Nature Protocols*, 2015, *10*, 875-886.

17. P. K. Yuen and V. N. Goral, *Lab on a Chip*, 2010, *10*, 384-387.

18. H. Becker and C. Gartner, *Electrophoresis*, 2000, *21*, 12-26.

19. S. Bhattacharya, A. Datta, J. M. Berg and S. Gangopadhyay, *Journal of Microelectromechanical Systems*, 2005, *14*, 590-597.

20. H.-J. Hettlich, F. Otterbach, C. Mittermayer, R. Kaufmann and D. Klee, *Biomaterials*, 1991, *12*, 521-524.

21. H. Hillborg and U. W. Gedde, *Polymer*, 1998, *39*, 1991-1998.

22. F. Camacho-Alanis, L. Gan and A. Ros, *Sensors and Actuators B: Chemical*, 2012, *173*, 668-675.

23. J. Melin and S. R. Quake, *Annual Review of Biophysics and Biomolecular Structure*, 2007, *36*, 213-231.

24. A. Mohammadzadeh, A. E. Fox-Robichaud and P. R. Selvaganapathy, *Journal of Micromechanics and Microengineering*, 2019, *29*, 015013.

25. H. S. Rho, Y. Yang, A. T. Hanke, M. Ottens, L. W. M. M. Terstappen and H. Gardeniers, *Lab on a Chip*, 2016, *16*, 305-311.

26. M. A. Unger, H.-P. Chou, T. Thorsen, A. Scherer and S. R. Quake, *Science*, 2000, *228*, 113-116.

27. C. J. Lee, H. J. Sheen, H. C. Chu, C. J. Hsu and T. H. Wu, *Journal of Micromechanics and Microengineering*, 2007, *17*, 439-446.

28. Y. Temiz, J. Skorucak and E. Delamarche, *Journal of Micro/Nanolithography, MEMS, and MOEMS*, 2014, *13*, 033018.

29. C.-S. Chen, D. N. Breslauer, J. I. Luna, A. Grimes, W.-c. Chin, L. P. Lee and M. Khine, *Lab on a Chip*, 2008, *8*, 622-624.

30. B.-H. Jo, L. M. Van Lerberghe, K. M. Motsegood and D. J. Beebe, *Journal of Microelectromechanical Systems*, 2000, *9*, 76-81.

31. A. R. Schor and C. R. Buie, *Journal of Micromechanics and Microengineering*, 2016, *26*, 105010.

32. T. B. Jones, *Electromechanics of Particles*, Cambridge University Press, New York, 1995.

33. R. Pethig, *Dielectrophoresis : theory, methodology and biological applications*, Hoboken, NJ : John Wiley & Sons, Ltd, 1st edn., 2017.

34. M. Castellarnau, A. Errachid, C. Madrid, A. Juarez and J. Samitier, *Biophysical Journal*, 2006, *91*, 3937-3945.

35. J. S. Crane and H. A. Pohl, *Journal of The Electrochemical Society*, 1968, *115*, 584-586.

36. F. H. Labeed, J. Lu, H. J. Mulhall, S. A. Marchenko, K. F. Hoettges, L. C. Estrada, A. P. Lee, M. P. Hughes and L. A. Flanagan, *PLoS One*, 2011, *6*, e25458.

37. G. H. Markx, Y. Huang, X.-F. Zhou and R. Pethig, *Microbiology*, 1994, *140*, 585-591.

38. S. K. Srivastava, P. R. Daggolu, S. C. Burgess and A. R. Minerick, *Electrophoresis*, 2008, *29*, 5033-5046.

39. X.-B. Wang, Y. Huang, J. P. H. Burt, G. H. Markx and R. Pethig, *Journal of Physics D: Applied Physics*, 1993, *26*, 1276-1285.

40. C.-F. Chou, J. O. Tegenfeldt, O. Bakajin, S. S. Chan, E. C. Cox, N. Darnton, T. Duke and R. H. Austin, *Biophysical Journal*, 2002, *83*, 2170-2179.

41. E. B. Cummings and A. K. Singh, *Analytical Chemistry*, 2003, *75*, 4724-4731.

42. T. N. G. Adams, A. Y. L. Jiang, P. D. Vyas and L. A. Flanagan, *Methods*, 2018, *133*, 91-103.

43. C. Asbury, L., A. H. Dierks and G. van den Engh, *Electrophoresis*, 2002, *23*, 2658-2666.

44. F. F. Becker, X.-B. Wang, Y. Huang, R. Pethig, J. Vykoukal and P. R. C. Gascoyne, *Proceedings of the National Academy of Sciences of the United States of America*, 1995, *92*, 860-864.

45. J. Ding, R. M. Lawrence, P. V. Jones, B. G. Hogue and M. A. Hayes, *Analyst*, 2016, *141*, 1997-2008.

46. M. P. Hughes, H. Morgan, F. J. Rixon, J. P. H. Burt and R. Pethig, *Biochimica et Biophysica Acta*, 1998, *1425*, 119-126.

47. P. V. Jones, A. F. DeMichele, L. Kemp and M. A. Hayes, *Analytical and Bioanalytical Chemistry*, 2014, *406*, 183-192.

48. B. H. Lapizco-Encinas, S. Ozuna-Chacon and M. Rito-Palomares, *Journal of Chromatography A*, 2008, *1206*, 45-51.

49. B. H. Lapizco-Encinas, B. A. Simmons, E. B. Cummings and Y. Fintschenko, *Analytical Chemistry*, 2004, *76*, 1571-1579.

50. H. Morgan and N. G. Green, *Journal of Electrostatics*, 1997, *42*, 279-293.

51. S. Otto, U. Kaletta, F. F. Bier, C. Wenger and R. Holzel, *Lab on a Chip*, 2014, *14*, 998-1004.

52. J. Regtmeier, T. T. Duong, R. Eichhorn, D. Anselmetti and A. Ros, *Analytical Chemistry*, 2007, *79*, 3925-3932.

53. H. Song, J. M. Rosano, Y. Wang, C. J. Garson, B. Prabhakarpandian, K. Pant, G. J. Klarmann, A. Perantoni, L. M. Alvarez and E. Lai, *Lab on a Chip*, 2015, *15*, 1320-1328.

54. S. J. R. Staton, P. V. Jones, G. Ku, S. D. Gilman, I. Kheterpal and M. A. Hayes, *Analyst*, 2012, *137*, 3227-3229.

55. M. Washizu, S. Suzuki, O. Kurosawa, T. Nishizaka and T. Shinohara, *IEEE Transactions on Industry Applications*, 1994, *30*, 835-843.

56. M. Washizu and O. Kurosawa, *IEEE Transactions on Industry Applications*, 1990, *26*, 1165-1172.

57. J. Ding, C. Woolley and M. A. Hayes, *Analytical and Bioanalytical Chemistry*, 2017, *409*, 6405-6414.

58. P. R. C. Gascoyne, J. Noshari, T. J. Anderson and F. F. Becker, *Electrophoresis*, 2009, *30*, 1388-1398.

59. A. LaLonde, M. F. Romero-Creel, M. A. Saucedo-Espinosa and B. H. Lapizco-Encinas, *Biomicrofluidics*, 2015, *9*, 064113.

**CHAPTER 3**

1. H. A. Pohl, *Journal of Applied Physics*, 1951, *22*, 869-871.

2. R. Pethig, *Journal of The Electrochemical Society*, 2016, *164*, B3049-B3055.

3. C. Asbury, L., A. H. Dierks and G. van den Engh, *Electrophoresis*, 2002, *23*, 2658-2666.

4. C.-F. Chou, J. O. Tegenfeldt, O. Bakajin, S. S. Chan, E. C. Cox, N. Darnton, T. Duke and R. H. Austin, *Biophysical Journal*, 2002, *83*, 2170-2179.

5. P. R. C. Gascoyne, J. Noshari, T. J. Anderson and F. F. Becker, *Electrophoresis*, 2009, *30*, 1388-1398.

6. P. V. Jones, A. F. DeMichele, L. Kemp and M. A. Hayes, *Analytical and Bioanalytical Chemistry*, 2014, *406*, 183-192.

7. B. H. Lapizco-Encinas, S. Ozuna-Chacon and M. Rito-Palomares, *Journal of Chromatography A*, 2008, *1206*, 45-51.

8. B. H. Lapizco-Encinas, B. A. Simmons, E. B. Cummings and Y. Fintschenko, *Analytical Chemistry*, 2004, *76*, 1571-1579.

9. G. H. Markx, Y. Huang, X.-F. Zhou and R. Pethig, *Microbiology*, 1994, *140*, 585-591.

10. S. Otto, U. Kaletta, F. F. Bier, C. Wenger and R. Holzel, *Lab on a Chip*, 2014, *14*, 998-1004.

11. J. Regtmeier, T. T. Duong, R. Eichhorn, D. Anselmetti and A. Ros, *Analytical Chemistry*, 2007, *79*, 3925-3932.

12. S. J. R. Staton, P. V. Jones, G. Ku, S. D. Gilman, I. Kheterpal and M. A. Hayes, *Analyst*, 2012, *137*, 3227-3229.

13. X.-B. Wang, Y. Huang, J. P. H. Burt, G. H. Markx and R. Pethig, *Journal of Physics D: Applied Physics*, 1993, *26*, 1276-1285.

14. M. Washizu, S. Suzuki, O. Kurosawa, T. Nishizaka and T. Shinohara, *IEEE Transactions on Industry Applications*, 1994, *30*, 835-843.

15. T. N. G. Adams, K. M. Leonard and A. R. Minerick, *Biomicrofluidics*, 2013, *7*, 64114.

16. P. V. Jones, S. J. R. Staton and M. A. Hayes, *Analytical and Bioanalytical Chemistry*, 2011, *401*, 2103-2111.

17. Y. Huang, R. Holzel, R. Pethig and X.-B. Wang, *Physics in Medicine and Biology*, 1992, *37*, 1499-1517.

18. T. B. Jones, *Electromechanics of Particles*, Cambridge University Press, New York, 1995.

19. R. Pethig, *Biomicrofluidics*, 2010, *4*, 022811.

20. H. A. Pohl, *Dielectrophoresis The behavior of neutral matter in nonuniform electric fields*, Cambridge University Press, New York, 1978.

21. M. Washizu and T. B. Jones, *Journal of Electrostatics*, 1994, *33*, 187-198.

22. J. S. Crane and H. A. Pohl, *Journal of Electrostatics*, 1978, *5*, 11-19.

23. Z. R. Gagnon, *Electrophoresis*, 2011, *32*, 2466-2487.

24. E. B. Cummings and A. K. Singh, *Analytical Chemistry*, 2003, *75*, 4724-4731.

25. F. F. Becker, X.-B. Wang, Y. Huang, R. Pethig, J. Vykoukal and P. R. C. Gascoyne, *Proceedings of the National Academy of Sciences of the United States of America*, 1995, *92*, 860-864.

26. A. Rohani, J. H. Moore, J. A. Kashatus, H. Sesaki, D. F. Kashatus and N. S. Swami, *Analytical Chemistry*, 2017, *89*, 5757-5764.

27. T. N. G. Adams, A. Y. L. Jiang, P. D. Vyas and L. A. Flanagan, *Methods*, 2018, *133*, 91-103.

28. S. K. Srivastava, P. R. Daggolu, S. C. Burgess and A. R. Minerick, *Electrophoresis*, 2008, *29*, 5033-5046.

29. P. V. Jones, S. Huey, P. Davis, R. Yanashima, R. McLemore, A. McLaren and M. A. Hayes, *Analyst*, 2015, *140*, 5152-5161.

30. W. A. Braff, D. Willner, P. Hugenholtz, K. Rabaey and C. R. Buie, *PLoS One*, 2013, *8*, e76751.

31. P. V. Jones and M. A. Hayes, *Electrophoresis*, 2015, *36*, 1098-1106.

32. A. LaLonde, M. F. Romero-Creel, M. A. Saucedo-Espinosa and B. H. Lapizco-Encinas, *Biomicrofluidics*, 2015, *9*, 064113.

33. A. R. Minerick, *AIChE Journal*, 2008, *54*, 2230-2237.

34. M. A. Saucedo-Espinosa and B. H. Lapizco-Encinas, *Electrophoresis*, 2015, *36*, 1086-1097.

35. S. J. R. Staton, K. P. Chen, T. J. Taylor, J. R. Pacheco and M. A. Hayes, *Electrophoresis*, 2010, *31*, 3634-3641.

36. J. T. Davies and E. K. Rideal, *Interfacial Phenomena*, Academic Press, New York, 1961.

37. N.-T. Nguyen and S. T. Wereley, *Fundamentals and Applications of Microfluidics*, Artech House, Boston, 2nd edn., 2006.

38. P. Tabeling, *Introduction to Microfluidics*, Oxford University Press, New York, 2005.

39. R. W. Clarke, J. D. Piper, L. Ying and D. Klenerman, *Physical Review Letters*, 2007, *98*, 198102.

40. H. Nili and N. G. Green, *Physical Review E: Statistical, Nonlinear, and Soft Matter Physics*, 2014, *89*, 063302.

41. A. Irimajiri, T. Hanai and A. Inoyue, *Journal of Theoretical Biology*, 1979, *78*, 251-269.

42. W. Bai, K. Zhao and K. Asami, *Colloids and Surfaces, B: Biointerfaces*, 2007, *58*, 105-115.

43. T. Kakutani, S. Shibatani and M. Sugai, *Bioelectrochemistry and Bioenergetics*, 1993, *31*, 131-145.

44. H. Ohshima and T. Kondo, *Journal of Colloid and Interface Science*, 1987, *116*, 305-311.

45. H. Ohshima and T. Kondo, *Journal of Colloid and Interface Science*, 1989, *130*, 281-282.

46. R. Sonohara, N. Muramatsu, H. Ohshima and T. Kondo, *Biophysical Chemistry*, 1995, *55*, 273-277.

47. E. Daly and B. R. Saunders, *Physical Chemistry Chemical Physics*, 2000, *2*, 3187-3193.

48. J. L. Ortega-Vinuesa, R. Hidalgo-Alvarez, F. J. de las Nieves, C. L. Davey, D. J. Newman and C. P. Price, *Journal of Colloid and Interface Science*, 1998, *204*, 300-311.

49. S. Takashima and H. Morisaki, *Colloids and Surfaces, B: Biointerfaces*, 1997, *9*, 205-212.

50. M. Torimura, S. Ito, K. Kano, T. Ikeda, Y. Esaka and T. Ueda, *Journal of Chromatography B*, 1999, *721*, 31-37.

51. J. L. Anderson, *Journal of Colloid and Interface Science*, 1985, *105*, 45-54.

52. M. C. Fair and J. L. Anderson, *Journal of Colloid and Interface Science*, 1989, *127*, 388-400.

53. M. D. Pysher and M. A. Hayes, *Langmuir*, 2005, *21*, 3572-3577.

54. M. Dinpajooh and D. V. Matyushov, *Journal of Chemical Physics*, 2016, *145*, 014504.

55. M. Dinpajooh and D. V. Matyushov, *Physica A: Statistical Mechanics and its Applications*, 2016, *463*, 366-375.

56. D. V. Matyushov, *Journal of Chemical Physics*, 2004, *120*, 1375-1382.

57. D. V. Matyushov, *Journal of Chemical Physics*, 2012, *136*, 085102.

58. D. V. Matyushov, *Molecular Physics*, 2014, *112*, 2029-2039.

59. S. Seyedi and D. V. Matyushov, *Chemical Physics Letters*, 2018, *712*, accepted (preprint available from corresponding author).

60. C. V. Crowther and M. A. Hayes, *Analyst*, 2017, *142*, 1608-1618.

61. W. A. Braff, A. Pignier and C. R. Buie, *Lab on a Chip*, 2012, *12*, 1327-1331.

62. F. Camacho-Alanis, L. Gan and A. Ros, *Sensors and Actuators B: Chemical*, 2012, *173*, 668-675.

63. J. Ding, R. M. Lawrence, P. V. Jones, B. G. Hogue and M. A. Hayes, *Analyst*, 2016, *141*, 1997-2008.

64. J. Ding, C. Woolley and M. A. Hayes, *Analytical and Bioanalytical Chemistry*, 2017, *409*, 6405-6414.

65. A. Nakano, F. Camacho-Alanis and A. Ros, *Analyst*, 2015, *140*, 860-868.

66. D. V. Polniak, E. Goodrich, N. Hill and B. H. Lapizco-Encinas, *Journal of Chromatography A*, 2018, *1545*, 84-92.

67. M. T. Rabbani, C. F. Schmidt and A. Ros, *Analytical Chemistry*, 2017, *89*, 13235-13244.

68. M. A. Saucedo-Espinosa, A. LaLonde, A. Gencoglu, M. F. Romero-Creel, J. R. Dolas and B. H. Lapizco-Encinas, *Electrophoresis*, 2016, *37*, 282-290.

69. B. Brazey, J. Cottet, A. Bolopion, H. Van Lintel, P. Renaud and M. Gauthier, *Lab on a Chip*, 2018, *18*, 818-831.

70. C.-H. Chuang and Y.-W. Huang, *Microelectronic Engineering*, 2012, *97*, 317-323.

71. B. H. Lapizco-Encinas, B. A. Simmons, E. B. Cummings and Y. Fintschenko, *Electrophoresis*, 2004, *25*, 1695-1704.

72. H. Moncada-Hernandez, J. L. Baylon-Cardiel, V. H. Perez-Gonzalez and B. H. Lapizco-Encinas, *Electrophoresis*, 2011, *32*, 2502-2511.

73. S. Ozuna-Chacon, B. H. Lapizco-Encinas, M. Rito-Palomares, S. O. Martinez-Chapa and C. Reyes-Betanzo, *Electrophoresis*, 2008, *29*, 3115-3122.

74. Z. Wang, T. Han, T.-J. Jeon, S. Park and S. M. Kim, *Sensors and Actuators B: Chemical*, 2013, *178*, 683-688.

75. Y. Tomizawa, E. Tamiya and Y. Takamura, *Physical Review E: Statistical, Nonlinear, and Soft Matter Physics*, 2009, *79*, 051902.

76. R. Pethig, *Dielectrophoresis : theory, methodology and biological applications*, Hoboken, NJ : John Wiley & Sons, Ltd, 1st edn., 2017.

77. G. H. Markx and C. L. Davey, *Enzyme and Microbial Technology*, 1999, *25*, 161-171.

78. R. Pethig and G. H. Markx, *Trends in Biotechnology*, 1997, *15*, 426-432.

79. R. Holzel, *Biochimica et Biophysica Acta*, 1999, *1450*, 53-60.

80. J. Olsson and P.-O. Glantz, *Archives of Oral Biology*, 1977, *22*, 461-466.

81. A. van der Wal, M. Minor, W. Norde, A. J. B. Zehnder and J. Lyklema, *Journal of Colloid and Interface Science*, 1997, *186*, 71-79.

82. W. W. Wilson, M. M. Wade, S. C. Holman and F. R. Champlin, *Journal of Microbiological Methods*, 2001, *43*, 153-164.

83. P. J. M. Kiers, R. Bos, H. C. van der Mei and H. J. Busscher, *Microbiology*, 2001, *147*, 757-762.

84. T. Schnelle, T. Muller, S. Fiedler and G. Fuhr, *Journal of Electrostatics*, 1999, *46*, 13-28.

85. E. Liang, R. L. Smith and D. S. Clague, *Physical Review E: Statistical, Nonlinear, and Soft Matter Physics*, 2004, *70*, 066617.

86. M. Washizu, T. B. Jones and K. V. I. S. Kaler, *Biochimica et Biophysica Acta*, 1993, *1158*, 40-46.

87. M. Washizu, *Journal of Electrostatics*, 1992, *29*, 177-188.

**CHAPTER 4**

1. K. Loewen, Y. Schreiber, M. Kirlew, N. Bocking and L. Kelly, *Canadian Family Physician*, 2017, *63*, 512-520.

2. F. D. Lowy, *The New England Journal of Medicine*, 1998, *339*, 520-532.

3. W. C. Noble, H. A. Valkenburg and C. H. L. Wolters, *Journal of Hygiene*, 1967, *65*, 567-573.

4. A. Hassoun, P. K. Linden and B. Friedman, *Critical Care*, 2017, *21*, 211.

5. R. P. Wenzel and T. M. Perl, *Journal of Hospital Infection*, 1995, *31*, 13-24.

6. D. J. Diekema, M. A. Pfaller, F. J. Schmitz, J. Smayevsky, J. Bell, R. N. Jones, M. Beach and S. P. Group, *Clinical Infectious Diseases*, 2001, *32*, S114-S132.

7. J. Miao, L. Chen, J. Wang, W. Wang, D. Chen, L. Li, B. Li, Y. Deng and Z. Xu, *Microbial Pathogenesis*, 2017, *107*, 17-28.

8. National Institute of Allergy and Infectious Diseases, History, Methicillin-Resistant Staphylococcus aureus, Antimicrobial Resistance, https://www.niaid.nih.gov/research/mrsa-antimicrobial-resistance-history, (accessed 4 October, 2018).

9. T. J. Foster, *FEMS Microbiology Reviews*, 2017, *41*, 430-449.

10. D. Lim and N. C. J. Strynadka, *Nature Structural Biology*, 2002, *9*, 870-876.

11. M. J. Pucci and T. J. Dougherty, *Journal of Bacteriology*, 2002, *184*, 588-591.

12. P. Sarkar, V. Yarlagadda, C. Ghosh and J. Haldar, *Medchemcomm*, 2017, *8*, 516-533.

13. F. P. Maurer, M. Christner, M. Hentschke and H. Rohde, *Infectious Disease Reports*, 2017, *9*, 18-27.

14. A. Kumar, D. Roberts, K. E. Wood, B. Light, J. E. Parrillo, S. Sharma, R. Suppes, D. Feinstein, S. Zanotti, L. Taiberg, D. Gurka, A. Kumar and M. Cheang, *Critical Care Medicine*, 2006, *34*, 1589-1596.

15. J. M. Entenza, B. Betrisey, O. Manuel, M. Giddey, O. Sakwinska, F. Laurent and A. Bizzini, *Journal of Clinical Microbiology*, 2014, *52*, 180-186.

16. A. Novais, M. Brilhante, J. Pires and L. Peixe, *Journal of Clinical Microbiology*, 2015, *53*, 3105-3107.

17. L. Poirel and P. Nordmann, *Journal of Clinical Microbiology*, 2015, *53*, 3003-3008.

18. B. H. Lapizco-Encinas, B. A. Simmons, E. B. Cummings and Y. Fintschenko, *Analytical Chemistry*, 2004, *76*, 1571-1579.

19. P. V. Jones, A. F. DeMichele, L. Kemp and M. A. Hayes, *Analytical and Bioanalytical Chemistry*, 2014, *406*, 183-192.

20. P. V. Jones, S. Huey, P. Davis, R. Yanashima, R. McLemore, A. McLaren and M. A. Hayes, *Analyst*, 2015, *140*, 5152-5161.

21. H. A. Pohl, *Journal of Applied Physics*, 1951, *22*, 869-871.

22. T. N. G. Adams, A. Y. L. Jiang, P. D. Vyas and L. A. Flanagan, *Methods*, 2018, *133*, 91-103.

23. J. Ding, R. M. Lawrence, P. V. Jones, B. G. Hogue and M. A. Hayes, *Analyst*, 2016, *141*, 1997-2008.

24. M. P. Hughes, H. Morgan, F. J. Rixon, J. P. H. Burt and R. Pethig, *Biochimica et Biophysica Acta*, 1998, *1425*, 119-126.

25. F. H. Labeed, J. Lu, H. J. Mulhall, S. A. Marchenko, K. F. Hoettges, L. C. Estrada, A. P. Lee, M. P. Hughes and L. A. Flanagan, *PLoS One*, 2011, *6*, e25458.

26. B. H. Lapizco-Encinas, S. Ozuna-Chacon and M. Rito-Palomares, *Journal of Chromatography A*, 2008, *1206*, 45-51.

27. G. H. Markx, Y. Huang, X.-F. Zhou and R. Pethig, *Microbiology*, 1994, *140*, 585-591.

28. H. Morgan and N. G. Green, *Journal of Electrostatics*, 1997, *42*, 279-293.

29. S. Otto, U. Kaletta, F. F. Bier, C. Wenger and R. Holzel, *Lab on a Chip*, 2014, *14*, 998-1004.

30. H. Song, J. M. Rosano, Y. Wang, C. J. Garson, B. Prabhakarpandian, K. Pant, G. J. Klarmann, A. Perantoni, L. M. Alvarez and E. Lai, *Lab on a Chip*, 2015, *15*, 1320-1328.

31. S. J. R. Staton, P. V. Jones, G. Ku, S. D. Gilman, I. Kheterpal and M. A. Hayes, *Analyst*, 2012, *137*, 3227-3229.

32. S. Velugotla, S. Pells, H. K. Mjoseng, C. R. E. Duffy, S. Smith, P. De Sousa and R. Pethig, *Biomicrofluidics*, 2012, *6*, 44113.

33. M. Washizu, S. Suzuki, O. Kurosawa, T. Nishizaka and T. Shinohara, *IEEE Transactions on Industry Applications*, 1994, *30*, 835-843.

34. T. B. Jones, *Electromechanics of Particles*, Cambridge University Press, New York, 1995.

35. H. A. Pohl, *Dielectrophoresis The behavior of neutral matter in nonuniform electric fields*, Cambridge University Press, New York, 1978.

36. E. B. Cummings and A. K. Singh, *Analytical Chemistry*, 2003, *75*, 4724-4731.

37. S. H. Hilton and M. A. Hayes, *Analytical and Bioanalytical Chemistry*, 2019, DOI: 10.1007/s00216-019-01757-7.

38. N.-T. Nguyen and S. T. Wereley, *Fundamentals and Applications of Microfluidics*, Artech House, Boston, 2nd edn., 2006.

39. R. Pethig, *Biomicrofluidics*, 2010, *4*, 022811.

40. R. Pethig, *Dielectrophoresis : theory, methodology and biological applications*, Hoboken, NJ : John Wiley & Sons, Ltd, 1st edn., 2017.

41. P. Tabeling, *Introduction to Microfluidics*, Oxford University Press, New York, 2005.

42. A. Lalonde, A. Gencoglu, M. F. Romero-Creel, K. S. Koppula and B. H. Lapizco-Encinas, *Journal of Chromatography A*, 2014, *1344*, 99-108.

43. P. V. Jones, S. J. R. Staton and M. A. Hayes, *Analytical and Bioanalytical Chemistry*, 2011, *401*, 2103-2111.

44. S. J. R. Staton, K. P. Chen, T. J. Taylor, J. R. Pacheco and M. A. Hayes, *Electrophoresis*, 2010, *31*, 3634-3641.

45. W. Schrott, Z. Slouka, P. Cervenka, J. Ston, M. Nebyla, M. Pribyl and D. Snita, *Biomicrofluidics*, 2009, *3*, 44101.

46. P. V. Jones and M. A. Hayes, *Electrophoresis*, 2015, *36*, 1098-1106.

47. L. D. Garza-García, V. H. Pérez-González, O. A. Pérez-Sánchez and B. H. Lapizco-Encinas, *Chemical Engineering & Technology*, 2011, *34*, 371-378.

48. H. Moncada-Hernandez, J. L. Baylon-Cardiel, V. H. Perez-Gonzalez and B. H. Lapizco-Encinas, *Electrophoresis*, 2011, *32*, 2502-2511.

49. M. E. Bayer and J. L. Sloyer Jr., *Journal of General Microbiology*, 1990, *136*, 867-874.

**CHAPTER 5**

1. T. A. de Campos, L. F. Goncalves, K. G. Magalhaes, V. de Paulo Martins, G. J. Pappas Junior, G. Peirano, J. D. D. Pitout, G. B. Goncalves, J. P. R. Furlan, E. G. Stehling and A. Pitondo-Silva, *Frontiers in Medicine*, 2018, *5*, 265.

2. I. Galdadas, S. Lovera, G. Perez-Hernandez, M. D. Barnes, J. Healy, H. Afsharikho, N. Woodford, R. A. Bonomo, F. L. Gervasio and S. Haider, *Scientific Reports*, 2018, *8*, 12916.

3. D. M. Livermore, *Journal of Antimicrobial Chemotherapy*, 2009, *64 Suppl 1*, i29-i36.

4. D. M. Livermore, R. Hope, G. Brick, M. Lillie and R. Reynolds, *Journal of Antimicrobial Chemotherapy*, 2008, *62 Suppl 2*, ii41-ii54.

5. P. I. P. Ramos, R. C. Picao, L. G. P. de Almeida, N. C. B. Lima, R. Girardello, A. C. P. Vivan, D. E. Xavier, F. G. Barcellos, M. Pelisson, E. C. Vespero, C. Medigue, A. T. R. de Vasconcelos, A. C. Gales and M. F. Nicolas, *BMC Genomics*, 2014, *15*.

6. A. M. Queenan and K. Bush, *Clinical Microbiology Reviews*, 2007, *20*, 440-458.

7. D. Z. Rechenchoski, A. M. L. Dambrozio, A. C. P. Vivan, P. A. Schuroff, T. d. N. Burgos, M. Pelisson, M. R. E. Perugini and E. C. Vespero, *Brazilian Journal of Microbiology*, 2017, *48*, 509-514.

8. D. J. Wolter, P. M. Kurpiel, N. Woodford, M.-F. I. Palepou, R. V. Goering and N. D. Hanson, *Antimicrobial Agents and Chemotherapy*, 2009, *53*, 557-562.

9. R. S. Arnold, K. A. Thom, S. Sharma, M. Phillips, J. K. Johnson and D. J. Morgan, *Southern Medical Journal*, 2011, *104*, 40-45.

10. H. Khalili, S. Dashti-Khavidaki, M.-R. Shahidi, A. Abdollahi, S. Jafari, Z. Jahangard-Rafsanjani and A.-H. Talasaz, *DARU Journal of Pharmaceutical Sciences*, 2012, *20*.

11. Centers for Disease Control and Prevention, *Facility Guidance for Control of Carbapenem-resistant Enterobacteriaceae (CRE) November 2015 Update - CRE Toolkit*, 2015.

12. Centers for Disease Control and Prevention, *Morbidity and Mortality Weekly Report*, 2009, *58*, 256-260.

13. A. R. McMullen, M. L. Yarbrough, M. A. Wallace, A. Shupe and C.-A. D. Burnham, *Clinical Chemistry*, 2017, *63*, 723-730.

14. S. Bratu, D. Landman, R. Haag, R. Recco, A. Eramo, M. Alam and J. Quale, *Archives of Internal Medicine*, 2005, *165*, 1430-1435.

15. S. Bratu, M. Mooty, S. Nichani, D. Landman, C. Gullans, B. Pettinato, U. Karumudi, P. Tolaney and J. Quale, *Antimicrobial Agents and Chemotherapy*, 2005, *49*, 3018-3020.

16. B. M. Lomaestro, E. Tobin, H., W. Shang and T. Gootz, *Clinical Infectious Diseases*, 2006, *43*, e26-e28.

17. P. Nordmann, G. Cuzon and T. Naas, *The Lancet Infectious Diseases*, 2009, *9*, 228-236.

18. P. V. Jones, S. Huey, P. Davis, R. Yanashima, R. McLemore, A. McLaren and M. A. Hayes, *Analyst*, 2015, *140*, 5152-5161.

19. S. H. Hilton, C. V. Crowther, A. McLaren and M. A. Hayes, *Analyst*, 2019, Submitted.

20. H. A. Pohl, *Journal of Applied Physics*, 1951, *22*, 869-871.

21. C. Asbury, L., A. H. Dierks and G. van den Engh, *Electrophoresis*, 2002, *23*, 2658-2666.

22. F. F. Becker, X.-B. Wang, Y. Huang, R. Pethig, J. Vykoukal and P. R. C. Gascoyne, *Proceedings of the National Academy of Sciences of the United States of America*, 1995, *92*, 860-864.

23. K. L. Chan, H. Morgan, E. Morgan, I. T. Cameron and M. R. Thomas, *Biochimica et Biophysica Acta*, 2000, *1500*, 313-322.

24. C.-F. Chou, J. O. Tegenfeldt, O. Bakajin, S. S. Chan, E. C. Cox, N. Darnton, T. Duke and R. H. Austin, *Biophysical Journal*, 2002, *83*, 2170-2179.

25. J. Ding, R. M. Lawrence, P. V. Jones, B. G. Hogue and M. A. Hayes, *Analyst*, 2016, *141*, 1997-2008.

26. J. Ding, C. Woolley and M. A. Hayes, *Analytical and Bioanalytical Chemistry*, 2017, *409*, 6405-6414.

27. M. P. Hughes, H. Morgan, F. J. Rixon, J. P. H. Burt and R. Pethig, *Biochimica et Biophysica Acta*, 1998, *1425*, 119-126.

28. P. V. Jones, S. J. R. Staton and M. A. Hayes, *Analytical and Bioanalytical Chemistry*, 2011, *401*, 2103-2111.

29. B. H. Lapizco-Encinas, B. A. Simmons, E. B. Cummings and Y. Fintschenko, *Electrophoresis*, 2004, *25*, 1695-1704.

30. B. H. Lapizco-Encinas, B. A. Simmons, E. B. Cummings and Y. Fintschenko, *Analytical Chemistry*, 2004, *76*, 1571-1579.

31. G. H. Markx, Y. Huang, X.-F. Zhou and R. Pethig, *Microbiology*, 1994, *140*, 585-591.

32. H. Morgan and N. G. Green, *Journal of Electrostatics*, 1997, *42*, 279-293.

33. J. Regtmeier, T. T. Duong, R. Eichhorn, D. Anselmetti and A. Ros, *Analytical Chemistry*, 2007, *79*, 3925-3932.

34. S. K. Srivastava, P. R. Daggolu, S. C. Burgess and A. R. Minerick, *Electrophoresis*, 2008, *29*, 5033-5046.

35. A. Lalonde, A. Gencoglu, M. F. Romero-Creel, K. S. Koppula and B. H. Lapizco-Encinas, *Journal of Chromatography A*, 2014, *1344*, 99-108.

36. H. A. Pohl, *Dielectrophoresis The behavior of neutral matter in nonuniform electric fields*, Cambridge University Press, New York, 1978.

37. E. B. Cummings and A. K. Singh, *Analytical Chemistry*, 2003, *75*, 4724-4731.

38. W. A. Braff, A. Pignier and C. R. Buie, *Lab on a Chip*, 2012, *12*, 1327-1331.

39. F. Camacho-Alanis, L. Gan and A. Ros, *Sensors and Actuators B: Chemical*, 2012, *173*, 668-675.

40. D. Chen and H. Du, *Microfluidics and Nanofluidics*, 2010, *9*, 281-291.

41. P. R. C. Gascoyne, J. Noshari, T. J. Anderson and F. F. Becker, *Electrophoresis*, 2009, *30*, 1388-1398.

42. B. H. Lapizco-Encinas, S. Ozuna-Chacon and M. Rito-Palomares, *Journal of Chromatography A*, 2008, *1206*, 45-51.

43. H. Moncada-Hernandez, J. L. Baylon-Cardiel, V. H. Perez-Gonzalez and B. H. Lapizco-Encinas, *Electrophoresis*, 2011, *32*, 2502-2511.

44. A. Nakano, F. Camacho-Alanis and A. Ros, *Analyst*, 2015, *140*, 860-868.

45. S. Ozuna-Chacon, B. H. Lapizco-Encinas, M. Rito-Palomares, S. O. Martinez-Chapa and C. Reyes-Betanzo, *Electrophoresis*, 2008, *29*, 3115-3122.

46. M. A. Saucedo-Espinosa, A. LaLonde, A. Gencoglu, M. F. Romero-Creel, J. R. Dolas and B. H. Lapizco-Encinas, *Electrophoresis*, 2016, *37*, 282-290.

47. H. Song, J. M. Rosano, Y. Wang, C. J. Garson, B. Prabhakarpandian, K. Pant, G. J. Klarmann, A. Perantoni, L. M. Alvarez and E. Lai, *Lab on a Chip*, 2015, *15*, 1320-1328.

48. S. J. R. Staton, K. P. Chen, T. J. Taylor, J. R. Pacheco and M. A. Hayes, *Electrophoresis*, 2010, *31*, 3634-3641.

49. P. Tabeling, *Introduction to Microfluidics*, Oxford University Press, New York, 2005.

50. P. V. Jones, A. F. DeMichele, L. Kemp and M. A. Hayes, *Analytical and Bioanalytical Chemistry*, 2014, *406*, 183-192.

51. S. J. R. Staton, P. V. Jones, G. Ku, S. D. Gilman, I. Kheterpal and M. A. Hayes, *Analyst*, 2012, *137*, 3227-3229.

52. S. H. Hilton and M. A. Hayes, *Analytical and Bioanalytical Chemistry*, 2019, DOI: 10.1007/s00216-019-01757-7.

**CHAPTER 6**

1. European Committee on Antimicrobial Susceptibility Testing, *Reading guide: EUCAST disk diffusion method for antimicrobial susceptibility testing, version 6.0*, 2019.

2. European Committee on Antimicrobial Susceptibility Testing, *EUCAST reading guide for broth microdilution, version 1.0*, 2019.

3. World Health Organization, *Global Action Plan on Antimicrobial Resistance*, World Health Organizaion, Geneva, Switzerland, 2015.

4. Centers for Disease Control and Prevention, Antibiotic Resistance: A Global Threat, https://www.cdc.gov/features/antibiotic-resistance-global/index.html, (accessed February 11, 2019).

5. E. H. Ibrahim, G. Sherman, S. Ward, V. J. Fraser and M. H. Kollef, *CHEST*, 2000, *118*, 146-155.

6. C.-I. Kang, S.-H. Kim, W. B. Park, K.-D. Lee, H.-B. Kim, E.-C. Kim, M.-d. Oh and K.-W. Choe, *Antimicrobial Agents and Chemotherapy*, 2005, *49*, 760-766.

7. World Health Organization, Antimicrobial resistance, https://www.who.int/en/news-room/fact-sheets/detail/antimicrobial-resistance, (accessed February 13, 2019).

8. Centers for Disease Control and Prevention, *Antibiotic Resistance Threats in the United States, 2013*, 2013.

9. H. Goossens, M. Ferech, R. Vander Stichele and M. Elseviers, *The Lancet*, 2005, *365*, 579-587.

10. S. Riedel, S. E. Beekmann, K. P. Heilmann, S. S. Richter, J. Garcia-de-Lomas, M. Ferech, H. Goosens and G. V. Doern, *European Journal of Clinical Microbiology and Infectious Diseases*, 2007, *26*, 485-490.

11. E. A. Grice and J. A. Segre, *Nature Reviews Microbiology*, 2011, *9*, 244-253.

12. W. E. Kloos and M. S. Musselwhite, *Applied Microbiology*, 1975, *30*, 381-395.

13. C. Vuong and M. Otto, *Microbes and Infection*, 2002, *4*, 481-489.

14. M. Otto, *Nature Reviews Microbiology*, 2009, *7*, 555-567.

15. T. Hermann, *Cellular and Molecular Life Sciences*, 2007, *64*, 1841-1852.

16. G. D. Wright, *Chemical Communications*, 2011, *47*, 4055-4061.

17. G. H. Miller, F. J. Sabatelli, R. S. Hare, Y. Glupczynski, P. Mackey, D. Shales, K. Shimizu and K. J. Shaw, *Clinical Infectious Diseases*, 1997, *24*, S46-S62.

18. T. N. G. Adams, A. Y. L. Jiang, P. D. Vyas and L. A. Flanagan, *Methods*, 2018, *133*, 91-103.

19. C. Asbury, L., A. H. Dierks and G. van den Engh, *Electrophoresis*, 2002, *23*, 2658-2666.

20. C.-F. Chou, J. O. Tegenfeldt, O. Bakajin, S. S. Chan, E. C. Cox, N. Darnton, T. Duke and R. H. Austin, *Biophysical Journal*, 2002, *83*, 2170-2179.

21. P. R. C. Gascoyne, J. Noshari, T. J. Anderson and F. F. Becker, *Electrophoresis*, 2009, *30*, 1388-1398.

22. M. P. Hughes, H. Morgan, F. J. Rixon, J. P. H. Burt and R. Pethig, *Biochimica et Biophysica Acta*, 1998, *1425*, 119-126.

23. P. V. Jones, A. F. DeMichele, L. Kemp and M. A. Hayes, *Analytical and Bioanalytical Chemistry*, 2014, *406*, 183-192.

24. F. H. Labeed, J. Lu, H. J. Mulhall, S. A. Marchenko, K. F. Hoettges, L. C. Estrada, A. P. Lee, M. P. Hughes and L. A. Flanagan, *PLoS One*, 2011, *6*, e25458.

25. B. H. Lapizco-Encinas, S. Ozuna-Chacon and M. Rito-Palomares, *Journal of Chromatography A*, 2008, *1206*, 45-51.

26. B. H. Lapizco-Encinas, B. A. Simmons, E. B. Cummings and Y. Fintschenko, *Electrophoresis*, 2004, *25*, 1695-1704.

27. B. H. Lapizco-Encinas, B. A. Simmons, E. B. Cummings and Y. Fintschenko, *Analytical Chemistry*, 2004, *76*, 1571-1579.

28. G. H. Markx, Y. Huang, X.-F. Zhou and R. Pethig, *Microbiology*, 1994, *140*, 585-591.

29. H. Morgan and N. G. Green, *Journal of Electrostatics*, 1997, *42*, 279-293.

30. S. Otto, U. Kaletta, F. F. Bier, C. Wenger and R. Holzel, *Lab on a Chip*, 2014, *14*, 998-1004.

31. J. Regtmeier, T. T. Duong, R. Eichhorn, D. Anselmetti and A. Ros, *Analytical Chemistry*, 2007, *79*, 3925-3932.

32. H. Song, J. M. Rosano, Y. Wang, C. J. Garson, B. Prabhakarpandian, K. Pant, G. J. Klarmann, A. Perantoni, L. M. Alvarez and E. Lai, *Lab on a Chip*, 2015, *15*, 1320-1328.

33. S. J. R. Staton, P. V. Jones, G. Ku, S. D. Gilman, I. Kheterpal and M. A. Hayes, *Analyst*, 2012, *137*, 3227-3229.

34. S. Velugotla, S. Pells, H. K. Mjoseng, C. R. E. Duffy, S. Smith, P. De Sousa and R. Pethig, *Biomicrofluidics*, 2012, *6*, 44113.

35. X.-B. Wang, Y. Huang, J. P. H. Burt, G. H. Markx and R. Pethig, *Journal of Physics D: Applied Physics*, 1993, *26*, 1276-1285.

36. M. Washizu, S. Suzuki, O. Kurosawa, T. Nishizaka and T. Shinohara, *IEEE Transactions on Industry Applications*, 1994, *30*, 835-843.

37. J. Ding, C. Woolley and M. A. Hayes, *Analytical and Bioanalytical Chemistry*, 2017, *409*, 6405-6414.

38. J. S. Crane and H. A. Pohl, *Journal of The Electrochemical Society*, 1968, *115*, 584-586.

39. J. S. Crane and H. A. Pohl, *Journal of Electrostatics*, 1978, *5*, 11-19.

40. H. A. Pohl, *Journal of Applied Physics*, 1951, *22*, 869-871.

41. H. A. Pohl, *Dielectrophoresis The behavior of neutral matter in nonuniform electric fields*, Cambridge University Press, New York, 1978.

42. E. B. Cummings and A. K. Singh, *Analytical Chemistry*, 2003, *75*, 4724-4731.

43. J. Ding, R. M. Lawrence, P. V. Jones, B. G. Hogue and M. A. Hayes, *Analyst*, 2016, *141*, 1997-2008.

44. P. V. Jones, S. J. R. Staton and M. A. Hayes, *Analytical and Bioanalytical Chemistry*, 2011, *401*, 2103-2111.

45. A. LaLonde, M. F. Romero-Creel, M. A. Saucedo-Espinosa and B. H. Lapizco-Encinas, *Biomicrofluidics*, 2015, *9*, 064113.

46. H. Moncada-Hernandez, J. L. Baylon-Cardiel, V. H. Perez-Gonzalez and B. H. Lapizco-Encinas, *Electrophoresis*, 2011, *32*, 2502-2511.

47. A. Nakano, F. Camacho-Alanis and A. Ros, *Analyst*, 2015, *140*, 860-868.

48. M. A. Saucedo-Espinosa, A. LaLonde, A. Gencoglu, M. F. Romero-Creel, J. R. Dolas and B. H. Lapizco-Encinas, *Electrophoresis*, 2016, *37*, 282-290.

49. Q. Jin, C. Cui, H. Chen, J. Wu, J. Hu, X. Xing, J. Geng and Y. Wu, *Frontiers of Environmental Science & Engineering*, 2019, *13*, 16.

50. M. Elitas, Y. Yildizhan, M. Islam, R. Martinez-Duarte and D. Ozkazanc, *Electrophoresis*, 2019, *40*, 315-321.

51. M. T. Rabbani, C. F. Schmidt and A. Ros, *Analytical Chemistry*, 2017, *89*, 13235-13244.

52. A. Rohani, J. H. Moore, J. A. Kashatus, H. Sesaki, D. F. Kashatus and N. S. Swami, *Analytical Chemistry*, 2017, *89*, 5757-5764.

53. D. V. Polniak, E. Goodrich, N. Hill and B. H. Lapizco-Encinas, *Journal of Chromatography A*, 2018, *1545*, 84-92.

54. A. Lalonde, A. Gencoglu, M. F. Romero-Creel, K. S. Koppula and B. H. Lapizco-Encinas, *Journal of Chromatography A*, 2014, *1344*, 99-108.

55. S. J. R. Staton, K. P. Chen, T. J. Taylor, J. R. Pacheco and M. A. Hayes, *Electrophoresis*, 2010, *31*, 3634-3641.

56. J. T. Davies and E. K. Rideal, *Interfacial Phenomena*, Academic Press, New York, 1961.

57. N.-T. Nguyen and S. T. Wereley, *Fundamentals and Applications of Microfluidics*, Artech House, Boston, 2nd edn., 2006.

58. R. Pethig, *Biomicrofluidics*, 2010, *4*, 022811.

59. R. Pethig, *Dielectrophoresis : theory, methodology and biological applications*, Hoboken, NJ : John Wiley & Sons, Ltd, 1st edn., 2017.

60. P. Tabeling, *Introduction to Microfluidics*, Oxford University Press, New York, 2005.

61. P. V. Jones, S. Huey, P. Davis, R. Yanashima, R. McLemore, A. McLaren and M. A. Hayes, *Analyst*, 2015, *140*, 5152-5161.

**CHAPTER 7**

1. A. Kumar, D. Roberts, K. E. Wood, B. Light, J. E. Parrillo, S. Sharma, R. Suppes, D. Feinstein, S. Zanotti, L. Taiberg, D. Gurka, A. Kumar and M. Cheang, *Critical Care Medicine*, 2006, *34*, 1589-1596.

2. P. V. Jones and M. A. Hayes, *Electrophoresis*, 2015, *36*, 1098-1106.

3. C.-C. Chung, I.-F. Cheng, H.-M. Chen, H.-C. Kan, W.-H. Yang and H.-C. Chang, *Analytical Chemistry*, 2012, *84*, 3347-3354.

4. K. F. Hoettges, Y. Hubner, L. M. Broche, S. L. Ogin, G. E. N. Kass and M. P. Hughes, *Analytical Chemistry*, 2008, *80*, 2063-2068.

5. S. Inoue, H.-B. Lee, A. L. Becker, K. M. Weigel, J.-H. Kim, K.-H. Lee, G. A. Cangelosi and J.-H. Chung, *Analytical and Bioanalytical Chemistry*, 2015, *407*, 7673-7680.

6. J. Kirchhoff, U. Glaser, J. A. Bohnert, M. W. Pletz, J. Popp and U. Neugebauer, *Analytical Chemistry*, 2018, *90*, 1811-1818.

7. A. Rohani, J. H. Moore, Y.-H. Su, V. Stagnaro, C. Warren and N. S. Swami, *Sensors and Actuators B: Chemical*, 2018, *276*, 472-480.

8. U.-C. Schroder, J. Kirchhoff, U. Hubner, G. Mayer, U. Glaser, T. Henkel, W. Pfister, W. Fritzsche, J. Popp and U. Neugebauer, *Journal of Biophotonics*, 2017, *10*, 1547-1557.

9. I.-H. Su, W.-C. Ko, C.-H. Shih, F.-H. Yeh, Y.-N. Sun, J.-C. Chen, P.-L. Chen and H.-C. Chang, *Analytical Chemistry*, 2017, *89*, 4635-4641.

10. Y.-H. Su, C. A. Warren, R. L. Guerrant and N. S. Swami, *Analytical Chemistry*, 2014, *86*, 10855-10863.

# APPENDIX A

# VALIDATION OF THE MATHEMATICAL MODEL OF DIELECTROPHORETIC DATA

The mathematical model of dielectrophoretic data presented in Chapter 3 has been validated using data from three *Listeria monocytogenes* bacterial strains [1]. The electrokinetic mobilities of these three strains were determined from particle tracking velocity measurements. Dielectrophoretic data from the three strains was collected as well. The independently-determined electrokinetic mobilities were used to calculate the slope of dielectrophoretic data of the three strains using the mathematical model. Since the dielectrophoretic mobility is not known, the capture onset potential can be made an adjustable parameter. This will not affect the slope, but rather only the capture onset potential. Other parameters were set as in the experiments. With these considerations, the slope calculated from the model found agreement with that determined experimentally though dielectrophoretic experiments (Figure A.1).

Comparing the electrokinetic mobilities determined from dielectrophoretic data using the model with those from velocity measurements is another way to validate the mathematical model of dielectrophoretic data (Table A.1). This comparison shows good agreement between the velocity-determined and dielectrophoresis-determined electrokinetic mobilities. One consideration in the mathematical model is the $s$ factor, which accounts for issues in the detection of analytes, including those arising from potential stacking of the analyte, scattering of the light, or saturation of the detection method. While a value of 15 for the $s$ factor was chosen in this case, it is likely that rather than arising from issues in detection of the analytes, this instead arises from considering the fluorescence intensity per particle to be lower than is seen in the

microchannel. An actual value for the fluorescence intensity per particle in each experiment could be found to assess this possibility.

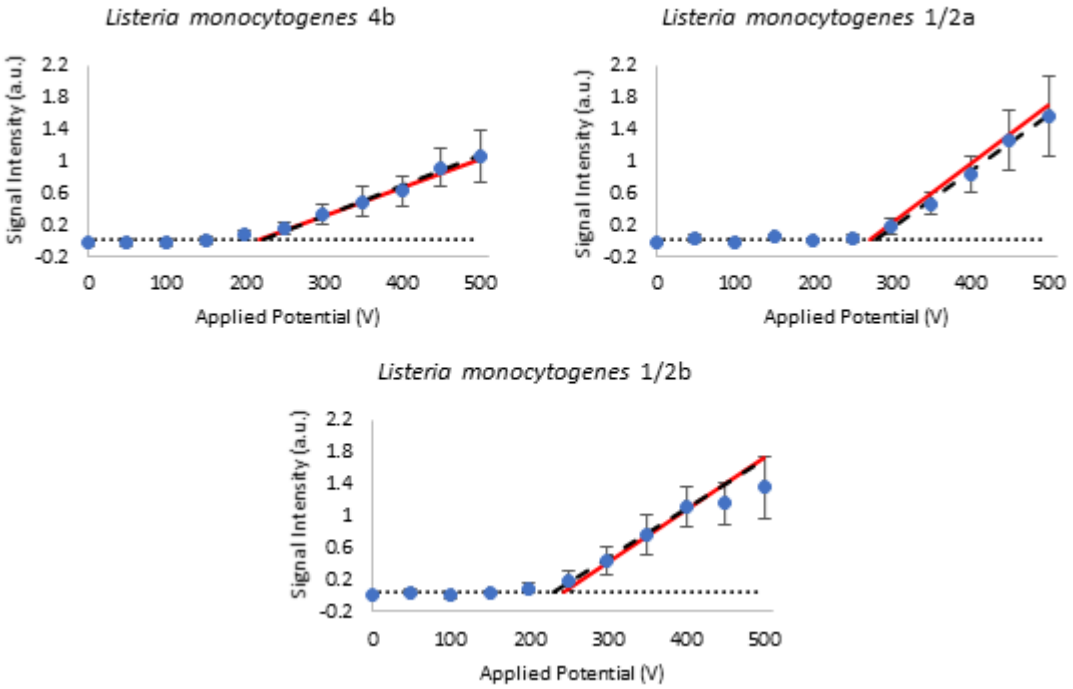



Figure A.1 Overlay of modeled slope from velocity-determined electrokinetic mobility (solid red line) with dielectrophoretic data (blue circles) and calculated slope (dashed black line) for three strains of *Listeria monocytogenes*: 4b (top left), 1/2a (top right), and 1/2b (bottom). Error bars are 95% confidence intervals of dielectrophoretic data.

Table A.1 Comparison of velocity-determined and dielectrophoresis-determined electrokinetic mobility

| | $\mu_{EK}$ Determined by Velocity $\left(\frac{m^2}{V \cdot s}\right)$ | $\mu_{EK}$ Determined by Dielectrophoresis $\left(\frac{m^2}{V \cdot s}\right)$ |
|---|---|---|
| *L. monocytogenes* 1/2a | $19 \pm 0.7 \times 10^{-9}$ | $18 \pm 0.6 \times 10^{-9}$ |
| *L. monocytogenes* 1/2b | $17 \pm 0.7 \times 10^{-9}$ | $16 \pm 0.6 \times 10^{-9}$ |
| *L. monocytogenes* 4b | $9.2 \pm 0.3 \times 10^{-9}$ | $9.9 \pm 0.4 \times 10^{-9}$ |

## A.1 Reference

1. C. V. Crowther, S. H. Hilton, L. Kemp and M. A. Hayes, *Analytica Chimica Acta*, 2019, In Press.

# APPENDIX B

## PUBLISHED PORTIONS

Portions of this dissertation have been previously published or submitted for publication, while others are in preparation for submission. In addition, figures 6.2 and 6.3 were adapted from a previous publication. These portions were included with permission from all co-authors.

Chapter 3:

Reprinted by permission from Springer *Analytical and Bioanalytical Chemistry* A mathematical model of dielectrophoretic data to connect measurements with cell properties, S.H. Hilton, M. A. Hayes © 2019

Chapter 4:

S. H. Hilton, C. V. Crowther, A. McLaren, M. A. Hayes, *Analyst*, 2019, Submitted.

Chapter 5:

S. H. Hilton, J. Bowers, M. A. Hayes, In Preparation.

Chapter 6:

Figures 6.2 and 6.3 adapted from P. V. Jones, S. Huey, P. Davis, R. Yanashima, R. McLemore, A. McLaren and M. A. Hayes, *Analyst*, 2015, *140*, 5152-5161 with permission from the Royal Society of Chemistry.

Copyright Clearance Center RightsLink®

Home | Account Info | Help

SPRINGER NATURE

Title: A mathematical model of dielectrophoretic data to connect measurements with cell properties
Author: Shannon Huey Hilton, Mark A. Hayes
Publication: Analytical and Bioanalytical Chemistry
Publisher: Springer Nature
Date: Jan 1, 2019
Copyright © 2019, Springer-Verlag GmbH Germany, part of Springer Nature

Logged in as:
Shannon Hilton
LOGOUT

## Order Completed

Thank you for your order.

This Agreement between Shannon Hilton ("You") and Springer Nature ("Springer Nature") consists of your license details and the terms and conditions provided by Springer Nature and Copyright Clearance Center.

Your confirmation email will contain your order number for future reference.

printable details

| | |
|---|---|
| License Number | 4553190466555 |
| License date | Mar 20, 2019 |
| Licensed Content Publisher | Springer Nature |
| Licensed Content Publication | Analytical and Bioanalytical Chemistry |
| Licensed Content Title | A mathematical model of dielectrophoretic data to connect measurements with cell properties |
| Licensed Content Author | Shannon Huey Hilton, Mark A. Hayes |
| Licensed Content Date | Jan 1, 2019 |
| Type of Use | Thesis/Dissertation |
| Requestor type | academic/university or research institute |
| Format | print and electronic |
| Portion | full article/chapter |
| Will you be translating? | no |
| Circulation/distribution | >50,000 |
| Author of this Springer Nature content | yes |
| Title | Analyzing Cellular Properties with Dielectrophoresis |
| Institution name | Arizona State University |
| Expected presentation date | Apr 2019 |
| Requestor Location | Shannon Hilton<br>Physical Sciences Center PSD-D102<br><br>TEMPE, AZ 85287<br>United States<br>Attn: Shannon Hilton |
| Total | 0.00 USD |